

IntechOpen

Organic Polymers

Edited by Arpit Sand and Elsayed Zaki



Organic Polymers

Edited by Arpit Sand and Elsayed Zaki

Published in London, United Kingdom



IntechOpen





Supporting open minds since 2005



Organic Polymers

<http://dx.doi.org/10.5772/intechopen.78486>

Edited by Arpit Sand and Elsayed Zaki

Contributors

Emmanuel Kweinor Tetteh, Sudesh Rathilal, Wenyi Huang, Panmanas Sirisomboon, Chin Hock Lim, Tao Yang, Rui Lu, Xiaobing Qu, Lu Zhang, Nana Zhu, Cengiz Soykan, Aline Dettmer, Marieli Rosseto, Cesar V.T. Riguetto, Daniela D.C. Krein, Naiana P. Balbé, Lillian A. Massuda, Aurélie Cayla, Christine Campagne, Juliette Minet, Arpit Sand, Aparna Vyas

© The Editor(s) and the Author(s) 2020

The rights of the editor(s) and the author(s) have been asserted in accordance with the Copyright, Designs and Patents Act 1988. All rights to the book as a whole are reserved by INTECHOPEN LIMITED. The book as a whole (compilation) cannot be reproduced, distributed or used for commercial or non-commercial purposes without INTECHOPEN LIMITED's written permission. Enquiries concerning the use of the book should be directed to INTECHOPEN LIMITED rights and permissions department (permissions@intechopen.com).

Violations are liable to prosecution under the governing Copyright Law.



Individual chapters of this publication are distributed under the terms of the Creative Commons Attribution 3.0 Unported License which permits commercial use, distribution and reproduction of the individual chapters, provided the original author(s) and source publication are appropriately acknowledged. If so indicated, certain images may not be included under the Creative Commons license. In such cases users will need to obtain permission from the license holder to reproduce the material. More details and guidelines concerning content reuse and adaptation can be found at <http://www.intechopen.com/copyright-policy.html>.

Notice

Statements and opinions expressed in the chapters are these of the individual contributors and not necessarily those of the editors or publisher. No responsibility is accepted for the accuracy of information contained in the published chapters. The publisher assumes no responsibility for any damage or injury to persons or property arising out of the use of any materials, instructions, methods or ideas contained in the book.

First published in London, United Kingdom, 2020 by IntechOpen

IntechOpen is the global imprint of INTECHOPEN LIMITED, registered in England and Wales, registration number: 11086078, 7th floor, 10 Lower Thames Street, London, EC3R 6AF, United Kingdom

Printed in Croatia

British Library Cataloguing-in-Publication Data

A catalogue record for this book is available from the British Library

Additional hard and PDF copies can be obtained from orders@intechopen.com

Organic Polymers

Edited by Arpit Sand and Elsayed Zaki

p. cm.

Print ISBN 978-1-78984-573-0

Online ISBN 978-1-78984-618-8

eBook (PDF) ISBN 978-1-78985-194-6

We are IntechOpen, the world's leading publisher of Open Access books Built by scientists, for scientists

4,700+

Open access books available

120,000+

International authors and editors

135M+

Downloads

151

Countries delivered to

Our authors are among the
Top 1%

most cited scientists

12.2%

Contributors from top 500 universities



WEB OF SCIENCE™

Selection of our books indexed in the Book Citation Index
in Web of Science™ Core Collection (BKCI)

Interested in publishing with us?
Contact book.department@intechopen.com

Numbers displayed above are based on latest data collected.
For more information visit www.intechopen.com



Meet the editors



Dr Arpit Sand is currently an Associate Professor in the Department of Chemistry at Manav Rachna University, India, a position he has held since 2014. He received his B.Sc. in Science and his M.Sc. in Chemistry from the University of Allahabad, India, in 2004 and 2006, respectively. He received his Ph.D. degree in Chemistry from the University of Allahabad in 2010.

Dr Arpit Sand is a reviewer for international journals including Carbohydrate Polymers, the International Journal of Biological Macromolecules, Fibers and Polymers, etc. He is also a life member of the Indian Science Congress and the Green Chemistry Network centre, and he has authored more than 20 international research articles and review articles in reputed SCI journals. He has made a significant contribution to the field of the modification and characterization of graft copolymers. His research interests include polymer synthesis using different polymerization techniques.



Dr Elsayed Zaki received his PhD in physical chemistry from the Department of Chemistry, Faculty of Science,– Mansoura University, Egypt. Currently, he is a Researcher visiting the Department of Chemical and Biomolecular Engineering, Iacocca Hall, Lehigh University, USA. He has been a researcher of applied chemistry in the Petroleum Applications Department, Egyptian Petroleum Research Institute from 1 March 2015 to present.

He is currently serving as an editorial member of several reputed journals such as Industrial & Engineering Chemistry Research, American Chemical Society, International Journal of Hydrogen Energy, Archives in Cancer Research, Herald Journal of Agriculture and Food Science Research, on the scientific and technical committee and editorial review board on Chemical and Molecular Engineering (WASET), Open Journal of Applied Sciences, Advances in Chemical Engineering and Science, Journal of the Chemical Society of Pakistan, International Conference on Chemical, Metallurgy and Environmental Engineering, Universal Researchers in Environmental & Biological Engineering, Asia-Pacific Chemical, Biological & Environmental Engineering Society, International Journal of Chemical and Biomolecular Science in Public Science Framework, Biomedical and Pharmacology Journal, International Academy of Chemical, Civil & Environment Engineering, International Journal of Ambient Energy, he was appointed to editorial board for the International Journal of Materials Science and Applications, he was appointed to editorial board for Advances in Materials, he was appointed to editorial board for International Journal of Science, Technology and Society, Organic & Medicinal Chemistry International Journal (OMCIJ), Universal Journal of Pharmaceutical Research, International Journal of Nano and Material Sciences, he is an advisory board member of World Journal of Pharmacy and Pharmaceutical Sciences, Cogent OA, Taylor & Francis Group, SciFed Journal of Polymerscience. He is a member of the Royal Society of

Chemistry (MRSC), Chemicals Development Services Center (CDSC), Egyptian Corrosion Society (ECS), The Arab Society of Material Science, Petroleum and Mineral Resources Society, Egyptian Petroleum Association, The Egyptian Society of Polymer Science and Technology, Egyptian Syndicate of Scientific Professions, Asia-Pacific Chemical, Biological & Environmental Engineering Society (APC-BEES), Society of Petroleum Engineers (SPE), World Academy of Science, Engineering and Technology (WASET), The International Association of Engineers (IAENG), Egyptian Association for Science and Engineering (EASE), Sesame User Office (SUO) Synchrotron- Light for Experimental Science and Applications in the Middle East, Sesame Users' Committee (SUC) Synchrotron-Light for Experimental Science and Applications in the Middle East, International Association of Advanced Materials (IAAM), The Society of Digital Information and Wireless Communications (SDIWC), The International Society for Environmental Information Sciences (ISEIS), The Organization for Women in Science for the Developing World (OWSD), and the International Union of Pure and Applied Chemistry.

Contents

Preface	XIII
Chapter 1 Introductory Chapter: Organic Polymer - Graft Copolymers <i>by Arpit Sand and Aparna Vyas</i>	1
Chapter 2 Rapid Evaluation of the Properties of Natural Rubber Latex and Its Products Using Near-Infrared Spectroscopy <i>by Panmanas Sirisomboon and Chin Hock Lim</i>	9
Chapter 3 Electron Donor-Acceptor Organic Polymers by “Click” Type Cycloaddition/Retroelectrocyclization Reaction <i>by Wenyi Huang</i>	27
Chapter 4 Application of Organic Coagulants in Water and Wastewater Treatment <i>by Emmanuel Kweinor Tetteh and Sudesh Rathilal</i>	51
Chapter 5 Directed Self-Assembly of Block Copolymers Based on the Heterogeneous Nucleation Process <i>by Rui Lu, Xiaobing Qu, Lu Zhang, Nana Zhu and Tao Yang</i>	69
Chapter 6 New Methods in the Synthesis of (Meth)Acrylates <i>by Cengiz Soykan</i>	85
Chapter 7 Biodegradable Polymers: Opportunities and Challenges <i>by Marieli Rosseto, Cesar V.T. Rigueto, Daniela D.C. Krein, Naiana P. Balb�e, Lillian A. Massuda and Aline Dettmer</i>	101
Chapter 8 Lignin as Sustainable Antimicrobial Fillers to Develop PET Multifilaments by Melting Process <i>by Juliette Minet, Aur�elie Cayla and Christine Campagne</i>	119

Preface

A polymer is a class of natural or synthetic substances composed of very large molecules, called macromolecules, that are multiples of simpler chemical units called monomers. Polymers make up many of the materials in living organisms, including, for example, proteins, cellulose, and nucleic acids. Moreover, they constitute the basis of such minerals as diamond, quartz, and feldspar and such man-made materials as concrete, glass, paper, plastics, and rubbers.

Other important natural polymers include the proteins, which are polymers of amino acids; and the nucleic acids, which are polymers of nucleotides—complex molecules composed of nitrogen-containing bases, sugars, and phosphoric acid. The nucleic acids carry genetic information in the cell. Starches, important sources of food energy derived from plants, are natural polymers composed of glucose.

Organic polymers play a crucial role in living things, providing basic structural materials and participating in vital life processes. For example, the solid parts of all plants are made up of polymers. These include cellulose, lignin, and various resins. Cellulose is a polysaccharide, a polymer that is composed of sugar molecules. Lignin consists of a complicated three-dimensional network of polymers. Wood resins are polymers of a simple hydrocarbon, isoprene. Another familiar isoprene polymer is rubber.

Many inorganic polymers are also found in nature, including diamond and graphite. Both are composed of carbon. In diamond, carbon atoms are linked in a three-dimensional network that gives the material its hardness. In graphite, used as a lubricant and in pencil lead, the carbon atoms link in planes that can slide across one another. Synthetic polymers are produced in different types of reactions.

Many simple hydrocarbons, such as ethylene and propylene, can be transformed into polymers by adding one monomer after another to the growing chain. Polyethylene, composed of repeating ethylene monomers, is an addition polymer. It may have as many as 10,000 monomers joined in long coiled chains. Polyethylene is crystalline, translucent, and thermoplastic—i.e., it softens when heated. It is used for coatings, packaging, molded parts, and the manufacture of bottles and containers. Polypropylene is also crystalline and thermoplastic but is harder than polyethylene. Its molecules may consist of from 50,000 to 200,000 monomers. This compound is used in the textile industry and to make molded objects. This book consists of eight chapters.

Arpit Sand
Associate Professor,
Department of Chemistry,
Manav Rachna University,
India

Elsayed Zaki
Egyptian Petroleum Research Institute,
Egypt

Introductory Chapter: Organic Polymer - Graft Copolymers

Arpit Sand and Aparna Vyas

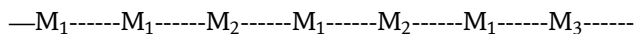
Polymers, high molecular weight compounds, have most essential position in the materials field today even though have been introduction in meaning full logic more recently. In performance, characteristics, and application predictions, polymers offer novelty and usefulness not to be found in other kinds of materials. The rapidity of the all-round developments in polymer science and technology and the unique pace of application development and developments in the design of products and parts and components of polymer processing equipment necessitate fresh efforts in organizing old and established thoughts, ideas, concepts, and practices and updating them in the light of the latest unfolding polymer. Polymer constitutes a diverse range of light- and energy-efficient materials discovered and developed in a large measure out of the sheer necessity of meeting the growing needs and demands of our higher-profile society. The present level of sophistication, growth, and advancements of our expanding society has been made possible in a large measure through continued imaginative and creative efforts of scientists, engineers, and technologists in the polymer field.

In recent years there is a considerable demand for specialty supplies, and there is an increasing affinity to design “intelligent polymers,” i.e., specialty polymers, which extend the scope of polymeric materials. Natural polymers have been used throughout the ages. From the beginning man has depended upon animal and vegetable matter for nutrition, shelter, warmth, and other requirements and desires. It is utilized in the field of pharmacology, diagnosis, and artificial respiration and in creation of articles of patient care. Commercially accessible synthetic polymeric materials are long lasting and have noble mechanical properties such as tensile strength and abrasion resistance, but because of the lack of functional groups in them, they resist dyeing and resist chemical reactions. The properties can be further improved by introducing various functional groups into their molecules. This ranges the scope of polymeric materials. Efforts have been made to use readily available natural polymers such as cellulose, proteins, gums and rubber, etc., for making polymers better properties. Copolymerization is an important method for the modification of polymers.

Copolymerization is defined as “a process in which two or more structurally different monomers are incorporated into the same polymeric chain.” The properties of polymer produced by copolymerization can be varied over a wide range by adjusting the monomer ratio. Copolymerization involves a chemical reaction between two or more different monomers, which results the formation of following different types of copolymers.

1. Random copolymer

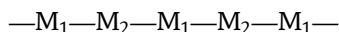
The distribution of the monomer units in the polymer chain does not follow any definite sequence:



This type of copolymer is produced in bulk, aqueous, suspension, or emulsion using free radical initiators of peroxide type or redox systems.

2. Alternate copolymer

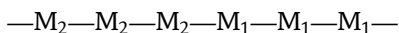
In these copolymers the monomers are arranged in an alternate sequence. These monomer units react with a high degree of order forming a polymer chain having a degree of alteration as



Special methods are used for manufacturing alternating copolymers. The reactivity of polar monomers can be enhanced by complexing them with metal halide or organo-aluminum halide. These complexed monomers participate in one electron transfer reaction with either an uncomplexed monomer or another electron donor monomer.

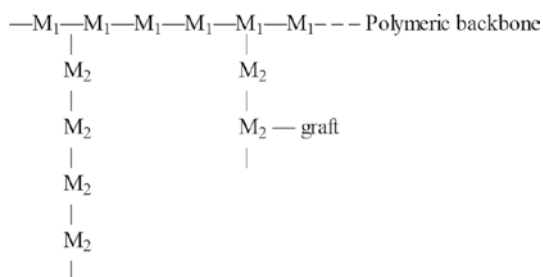
3. Block copolymer

These copolymers are built up of chemically different terminally connected segments. Block copolymers are generally prepared by sequential anionic addition or ring opening or step growth polymerization:



4. Graft copolymer

Graft copolymers are branched molecules where the main chain is made entirely of one repeat unit, while branch chains are made of yet additional repeat unit. The structure of such copolymer may be represented as



Schematic representation of graft copolymer

Grafting by most of the known methods includes the attachment of only a small number of side chains on the backbone polymer. During grafting there is little agitation, and, therefore, the bulk properties of polymer undergo little changes. The side chains disturb the uniformity of lattice, and the crystalline content of such polymer becomes smaller with an increasing degree of branching. However, the

most attractive method of modifying the nature of polymer is graft copolymerization.

Graft copolymers are generally prepared by free radical and anionic or cationic initiation process creating the active centers at polymer backbone. The mode of synthesis was first recommended by Flory [1] in 1937. The concept of graft copolymerization was first familiarized by Bandel and Alfrey [2]. Thus, graft copolymer is a macromolecule consisting of a block of constitutional units of backbone and blocks of unit grafts attached to the backbone.

Random and alternating copolymers, ready by polymerizing two kinds of monomers, possess better properties than constituent homopolymer; on the other hand, graft and block copolymers exhibit many properties that are characteristics of each constituent homopolymer. Conditions are usually so chosen as to retain the desirable properties and to eliminate the less desirable properties of the individual block or graft components. By grafting, some new properties allied with the side chains are added without drastically changing the basic properties of the substrate polymer.

The properties such as thermal stability and improvement in metal ion uptake, viscosity, ion exchange capacity, resistance to biodegradation, flocculation, etc. have been achieved on natural and synthetic polymers over graft copolymerization [1, 3–14]. These modified polymers called as graft copolymers have been found to be useful in oil recovery [15–17].

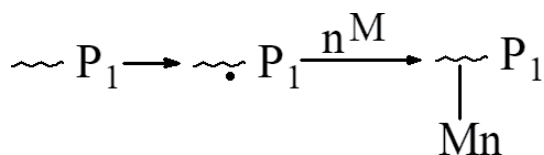
Graft copolymer of vinyl monomers bearing (+ve) charge or episulfide groups onto certain fibers has newly been reported to possess antibacterial activity. Synthetic MMA-grafted polysaccharides have been used as a hydrophilic matrix for controlled release forms [18].

5. Synthesis of graft copolymers

Most of the method of producing graft copolymers involves the use of radical polymerization although ionic graft copolymerizations are also possible. Graft copolymerization can be carried out either in homogeneous or heterogeneous systems depending whether the polymer being grafted and monomer is soluble or insoluble in the solvent being used. Usually grafting can occur by either the “grafting from” or “grafting onto” method as illustrated by the following:

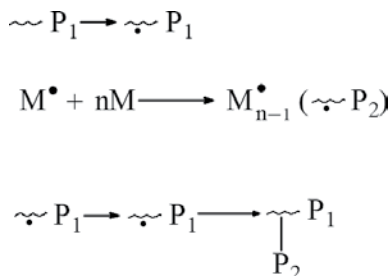
5.1 Grafting from

An active site generated along a polymer backbone starts to propagate monomer and thus produces branches.



5.2 Grafting onto

A growing polymer chain P_2 attacks another polymer P_1 .



The preparation of a graft (–ve) copolymer in most cases starts from a homopolymer (A) which is suitably activated, and then the growth of the graft of monomer (B) is initiated. The model must fulfill the following requirements:

1. The copolymer is of poly (A-g-B) type.
2. The probability that a graft will grow on a given unit of the backbone is not contingent on the number or size of the other grafts in the molecule or on the size of the backbone to which it is attached.

The efficiency of grafting is dependent upon several competing reactions:

- Competition between the various species present in the reaction mixture such as monomer, solvent, and backbone for the growing polymer radical, which means that there is competition between chain growth and various chain transfer steps.
- Competition for the initiator radical between monomer and backbone.
- Competition among the terminating process such as disproportionation after the polymer radical has formed.
- Competition among the terminating process in growing grafted species.

If the termination occurs through recombination of rising polymeric chains, it should lower the grafting efficiency. But even though the efficiency of this process is low, it has received considerable use because the reaction is easily carried out. The other reaction parameters, such as concentration of the initiator monomer, temperature, and the time of reaction, affect the grafting efficiency. The nature of the initiating radicals appears to bear a strong influence on the efficiency of grafting.

The graft copolymer is detached from the homopolymer by the solvent extraction method. Often graft copolymer prepared from water-soluble backbone polymers and water-soluble vinyl monomers is also water-soluble. In such cases graft copolymer is precipitated by using appropriate precipitating agent, and homopolymer is also separated. This method of parting has been successfully applied in many systems [19–27]. However, if it is not possible to separate the homopolymer from graft copolymer, such products are referred to as composites. Evidence for grafting in such case has been gotten from turbidimetric studies [27, 28].

5.3 Method of grafting

Combination and characterization of graft copolymers have received considerable interest in recent years due to its industrial importance. The chemistry of graft copolymerization essentially involves the generation of active site on the backbone polymer where appropriate monomer can be grafted. Different methods of activation include:

I. Physical activation

II. Chemical activation

III. Radiation activation

5.3.1 Physical activation

Physical activation contains the application of stress to polymeric backbone swelling it with suitable solvents [7, 29]. Application of stress to polymeric backbone causes segmental motions and molecular flow, which may lead to bond scission and consequent formation of free radicals. Freezing and thawing of the polymer-monomer mixture also make active sites. Free radicals may also be generated by mastication and milling of the backbone polymer. Production of a polymer with pendant basic moieties was performed by grafting dimethylamino-ethyl-methacrylate to linear low-density polyethylene (LDPE) in the melt in a batch-type internal mixer.

5.3.2 Chemical activation

This method of activation includes two different mechanisms:

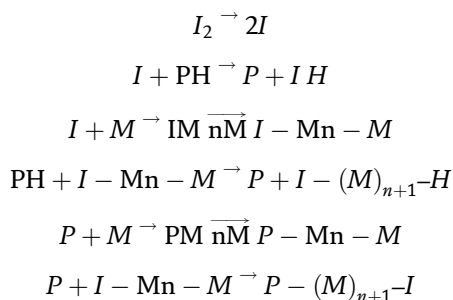
i. Free radical mechanism

ii. Ionic mechanism

5.3.2.1 Free radical mechanism

5.3.2.1.1 Radical initiators

In the existence of radical initiators such as benzoyl peroxide (BPO), azobisisobutyronitrile (AIBN), persulfates ($S_2O_8^{2-}$), etc., grafting of vinyl monomers onto polymeric backbones involves generation of free radical sites by hydrogen abstraction and chain transfer processes as described below:



where I_2 represents initiator molecules and PH and M are the polymeric backbone and monomer, respectively.

The extent of grafting is dependent on various reaction parameters, such as concentrations of initiator and monomer, reaction time, temperature, etc. The nature of initiator and monomer influences the reactivity of initiator and monomer toward grafting. Misra et al. have observed that during grafting of vinyl monomer onto starch, wool, or rubber, conservative free radical initiators show different reactivity toward grafting.

Although this process is not very efficient, it has received considerable importance because it is industrially important. The major drawback of this process is that it produces considerable amount of homopolymer. Therefore, various radical initiators are employed to graft different vinyl monomers on natural and synthetic polymeric backbones so as to minimize the production of homopolymer.

5.3.2.1.2 Redox systems

In redox systems the free radicals, which initiate polymerization, are generated as transient intermediates in the course of redox reaction. Essentially this involves an electron transfer process followed by scission to give free radicals. A wide variety of redox reactions, linking both organic and inorganic components, are used for this purpose. These reactions take place in aqueous media and occur rather rapidly even at relatively low temperatures. The general mechanism of grafting involves an abstraction of the hydrogen atom from the backbone of the polymeric material by the transient radical formed during the redox reaction, thus generating macro radicals onto which the monomer molecules are added to produce graft copolymer.

Author details

Arpit Sand^{1*} and Aparna Vyas²

1 Department of Chemistry, Manav Rachna University, Faridabad, India

2 Department of Mathematics, Manav Rachna University, Faridabad, India

*Address all correspondence to: sand.arpit@gmail.com

IntechOpen

© 2020 The Author(s). Licensee IntechOpen. This chapter is distributed under the terms of the Creative Commons Attribution License (<http://creativecommons.org/licenses/by/3.0>), which permits unrestricted use, distribution, and reproduction in any medium, provided the original work is properly cited. 

References

- [1] Flory PJ. The mechanism of vinyl polymerizations. *Journal of the American Chemical Society*. 1937;**59**:241
- [2] Alfrey, Bandel D. Presented at 118th American Chemical Society Meeting, Chicago, Sept. 4 (1950) through H. Mark Res. Chem. Progr. 1951;**12**(3):139
- [3] Hummel DO. Fluorinated polymers with functional groups. *Journal of Polymer Science, Polymer Symposia*. 1980;**67**:169
- [4] Sperling LH, editor. *Recent Advances in Polymer Blends, Graft and Blocks*. New York: Plenum Press; 1974
- [5] David NS. Graft copolymerization of lignocellulosic fibres. *ACS Symposium Series*. Vol. 187. 1982
- [6] Ranby B, Zuchowska D. Mechanical properties of multicomponent polymer preparation and characterization of interpenetrating network beads of poly(vinyl alcohol)-grafted-poly(acrylamide) with sodium alginate and their controlled release characteristics for cypermethrin pesticide. *Polymer Journal*. 1987; **19**(15):623
- [7] Sedlacek B, Overberger CG, Mark HF, editors. *Medical polymers chemical problems*. In: *Proceedings of 17th Prague IUPAC Microsymposium on Macromolecules*; Prague, Czechoslovakia; 1977. *Journal of Polymer Science: Polymer Symposia*. 1979;**66**
- [8] Sakamoto M, Hasuie H, Itoh M, Ishizuka Y, Yoshida K, Wtamoto H, et al. Modification of polymers by graft copolymerization. *Cellulosics: Chemical, Biochemical and Material Aspects*. 1993: 391-396
- [9] Iyer V, Varadaragan PV, Sawakhande KH, Nachave ND. Water-superabsorbent polymers through gamma radiation-induced graft-copolymerization of acrylonitrile on guar gum. *Journal of Applied Polymer Science*. 1990;**39**(11-12):2259
- [10] Miyata N, Sakata I. Experimental and theoretical considerations of electrolyte conductivity in glucose alkaline fuel cell. *Japanese Kokai Tokkyo Koho*. 1988;**6**(397):612
- [11] Takagi T, Nitta A, Ito H, Nagai K. Inhibitory effects of purified green tea epicatechins on contraction and proliferation of arterial smooth muscle cells. *Japanese Kokai Tokkyo Koho*. 1988;**1**:89, 252, 610
- [12] Saito T, Sesaki M, Mafande Y. Antifungal activity of polymer-based copper nanocomposite coatings. *Japanese Kokai Tokkyo Koho*. 1986;**61**: 86, 101, 506
- [13] Ghosh P, Biswas S, Datta C. *Concise polymeric materials encyclopedia*. *Journal of Materials Science*. 1989; **24**(1):205
- [14] Tripathi M, Karmakar NC, Singh RP. Modification of polymers by graft copolymerization. *International Journal of Polymeric Materials*. 2000;**46**(2):81-93
- [15] Yazdani-Pedram M, Retwart. Understanding biomaterial-tissue interface quality: Combined in vitro evaluation. *Soc. Symp. Proc. (Biomedical material-drug delivery, implants and tissue engineering)*. *Journal of Materials Research*. 1999;**550**: 29-34
- [16] Leansheng Z. *European Patent Application*. 1990;**356**:241
- [17] Meister JJ. U.S. 454, 889, 902. 1989
- [18] Zhang L-M, Tan Y-B, Li Z-M. *Heterogeneous emulsion graft*

- polymerization of glycidyl methacrylate on a wood matrix. *Applied Polymer Science*. 2001;**77**(1):195-201
- [19] Castellano I, Goni I, Ferrero MC, Munoz A, Manez-Castellanos R, Gurruchaga M, et al. Selective separation of some heavy metals by poly(vinyl alcohol)-grafted membranes. *The Indiana Pharmacist*. 1999;**25**(12): 1249-1257
- [20] Behari K, Pandey PK, Kumar R, Taunk K. Graft copolymerization of acrylamide onto xanthan gum. *Carbohydrate Polymers*. 2001;**46**(2): 185-189
- [21] Behari K, Kumar R. Graft copolymerization of methacrylamide onto guar gum using potassium chromate/malonic acid redox pair. *Polymeric Materials: Science and Engineering Division (American Chemical Society)*. 2001;**85**:361
- [22] Behari K, Taunk K. Graft copolymerization of acrylic acid onto Guar Gum. *Journal of Applied Polymer Science*. 2002;**84**(13):2380-2385
- [23] Behari K, Kumar R, Srivastava A. Studies on aqueous polymerization of 2 acrylamido 2 methyl 1 propane sulphonic acid initiated by peroxydiphosphate/Ag(I)—A kinetic study. *Polymer Preprints (ACS)*. 2003; **44**(1):882
- [24] Behari K, Kumar R. Polymerization of N,N'-methylenebis acrylamide by potassium peroxydiphosphate in presence of Mn II and Ag I. *Polymer Materials Science & Engineering*. 2003; **88**:459
- [25] Behari K, Pandey PK, Taunk K, Banerjee J. Synthesis and characterization of xanthan gum-g-N-vinyl formamide with a potassium monopersulfate/Ag(I) system. *Journal of Applied Polymer Science*. 2003;**89** (5):1341
- [26] Behari K, Kumar R. Synthesis of carboxymethyl cellulose g acrylamide using ferrous sulphate potassium bromate redox pair. *Polymer Preprints (ACS)*. 2003;**44**(1):1251
- [27] Kaur I, Misra BN, Barsala R, Singh K. The estimation of mechanical properties of polymers from molecular structure. *Journal of Applied Polymer Science*. 1993;**47**:1165
- [28] Kaur I, Misra BN, Chauhan S, Chauhan MS, Gupta A. Phenolphthalein-based cardo poly(arylene ether sulfone): Preparation and application to separation membranes. *Journal of Applied Polymer Science*. 1996;**59**:389
- [29] Kaur I, Maheshwari S, Gupta A, Misra BN. Viscometric and conductometric studies of poly(vinyl alcohol)-g-polyacrylamide composites. 1941

Rapid Evaluation of the Properties of Natural Rubber Latex and Its Products Using Near-Infrared Spectroscopy

Panmanas Sirisomboon and Chin Hock Lim

Abstract

The parameters including physico-chemical properties such as dry rubber content (DRC), total solids content (TSC), volatile fatty acid (VFA) number, alkalinity (ammonia content) and potassium hydroxide (KOH) number and physical properties such as viscosity and cross-link density are important to the trading and processing of natural rubber latex and its products. Traditionally these properties of field and concentrated latices and their products including thin and thick films are evaluated with chemicals and time-consuming methods and with the need of technical experts. The near-infrared (NIR) spectroscopy is a nondestructive, rapid, accurate and environment-friendly technique. It needs no chemical. This chapter describes the application of NIR spectroscopy on evaluation of the properties of natural rubber latex and its products.

Keywords: latex, thin and thick films, physico-chemical properties, near-infrared spectroscopy, ISO standards

1. Importance of physico-chemical properties of natural rubber latex and its products on trading and process control

Importance of physico-chemical properties of natural rubber latex and its products on trading and process control. The parameters include properties such as dry rubber content (DRC), total solids content (TSC), volatile fatty acid (VFA) number, alkalinity, potassium hydroxide (KOH) number, viscosity and cross-link density.

1.1 Historical background and introduction

The manufacturing of products directly from natural rubber latex takes place today in virtually every country of the world, and taken as a whole, the latex product industry is one of the most important non-tyre consumers of natural rubber.

Mankind has been making articles from natural latex for hundreds of years since Charles de la Condamine who made a journey across South America in 1736, reported the Amazonian Indians were producing shoes and bottles [1] from it. Nevertheless, a further 100 years had to pass before the beginnings of modern latex product industry can be discerned when in 1839 Charles Goodyear discovered

that the rubber samples after being baked in sulphur and white lead subsequently underwent little change through heat or cold [2]. This process was later coined as 'vulcanization' (from Vulcan the God of Fire) by Thomas Hancock.

The discovery of vulcanization was a milestone in the history of the rubber industry. As the demand for rubber increased and the supply of rubber from the wild *Hevea brasiliensis* trees of the Amazon Valley was unreliable, plantation rubber [2] began in Malaya in 1877, spreading to Southeast Asian countries and other tropical countries worldwide where millions of people's livelihoods depended on it.

Natural rubber latex is a stable colloidal dispersion of polymeric materials (latex particles) in an aqueous medium [3] containing no less than 60% by weight of polymer. Latex or rubber products, without vulcanization, suffer severely from poor physical properties, poor resistance to light and swelling in solvents and above all are susceptible to extremes of temperatures [4], becoming sticky in hot weather and hard when cold. The vulcanization process is brought about by the linking of macromolecules at their reactive sites. The cross-linking of rubber is also referred to as curing. During the progress of vulcanization [5], the modulus, hardness, elastic properties, resistance to swelling, etc. are considerably modified. In brief, vulcanization converts raw rubber molecules into a useful network by the formation of cross-links. The properties of vulcanized rubber are determined by the state of cure [6].

1.2 Types of natural latex concentrate

A range of natural latex concentrates is commercially available. The types of latex indicate the methods of concentration and the nature of the preservative systems. In all these latices, the polymer is the same, i.e. cis-1,4-polyisoprene; the differences lie in the quantity and the nature of the non-rubber substances present and the specific characteristics imparted by the preservatives.

The centrifuge-concentrated types of natural latex account for over 90% of total latex production, and of these the high ammonia (HA), low ammonia-TMTD/ZnO (LA-TZ) and medium ammonia (MA) types predominate. Centrifuged latices are used in virtually all latex processes, whereas other concentrates are used more selectively. Creamed latex, for example, is used almost exclusively for the production of extruded latex thread. Evaporated latex, which is characterized by a high solids content and by high stability, is used in processes where these properties are particularly desirable, e.g. in modifying bitumen or asphalt for road construction and as a binders or adhesives.

Latex particles are lighter than the serum in which they are suspended. There is a tendency to rise towards the surface (creaming). This movement is normally slow, and the rise of the rubber particles is covered by Stokes' law [2] as in the formula

$$V = \frac{2}{9} g \frac{(d - d_1)}{\eta} r^2$$

where V = rate of rise (mm/s)

g = acceleration due to gravity (cm/s/s)

d = density of serum (1.021 g/cc)

d_1 = density of rubber particle (0.91 g/cc)

r = radius of particle (av. 0.5 μm)

η = viscosity of medium (about 0.02 poises)

From Stokes' formula the rate of rise of a particle depends on the gravitational force, g . As g may be increased by some 2000–3000 times that of earth gravity using centrifuge, this method is used to concentrate the latex. If the rotating bowl is fed continuously with field latex, the concentrate (about 60% DRC) at the centre can

be withdrawn, while the dilute skim fraction is drained from the circumference. The ease and speed at which the field latex can be concentrated explains why the centrifugation is the preferred method commercially.

1.3 Properties of latex concentrates

It is appropriate to summarize here those properties of the major types of latex concentrate which may determine their use for any particular produce in **Table 1**.

1.3.1 HA-centrifuged latex

This is the most widely used form of concentrate and has the great advantage that the only preservative (ammonia) it contains is volatile. Consequently it may be used confidently in food applications and for medical or surgical goods. The disadvantages of HA latex are the strong odour of ammonia and the need for deammoniation in certain processes.

HA latex is the starting material for a wide range of products. It is used extensively for the manufacture of dipped products (e.g. examination gloves, household gloves, surgical gloves, industrial gloves, balloons, condoms, catheters) and in latex thread, latex foam, binder, adhesive and other miscellaneous applications. The level of ammonia is 0.6% minimum as specified in ISO 2004:2017 Natural rubber latex concentrate-centrifuged or creamed ammonia-preserved type specifications [8].

1.3.2 LA-TZ and MA-centrifuged latices

The LA-TZ latex is the most common of the LA types where tetramethylthiuram disulphide (TMTD) and zinc oxide (ZnO) are used as secondary preservatives. It is preserved with a blend of tetramethylthiuram disulphide and zinc oxide at ratio of 1:1. For MA, the amounts of preservatives (TMTD and ZnO) used are intermediate between HA and LA-TZ.

Unlike HA latex, low ammonia (LA-TZ) latex contains ammonia not more than 0.29% (by mass); MA has ammonia between 0.30 and 0.59% (by mass) and has less objectionable odour. The disadvantage is that the presence of TMTD in LA and MA latices may result in the occurrence of nitrosamines and nitrosatable substances that are carcinogenic. As such manufacturers of baby teats, balloons and those products that are in contact with food avoid using LA-TZ or MA latices.

Type of latex concentrates	Preservatives
Centrifuged concentrate, min. 60% DRC	
High ammonia (HA)	0.7% ammonia 0.025% ammonium laurate
Low ammonia – tetramethylthiuram disulphide/zinc oxide (LA-TZ)	0.2% ammonia + 0.013% TMTD + 0.013% ZnO + 0.05% ammonium laurate
Medium ammonia – tetramethylthiuram disulphide/zinc oxide (MA)	0.5% ammonia + 0.006% TMTD + 0.006% ZnO + 0.04% ammonium laurate

All chemical additions are based on weight/weight of whole latex.

Table 1.
Types of natural rubber latex concentrates [7].

1.4 Physico-chemical properties

1.4.1 Specified properties

Natural rubber latex concentrates are very highly specified materials, and a large measure of international agreement has been achieved regarding the limits to be imposed on their basic properties (**Table 2**). This international agreement is exemplified by the specifications published by the International Standards Organization (ISO) [7].

The natural rubber latex properties that are of chief significance to the users are total solids content, dry rubber content, non-rubber solids (NRS), alkalinity, volatile fatty acid number, mechanical stability time (MST), potassium hydroxide number (KOH no.) and magnesium content. The methods of measuring these properties have been established for many years in the ISO standards and are usually considered adequate.

1.4.2 Testing of latex

A brief description of each of the test procedure is given below. These details are not sufficient for practical use—the appropriate standards must be consulted.

The TSC is the weight percentage of all the solids (rubber plus non-rubber solids) present in the latex (ISO 124) [9]. It is determined by drying in a hot air oven at $70 \pm 5^\circ\text{C}$ for 16 h or $105 \pm 5^\circ\text{C}$ for 2 h a known weight of latex and weighing the dried rubber film thus produced. This is essentially a simple test to perform, and the reproducibility of the test between laboratories is normally very good. This is an important parameter as both VFA and KOH numbers are based on a quantity of latex containing 100 g of total solids (TS).

The DRC is the weight percentage of rubber hydrocarbon present in the latex. It is determined by coagulating a known weight of latex with dilute acetic acid, washing and sheeting the coagulum and then drying at 70°C for 16 h as in ISO 126 [10]. This test is time consuming, and it usually shows a high degree of reproducibility

Characteristic	Limits			Method of test
	Type HA	Type LA	Type MA	
TSC, min., % (by mass)	61	61	61	ISO 124
DRC, min., % (by mass)	60	60	60	ISO 126
Non-rubber solids, max., % (by mass)	1.7	1.7	1.7	TSC-DRC
Alkalinity (as NH_3), % (by mass)	0.60 min	0.29 max	0.30–0.59	ISO 125
MST, min, s	650	650	650	ISO 35
Coagulum content, max., % (by mass)	0.02	0.02	0.02	ISO 706
Cu content max., ppm of total solids	8	8	8	ISO 8053
Mn content max., ppm of total solids	8	8	8	ISO 7780
Sludge content, max., % (by mass)	0.06	0.06	0.06	ISO 2005
VFA no. max	0.06	0.06	0.06	ISO 506
KOH no. max	0.7	0.7	0.7	ISO 127

Table 2.
ISO specifications for centrifuged natural rubber latex [8].

between laboratories. This parameter is of extreme importance for commercial purpose as the prices depended on the dry rubber content.

The difference between the TSC and DRC values represents the weight percentage of NRS which comprises most of the non-rubber solids materials like proteins, fatty acid soaps and salts, together with a variety of other materials present in low concentrations. Hence, NRS is an indication of the cleanliness of the latex.

The VFA no. of a latex is the number of grammes of potassium hydroxide equivalent to the steam distillable fatty acids present in a quantity latex containing 100 g of total solids.

Fifty grammes of latex is coagulated with ammonium sulphate and the coagulum is removed. Twenty-five millilitre of serum is taken and acidified with sulphuric acid, and a 10 ml sample is steam distilled. The distillate is aerated with carbon dioxide-free air and titrated against barium hydroxide, phenolphthalein as indicator.

It has been found that majority of the volatile acid measures in the VFA test (ISO 506) [11] is acetic acid which is a by-product of bacterial activity in the latex. As such VFA no. is the primary measure of the state of preservation of the latex.

The alkalinity of the latex is the weight percentage of alkali present, determined by volumetric titration with a standard solution of dilute hydrochloric acid (ISO 125) [12]. As most natural latices are preserved with ammonia, the alkalinity is expressed as the percentage of ammonia present.

Five to ten grammes of latex is weighed out to within 10 mg and diluted with about 200 ml of water to which a stabilizer solution has been added. This solution is titrated against 0.1 M hydrochloric acid with continual stirring, either electrometrically taking $\text{pH } 6 \pm 0.05$ as the endpoint or using methyl red indicator.

The ammonia added to the natural latices acts as a preservative, i.e. as a bactericide, to prevent the bacterial activity that would otherwise cause putrefaction.

The actual level of ammonia present in the latex is of significance in a number of latex processes where the control of pH is necessary.

The KOH no. is defined as the number of grammes of potassium hydroxide equivalent to all the acid radicals combined with ammonia in a quantity of latex containing 100 g of total solids. It is measured by potentiometric titration of the latex with potassium hydroxide solution and determining the inflection point in the titration curve (ISO 127) [13]. For a well-preserved latex, the KOH no. can be used as an indication of the age of the latex.

The viscosity, in centipoises (cps), of a latex sample is determined by Brookfield viscometer which measures the torque on a specific spindle at a constant rotational frequency and at a controlled rate of shear while immersed to a specified depth in the latex (ISO 1652) [14]. The latex test sample is diluted to 60% TSC and the viscometer set at 60 rpm using spindle no. 1.

Zinc-oxide viscosity tests may be useful in providing a qualitative indication of the chemical stability of the latex but not for quantitative measure. The principle of zinc-oxide viscosity tests is to determine the change in viscosity when the latex is compounded with zinc oxide under specific conditions. The smaller is the viscosity change, the more chemically stable is the latex deemed to be [3].

1.5 Maturation and vulcanization

In most latex processes, the compounded latices are either partially or completely matured and stored before use. Most compounded latices contain accelerators (dithiocarbamates) which can cause a measure of the rubber cross-linking during maturation. The extent of cross-linking depends largely on the nature and amount of curatives as well as on storage conditions. The prevulcanized latex production may be considered as a special form of maturation. Both processes require a

means of measuring the extent of latex vulcanization because of the influence it has on processing behaviour of latex product properties [15].

Toluene swell is universally used by rubber factories to measure the degree of cross-link of compound at different stages of production. The benefits of the toluene swelling tests are that the results are directly related to the cross-link density and are also quite reproducible. Its weak points are that it is relative slow procedure since reliable measurements can only be made at equilibrium. The time taken to reach equilibrium is largely dependent on the latex film thickness used. The total time for the test, including the film drying, is approximately 1 h or more [15]. The procedure requires a skilled technician and is time consuming.

2. Application of near-infrared (NIR) spectroscopy on evaluation of the properties of natural rubber latex and its products

2.1 NIR spectroscopy for quantitative analysis

NIR spectroscopy measures the interactions between the electromagnetic radiation in the NIR region and the materials, and the fundamental absorptions occurring in the infrared region extend down to lower wavelengths as overtones and combination vibrations [16]. The NIR region is located between the red band of the visible light and the mid-IR region as wavelength from 780 to 2500 nm ($12821\text{--}4000\text{ cm}^{-1}$). The NIR spectroscopy is a rapid quantifying method with repeatability, reproducibility and accuracy equivalent to most reference methods and not prone to subjective operator errors. The NIR spectroscopy offers many benefits to research laboratory and quality control department in the factory. The method is environmentally friendly as no chemical is used. The instruments are simple to install and operate with little or no sample preparation and have the ability of evaluating many constituents at a time. According to Sirisomboon et al. [16], the instruments can be networked to use the same calibration, with their performance controlled from a single control centre.

Due to broad absorption peak and overlapping peak in NIR spectrum, NIR spectroscopy needs calibration modelling which relates to the absorbance vector, i.e. the inverse logarithm of the transmittance or the apparent absorbance vector which is the inverse logarithm of the diffuse reflectance (variable X) to the constituent vector (variable Y). The absorbance vector is obtained from NIR spectrometer, i.e. the spectra of calibration set samples. For example, the spectra of samples are scanned between 800 and 2500 nm ($12500\text{--}4000\text{ cm}^{-1}$) by Fourier transform NIR (FT-NIR) spectrometer. The constituent vector is obtained from the reference measurement of the interested parameter for calibration set samples, such as the dry rubber content (DRC), TSC, viscosity and so on. The widely used calibration method is based on variable reduction where the principle is compressing the information in the whole spectrum into small number of variables. The most popular method is partial least squares regression and its diversified algorithms. In general, before the modelling, the spectral pretreatment is performed for noise suppressing, multiplicative scatter correction, baseline correction and spectral normalization. The pretreatment spectra may provide better model performance than that of raw spectra. After the model is developed, it has to be validated by either internal or external validation. The internal validation is used for the model that developed from a small number of samples (normally <100 samples), and the samples for calibration set and validation set are same. It can be by full cross-validation or segmented cross-validation. The external validation is used for more number of samples where the total samples are divided into calibration set and validation set. The prediction performance of the model is indicated by

the coefficient of determination (r^2), standard error of prediction (SEP), root mean square error of prediction (RMSEP), bias, ratio of prediction to deviation (RPD) and ratio of performance to interquartile (RPIQ). The r^2 is from 0 to 1. The higher r^2 indicates that the absorbance variable (variable X) can explain more the constituent variable (variable Y). The SEP is calculated from standard deviation (SD) of error in validation set. It indicates the precision of the model. The lower the SEP, the higher the model precision will be. The RMSEP is the error of validation set (without sign), while the bias is the error with plus or minus sign. The RMSEP and bias indicate the accuracy of the model. The RPD and RPIQ are the indicators for the model robustness. The model is acceptable if their value is more than 3. The RPD is used when the reference data are normal distribution, and RPIQ is used when the data are skewed distribution. The RPD is calculated from the ratio of standard deviation of reference value of prediction set to the standard error of prediction. For RPIQ, the SD of the prediction set in the RPD formula was replaced by the interquartile (Q_3-Q_1) where Q_3 and Q_1 were the value below which 75 and 25%, respectively, of the samples were found [17].

2.2 Near-infrared scanning of natural rubber latex and film

The scanning of rubber latex can be done in transmission, diffuse reflection and interaction modes. **Figure 1** shows the spectral measurement of latex in transmission mode using quartz cuvette with the size of 1×0.5 cm by UV-VIS-NIR spectrometer [AVA-Spec-2048-USB2, Avantes, Netherlands] at the wavelength range of 350–1100 nm with the 2.4-nm resolution. **Figure 2** shows the latex scanning using Fourier transform NIR spectrometer (NIRFlex solid, Buchi, Switzerland) in diffuse reflection mode over the wavenumber range of 4000–10000 cm^{-1} at 4-cm^{-1} resolution. The latex sample is placed in a Petri dish (25-mm depth and 150-mm diameter) at 3/4 of the dish depth. **Figure 3** shows a 200 mL latex sample in a glass beaker (250 mL) scanned by a portable NIR spectrometer (FQA-NIR GUN, Shizuoka, Japan) over the wavelength range of 700–1050 nm with a resolution of 2 nm and an integrating time of 15 ms. **Figure 4** shows the spectral scanning of latex in interaction mode using optic fibre probe dipped in a latex cup by UV-VIS-NIR spectrometer [AVA-Spec-2048-USB2, Avantes, Netherlands] at the wavelength range of 350–1100 nm with the 2.4-nm resolution.

According to Lim and Sirisomboon [18], for the scanning experiment of thin and thick films, the aluminium plates ($90 \times 220 \times 0.5$ mm) were dipped into the latex and dried. In the case of the thick film, the plate was dipped into 5% calcium chloride solution and dried prior to dipping into the latex compound. For thin film, it was a straight dipped, i.e. without the use of coagulant. Both thin and thick films were dried in an oven at 70°C for 5 min and 1 h, respectively. They were then subjected to NIR radiation using the FT-NIR spectrometer by placing on the integrating sphere window (2.3 cm in diameter).

The spectra could not be directly referred to the physico-chemical properties. It needs chemometric to analyse for the correlation.

2.3 NIR spectroscopy for chemical properties of natural rubber latex

2.3.1 Dry rubber content and total solids content

Cornish et al. [19] established an NIR spectroscopic method for the quick quantification of latex in both wet and dried *Parthenium argentatum* (guayule) homogenate and purified latex samples. The coefficients of determination (r^2) of the measured rubber content and the predicted rubber content by NIR for the dry and wet samples were 0.92 and 0.83, respectively.

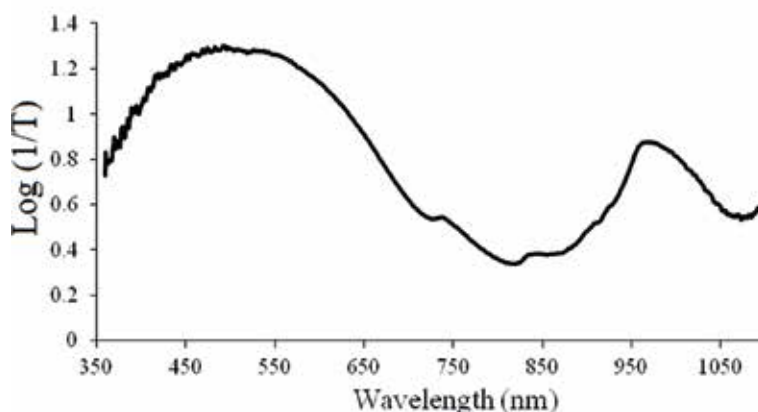


Figure 1.
Scanning of rubber latex in transmission mode and latex spectrum.

FT-NIR spectrometer in long wavelength between 1000 and 2500 nm ($10000\text{--}4000\text{ cm}^{-1}$) in diffuse reflection mode was applied to evaluate the DRC of field latex and concentrated latex from Para rubber and provided excellent prediction performance [16]. The result showed that the best model was established using the partial least squares regression (PLSR) from the spectra and corresponding DRC evaluated by reference method, which were the second derivative pretreated spectra, where the values of 0.997, 0.3398 and -0.0239% were the r^2 , SEP and bias, respectively. The ratio of SD to SEP of the reference data in the prediction sample set (RPD) and the ratio of the range to the SEP of the prediction set (RER) were 18.18 and 74.4, respectively. The model was validated using unknown samples, and the prediction performance was good with an r^2 , SEP and a bias of 0.999, 0.3898 and -0.0008% , respectively. Therefore, the NIR spectroscopy technique can be used as an accurate and quick method for estimating the DRC of both field and concentrated latices of Para rubber.

The shortwave NIR (700–1100 nm) spectroscopy was also used for the evaluation of DRC and TSC in Para rubber field and concentrated latices [20]. The transmittance spectra were obtained. There were 282 samples including 171 samples of field latex, 86 samples of concentrated latex and 25 of concentration-adjusted concentrated

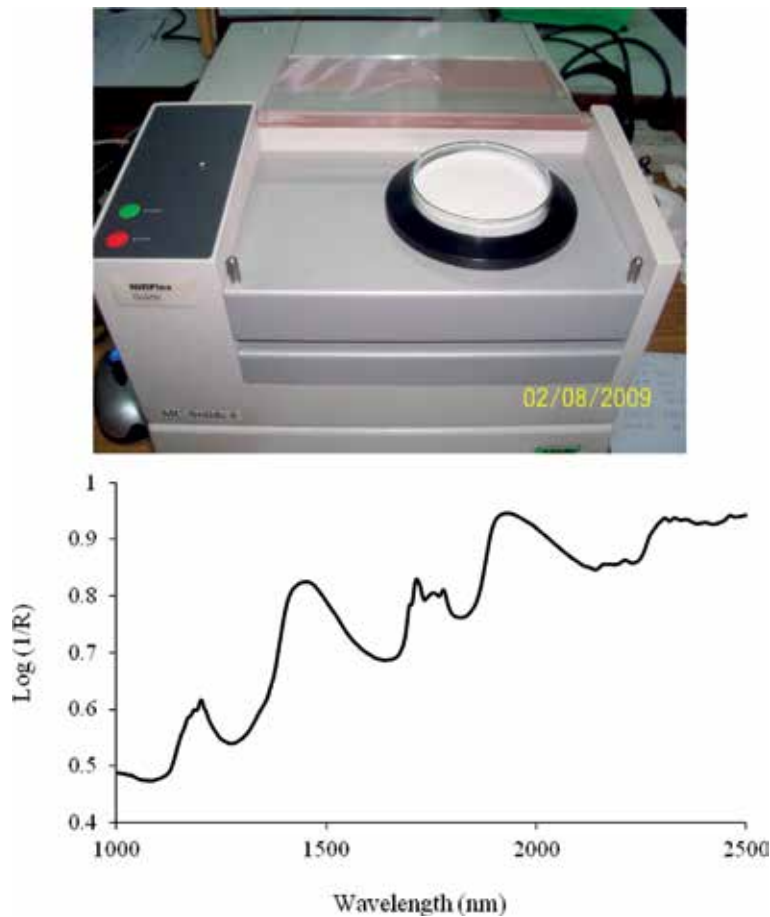


Figure 2.
Scanning of rubber latex in diffuse reflection mode and latex spectrum.

latex. The field latex and the concentrated latex had around 30 and 60% DRC, respectively. The concentration-adjusted concentrated latex was 55, 50, 45, 40 and 35% DRC. The PLSR calibration models were developed using original and pretreated absorbance spectra. The model developed from smoothing and range normalization pretreated spectra in the wavelength range of 700–950 nm provided the best prediction accuracy for DRC, and the models using raw spectra in the same wavelength range gave the best results for TSC. The slope, offset, r^2 , SEP and bias were 1.0154, -0.6286 , 0.992, 1.1092 and 0.0321%, respectively, for the DRC prediction and 1.0084, -0.2332 , 0.991, 1.3611 and 0.1456%, respectively, for the TSC prediction. The best models were validated using new unknown sample sets of 50 and 35 samples for DRC and TSC, respectively. The models provided an r^2 , SEP, RPD and bias of 0.988 and 0.974, of 1.4296 and 2.1255, of 10.0 and 6.2 and of -0.6191 and 0.5476% for DRC and TSC, respectively. This work showed that the SW-NIR spectroscopy protocol in the evaluation of TSC had high accuracy for quality assurance and process control in the concentrated rubber latex factory. However, for prediction of DRC, the accuracy was still not acceptable for the latex factory because a bias of more than 0.01% can incur considerable profits or losses when large volumes of latex are involved.

Lim and Sirisomboon [21, 22] updated the above DRC and TSC models. The updated DRC model was done by adding the 180 samples merged into the 280 original samples. The slope, offset, r , SEP and bias were 1.0126, -0.3729 , 0.9931, 1.2654 and 0.1103%, respectively. The updated TSC model was done by adding the

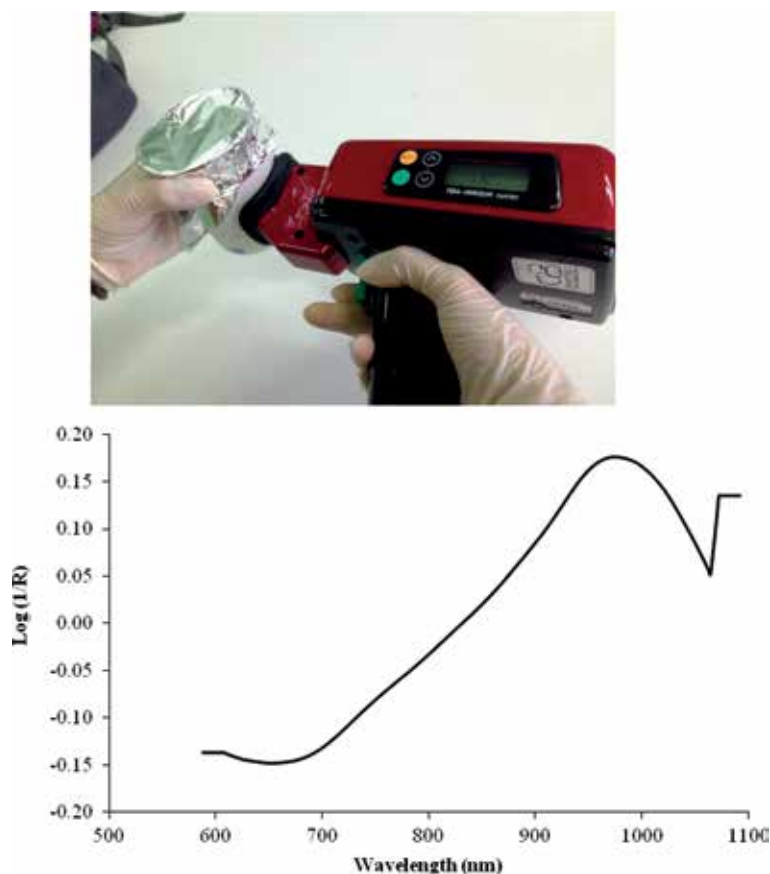


Figure 3. Scanning of rubber latex in diffuse reflection mode using FQA-NIR GUN spectrometer and latex spectrum (Thanking Dr. Ronnarit Rittiron, Kasetsart University, Thailand, for the the photos).

160 samples merged into the 280 original samples. The slope, offset, r , SEP and bias were 0.9795, 0.7150, 0.9834, 1.6186 and -0.0802% , respectively. Therefore, the more accurate, robust and faster updated model by NIRS technique was obtained for TSC of Para rubber latex, for both field latex and concentrated latex.

By the research conducted by Inagaki et al. [23], the ultraviolet-near-infrared (UV-NIR, 370–1085 nm) spectra of latex were measured in transmittance mode. Calibrations for TSC and DRC were developed using spectral data set of 57 samples with aid of PLSR. The latex UV-NIR spectra provided good regression models with r^2 for cross-validation of 0.96 and 0.97, for TSC and DRC, respectively. The PLS factors were 2 and 1, respectively. This study suggests UV-NIR spectroscopy with high-accuracy in-line quality control of latex. Inagaki et al. [23] also investigated the short-wavelength NIR spectra of bark which were scanned to check the feasibility of on-site evaluation of latex quality by measuring the NIR spectra of standing tree. This result suggested that the focal point should be on the outer part of bark to get the signal of latex when we measured the spectra of standing tree.

Three-fibre-based diffuse reflectance spectroscopy (TFDRS) was employed by Inagaki et al. [24] for the measurement of TSC in natural rubber latex samples. It was reported that TSC could be accurately predicted using the relative absorbance ratio even if the samples have significant variation in polyisoprene particle sizes (i.e. significant variation of reduced scattering coefficient). This group of researchers designed a user-friendly and inexpensive TFDRS system using a halogen light

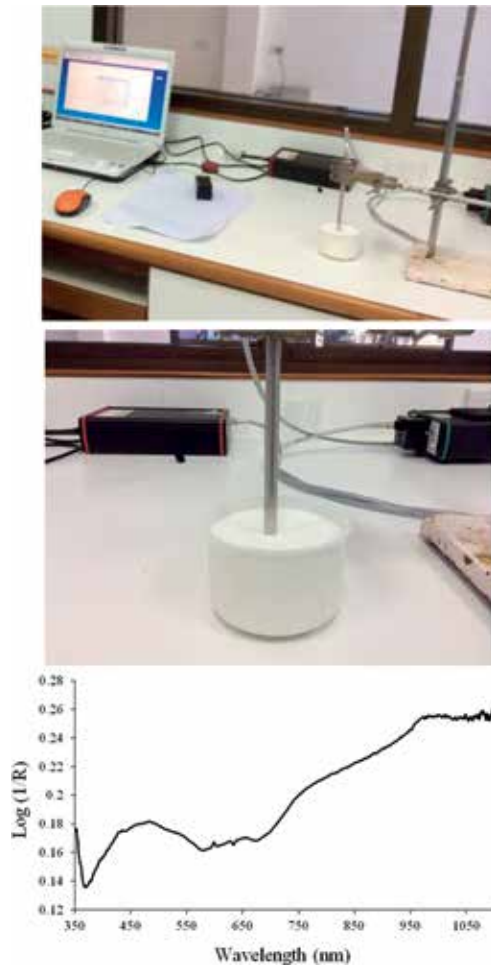


Figure 4.
Scanning of rubber latex in interaction mode and latex spectrum.

source and two spectrometers. Although compared to the Ti:Sapphire tunable laser system, the wavelength resolution was much lower. A strong relationship with r^2 of 0.97 was found between the relative absorbance ratio (970, 909, 849 nm) and TSC.

2.3.2 Volatile fatty acid number

Narongwongwattana et al. [25] reported that most factories analysed VFA number by the method in ISO 506:1992(E). However, the procedure was complicated, time and chemical consuming and also skilled technician required. Therefore, they applied NIR spectroscopy which is a quick, accurate and environment-friendly method to determine the VFA number in field and concentrated latex based on quantification and discriminant models. The standard normal variate (SNV) spectra provided the best calibration equation which was obtained from the region of $6109.7\text{--}5770.3$, $4613.1\text{--}4242.9\text{ cm}^{-1}$ with correlation coefficient (r) of 0.832, standard error of cross-validation (SECV) of 0.036 and no bias. It was shown statistically that SECV and bias were low enough for practical use, and the predicted value was not different significantly from actual value at 95% confidence level. Moreover, discriminant model was established to separate good-quality latex from the deteriorated latex using VFA number at 0.06 as standard as in ISO 2004:2017(E). The model could

screen the latex with overall accuracy of 91.86% in validation set. Moryadee et al. [26] also used the FT-NIR spectrometer in diffuse reflectance mode in the wavenumber of 12500–3600 cm^{-1} for evaluation of VFA number. There were totally 168 samples including 117 field latex samples and 51 concentrated latex samples. The calibration models were developed by PLSR using original and pretreated absorbance spectra. By statistical analysis, the vector normalization (SNV) pretreated spectra provided the model in the wavenumber of 7506.0–4597.7 cm^{-1} and with the PLS factors of 10 provided the r^2 , RMSEP, RPD and bias of 0.6044, 0.107, 1.650 and 0.029, respectively.

2.3.3 Alkalinity and potassium hydroxide number

Narongwongwattana et al. [27] reported that all factories monitor NH_3 content or alkalinity during processing and storage as it is an important parameter. Ammonia is a preservative for latex. Alkalinity is determined as a percentage (by mass) of ammonia by the standard analytical method, acid-based titration, as detailed in ISO 125:2011(E) Natural Rubber Latex Concentrate-Determination of Alkalinity. This method requires a skilled analyst and also the use of chemicals. The alkalinity predicting calibration equations were developed where the relationship between the latex absorbance spectra measured using a portable NIR and a Fourier transform NIR spectrometer and the alkalinity content of the latex was established. The best equation obtained using the portable and the FT-NIR spectrometers could be applied to evaluate the latex alkalinity with r^2 , SEP and RPD of 0.63, 0.101% and 1.62 and 0.97, 0.027% and 6.07, respectively. From the statistic testing as recommended in ISO12099:2010, the NIR-predicted values were no different from actual values at the 95% confidence level. The best equation from the more reliable calibration obtained using the FT-NIR spectrometer was attributed to the longer wavelength range.

Sompiw [28] collected the samples of Para rubber-concentrated latex which were from the factory of the Thai Rubber Latex Corporation (Thailand) Public Company Limited in the Nong Yai District, Chonburi Province, Thailand. There were 220 concentrated latex samples. The experiment was conducted at $25 \pm 2^\circ\text{C}$ room temperature. A latex sample without bubbles was scanned in glass cuvette with the size of $1 \times 0.5 \text{ cm}$ (**Figure 1**) over the wavelength range of 359–1100 nm by a spectrometer in transmission mode. The Teflon with the thickness of 1 cm was used for scanning as the reference material. The samples were separated into calibration set and prediction set with the ratio of 3:1. The calibration model development was done using raw spectra by PLSR. The model developed provided the r^2 , RMSEP, SEP, RPD and bias of 0.880, 0.070, 0.70, 2.980 and -0.00017 for alkalinity and of 0.422, 0.086, 0.086, 1.334 and -0.001 for KOH number, respectively. In addition, latex sample without bubbles was scanned in a glass Petri dish with the height of 1.5 cm and diameter of 9.5 cm over the wavenumber of 12500–3600 cm^{-1} by a FT-NIR spectrometer in a diffuse reflectance mode. The gold plate was used for scanning as the reference material. The samples were separated into calibration set and prediction set with the ratio of 1:1. The calibration model development was done by PLSR. The model developed provided the r^2 , RMSEP, RPD and bias of 0.978, 0.030, 6.570 and 0.002 for alkalinity and of 0.862, 0.045, 2.71 and -0.005 for KOH number, respectively.

2.4 Near-infrared spectroscopy for physical properties of natural rubber latex and film

2.4.1 Viscosity

The FT-NIR spectroscopy in diffuse reflection mode was used to evaluate the apparent viscosity of Para rubber field latex and concentrated latex over the

wavelength range of 1100–2500 nm, using PLSR [29]. The sample in a Petri dish was scanned (**Figure 2**). The model with 10 PLS factors developed using the raw spectra accurately predicted the apparent viscosity with r , SEP and bias of 0.974, 8.6 and -0.4 cP, respectively. The RPD and RER of the predictive model were 4.4 and 16.7, respectively. Therefore, the model can be used for measurement of the apparent viscosity of field and concentrated latex in the factory for quality assurance and process control.

2.4.2 Cross-link density

The analysis of the cross-link density of prevulcanized natural rubber latex using near-infrared spectroscopy was conducted [30] using a FT-NIR spectrometer in diffuse reflection mode over the wavenumber range of 12500–3600 cm^{-1} . As the cross-link density is an indication of the cure degree, hence the properties of the latex products, the proposed method is useful for industrial purposes. For prevulcanized latex of 50% total solids content (i.e. PV50%) samples at 100% extension (prevulcanizate-relaxed modulus 100%), the best model was developed using the PLSR from the first derivative pretreated spectra, where the r^2 , RMSEP and bias were 0.66, 6.06×10^4 and $1.63 \times 10^4 \text{ Nm}^{-2}$, respectively. The RPD was 1.8. This model could be used for screening. For samples at 300% extension (prevulcanizate-relaxed modulus 300%) for PV 50%, the best model was developed using spectra pretreated for scattering correction: r^2 , RMSEP and bias were 0.88, $6.74 \times 10^4 \text{ Nm}^{-2}$ and $1.35 \times 10^4 \text{ Nm}^{-2}$, respectively, and the RPD was 3.0. Hence, the near-infrared spectroscopy technique can be utilized as a rapid screening method for estimating the cross-link densities of prevulcanized natural rubber latex.

In addition, Lim and Sirisomboon [18] indicated that the toluene swell or equilibrium swelling is universally used by rubber factories to measure the degree of cross-link of their compounded or prevulcanized latices at different stages of production. They applied NIR spectroscopy for rapid and accurate quality control, spectral acquisition of prevulcanized latex and thin and thick films performed using a FT-NIR spectrometer in diffuse reflection mode across the wavenumber range of 12500–3600 cm^{-1} . For prevulcanized latex an effective model was developed using partial least squares regression with preprocessing (first derivative and straight line subtraction method). The r^2 , RMSECV and bias of the validation set were 0.71, 3.93 and -0.005% , respectively. For the thin-film model, the r^2 , RMSECV and bias were 0.65, 4.01 and -0.028% , respectively, whereas for the thick-film model, the r^2 , RMSECV and bias were 0.70, 4.00 and -0.006% , respectively. Three models including prevulcanized latex and thin and thick films were validated by 23 unknown samples, providing SEP and bias of 5.357 and 2.494, 4.565 and 1.001 and 3.641 and -0.961% , for prevulcanized latex and thin and thick films, respectively. It was shown that the thick-film spectra model gave the best results.

3. Pros and cons of methods used

A NIR spectrometer is a computerized super-microscope. It sees past the surface of the material being scanned, through the cells or matrix of which the material is composed, and into the actual molecules of which the materials are made [31].

The advantages of NIR spectroscopy for rubber latex technology are summarized as follows:

The processing of field latices to concentrates, compounding and control on production lines are hampered by the relatively cumbersome latex quantification methods of the ISO currently employed. Current methods, as specified in ISO 2004 on latex specifications [8], require several hours before analytical results can be obtained [19]. NIR spectroscopy once calibrated enables properties to be obtained in minutes with repeatability and reproducibility equivalent to most reference methods and not prone to subjective operator errors [18].

It is environmentally clean (no chemical is used) and flexible as many constituents can be tested simultaneously. Little or no sample preparation is required. They are stand-alone instruments and are easy and cheap to install. In addition, the measured cost per sample is cheap, and the samples to be tested can be many or every sample because the NIR spectroscopy is a nondestructive test.

There are also some disadvantages associated with NIRS technology. These include:

Separate calibrations are needed for every commodity and constituent, and the user has to monitor their performances. There is a need to monitor the accuracy and reproducibility including the reference analysis. The instruments are expensive to purchase. The lack of knowledge as to how to operate the instrument efficiently can affect the accuracy of their determinations.

4. Conclusions

From the review of NIR spectroscopy and its application on natural rubber latices (field latex and concentrated latex) and its products, i.e. thin and thick films, it is indicated that the technology is suitable for using in the quality, process control and assurance of the products in the factories.

NIR spectroscopy is rapid and reasonably accurate for determination of the various physico-chemical parameters of natural rubber field latex and concentrated latex and its latex products without chemicals. The developed calibration equation obtained from the NIR spectrometer is usable in most applications including quality assurance for coefficient of determination between 0.92 and 0.96 and excellent to use in any application for $r^2 > 0.98$ [31].

The latex products are prevulcanized latex and latex films. The thin and thick films are used to simulate the manufacture of condoms and gloves which are the two main dipped products made from natural rubber latex. The coefficient of determination of 0.66–0.81 means that this NIR spectroscopy method is usable for screening purpose and approximate calibration [31].

The rapidity of testing (<5 min/sample) by NIR would allow a factory to increase the frequency of monitoring the process resulting in improvement of the quality of the products being manufactured.

Consistency of properties of the latex became an important issue for the latex users. As such testing methods had to be devised in order to determine the property and quality of the latex raw material.

As consumers become more demanding, the importance grows of guaranteeing the quality of products. The employment of reliable testing techniques that assure the origin and characteristics of the inputs used by industry is a key factor in this respect.

Author details

Panmanas Sirisomboon^{1*} and Chin Hock Lim²

1 Department of Agricultural Engineering, Faculty of Engineering, King Mongkut's Institute of Technology Ladkrabang, Bangkok, Thailand

2 Thai Rubber Latex Corporation (Thailand) Public Company Limited, Chonburi, Thailand

*Address all correspondence to: panmanas.si@kmitl.ac.th

IntechOpen

© 2019 The Author(s). Licensee IntechOpen. This chapter is distributed under the terms of the Creative Commons Attribution License (<http://creativecommons.org/licenses/by/3.0>), which permits unrestricted use, distribution, and reproduction in any medium, provided the original work is properly cited. 

References

- [1] Gorton T. Latex product manufacturing technology. In: Bhowmick AK, Hall MM, Benarey HA, editors. *Rubber Products Manufacturing Technology*. New York, USA: Marcel Dekker Inc; 1994. pp. 823-844
- [2] Stern HJ. *Rubber: Natural and Synthetic*. 2nd ed. London: Maclaren & Sons Ltd; 1967. p. 519
- [3] Blackley DC. *Polymer Latices, Science and Technology*. Vol. 1: *Fundamental Principles*. 2nd ed. London: Chapman & Hall; 1997. p. 559
- [4] To BH. Sulphur cure systems. In: Dick JS, editor. *Rubber Technology Compounding and Testing for Performance*. Munich: Hanser Publishers; 2001. pp. 380-394
- [5] Hofmann W. *Vulcanization and Vulcanizing Agents*. London: Maclaren and Sons Ltd; 1967. p. 371
- [6] Bhowmick AK, Mangaraj D. *Vulcanization and curing techniques*. In: Bhowmick AK, Hall MM, Benarey HA, editors. *Rubber Products Manufacturing Technology*. New York, USA: Marcel Dekker Inc; 1994. pp. 315-396
- [7] Gazeley KF, Gorton ADT, Pendle TD. Latex concentrates: Properties and composition. In: Roberts AD, editor. *Natural Rubber Science and Technology*. Oxford, UK: Oxford University Press; 1988. pp. 63-98
- [8] The International Organization for Standardization. *Natural Rubber Latex Concentrate—Centrifuged or Creamed Ammonia Preserved Types—Specifications* (ISO Standard No. 2004). 6th ed. Geneva, Switzerland: The International Organization for Standardization; 2017
- [9] The International Organization for Standardization. *Latex, Rubber—Determination of Total Solids Content* (ISO Standard No. 124). 7th ed. Geneva, Switzerland: The International Organization for Standardization; 2014
- [10] The International Organization for Standardization. *Natural Rubber Latex Concentrate—Determination of Dry Rubber Content* (ISO Standard No. 126). 5th ed. Geneva, Switzerland: The International Organization for Standardization; 2005
- [11] The International Organization for Standardization. *Rubber Latex, Natural, Concentrate—Determination of Volatile Fatty Acid Number* (ISO Standard No. 506). 3rd ed. Geneva, Switzerland: The International Organization for Standardization; 1992
- [12] The International Organization for Standardization. *Natural Rubber Latex Concentrate—Determination of Alkalinity* (ISO Standard No. 125). 6th ed. Geneva, Switzerland: The International Organization for Standardization; 2011
- [13] The International Organization for Standardization. *Rubber, Natural Latex Concentrate—Determination of KOH Number* (ISO Standard No. 127). 5th ed. Geneva, Switzerland: The International Organization for Standardization; 2018
- [14] The International Organization for Standardization. *Rubber Latex—Determination of Apparent Viscosity by the Brookfield Test Method* (ISO Standard No. 1652). 4th ed. Geneva, Switzerland: The International Organization for Standardization; 2011
- [15] Gorton ADT, Pendle TD. A new rapid measurement of crosslink density in compounded natural latices. *NR Technology*. 1976;7:77-80

- [16] Sirisomboon P, Kaewkuptong A, Williams P. Feasibility study on the evaluation of the dry rubber content of field and concentrated latex of Para rubber by diffuse reflectance near infrared spectroscopy. *Journal of Near Infrared Spectroscopy*. 2013;**21**:81-88
- [17] Véronique BM, Elvira FA, Bernard P, Roger JM, Alex MB. Critical review of chemometric indicators commonly used for assessing the quality of the prediction of soil attributes by NIR spectroscopy. *Analytical Chemistry*. 2010;**29**:1073
- [18] Lim CH, Sirisomboon P. Near infrared spectroscopy as an alternative method for rapid evaluation of toluene swell of natural rubber latex and its products. *Journal of Near Infrared Spectroscopy*. 2018;**26**(3):159-168
- [19] Cornish K, Myers MD, Kelley SS. Latex quantification in homogenate and purified latex samples from various plant species using near infrared reflectance spectroscopy. *Industrial Crops and Products*. 2004;**19**(3):283
- [20] Sirisomboon P, Deeprommit M, Suchaiboonsiri W, Lertsri W. Shortwave near infrared spectroscopy for determination of dry rubber content and total solids content of Para rubber (*Hevea brasiliensis*) latex. *Journal of Near Infrared Spectroscopy*. 2013;**21**(4):269-279
- [21] Lim CH, Sirisomboon P. Updated model for fast dry rubber content determination in natural rubber latex using shortwave near infrared spectroscopy. *KMITL Science and Technology Journal*. 2014;**14**(1):34-36
- [22] Lim CH, Sirisomboon P. An updated model for fast total solids content determination in natural rubber latex using shortwave near infrared spectroscopy. *Thai Society of Agricultural Engineering Journal*. 2014;**20**(1):60-63
- [23] Inagaki T, Sirisomboon P, Liu C, Thanapase W, Tsuchikawa S. High accuracy rapid prediction and feasibility of on-site nondestructive estimation of Para rubber quality by spectroscopic methods. *Journal of Wood Science*. 2013;**59**(2):119-126
- [24] Inagaki T, Nozawa D, Shimomura Y, Tsuchikawa S. Three-fibre-based diffuse reflectance spectroscopy for estimation of total solid content in natural rubber latex. *Journal of Near Infrared Spectroscopy*. 2016;**24**:327-335
- [25] Narongwongwattana S, Rittiron R, Lim CH. The rapid determination of volatile fatty acid number in Para rubber latex using Fourier transform-near infrared spectroscopy based on quantification and discrimination model. *Journal of Innovative Optical Health Sciences*. 2015;**8**(5):1550042
- [26] Moryadee C, Surason P, Kaeophanth W. Evaluation of volatile fatty acid number of field and concentrated latex of Para rubber by near infrared spectroscopy [Bachelor thesis]. Bangkok, Thailand: Department of Agricultural Engineering, Faculty of Engineering, King Mongkut's Institute of Technology Ladkrabang; 2012
- [27] Narongwongwattana S, Rittiron R, Lim CH. Rapid determination of alkalinity (ammonia content) in Para rubber latex using portable and Fourier transform-near infrared spectrometers. *Journal of Near Infrared Spectroscopy*. 2015;**23**:181-188
- [28] Sompiw A. Nondestructive evaluation technique for viscosity, alkalinity and potassium hydroxide number of concentrated Para rubber latex by near infrared spectroscopy [Master thesis]. Bangkok, Thailand: Department of Agricultural

Engineering, Faculty of Engineering,
King Mongkut's Institute of Technology
Ladkrabang; 2015

[29] Sirisomboon P, Chowbankrang R,
Williams P. Evaluation of apparent
viscosity of Para rubber latex by
diffuse reflection near infrared
spectroscopy. *Applied Spectroscopy*.
2012;**66**(5):595-599

[30] Lim CH, Sirisomboon P. Evaluation
of prevulcanisate relaxed modulus of
prevulcanised natural rubber latex
using Fourier transform near infrared
spectroscopy. *Journal of Near Infrared
Spectroscopy*. 2017;**25**(6):407-415

[31] Williams P. Near-infrared
Technology-Getting the Best out of
Light. Nanaimo, British Columbia/
Winnipeg, Manitoba, Canada: PDK
Projects, Inc.; 2007

Electron Donor-Acceptor Organic Polymers by “Click” Type Cycloaddition/Retroelectrocyclization Reaction

Wenyi Huang

Abstract

The “click” type cycloaddition/retroelectrocyclization reaction is an intriguing approach for synthesizing electron donor-acceptor organic polymers. This chapter covers the fundamental reaction mechanism and the basic principles of applying this reaction to the synthesis of organic polymers via postfunctionalization or step-growth polymerization. The electron donor-acceptor moieties can be incorporated into the main-chain and/or side-chain of both conjugated and nonconjugated polymers. These polymers feature attractive properties including intramolecular charge-transfer bands, nonlinear optical properties, redox activities, third-order nonlinear optical properties, and enhanced thermal stability. Because of this, these polymers have found a variety of applications such as colorimetric chemosensors of metal ions, nonlinear optics, and solar cells. This novel “click” chemistry paves a unique path toward the synthesis of next-generation functional materials that cannot be accomplished by the incumbent synthetic methods.

Keywords: electronic donor-acceptor polymers, click reaction, cycloaddition/retroelectrocyclization reaction

1. Introduction

The “click” chemistries such as Diels-Alder cycloaddition, Cu-catalyzed azide/alkyne cycloaddition (CuAAC), and thiol-ene reaction have revolutionized the polymer science over the past two decades and have become an indispensable tool in synthesizing new polymers or incorporating new functionality into macromolecules [1–10]. In recent years, a new “click” chemistry of cycloaddition/retroelectrocyclization reaction has gained momentum in both organic synthesis and polymer synthesis. The “click” type cycloaddition/retroelectrocyclization reaction was first discovered by Bruce et al. [11] for the synthesis of metal acetylides in the 1980s. The first step of cycloaddition/retroelectrocyclization reaction involves the reaction of electron-rich alkynes activated by strong electron-donating groups (EDGs) with a strong electron-accepting cyanoolefinic molecule via a [2+2] cycloaddition to form the cyclobutene rings, and in the subsequent step, these cyclobutene rings are spontaneously opened to produce the donor-acceptor type chromophores in quantitative yields under mild conditions [12]. The currently available electron-donating groups for almost quantitative yields include aromatic amines [13–16], ferrocene [17, 18],

azulene, and organometallic derivatives [19, 20]. Examples of electron-accepting cyanoolefinic molecules are tetracyanoethylene (TCNE), 7,7,8,8-tetracyanoquinodimethane (TCNQ) and its derivatives [21–24], as well as dicyanovinyl and tricyanovinyl derivatives [25, 26]. Among these electron-accepting molecules, TCNE is one of the strongest organic electron acceptors, and its high chemical reactivity toward nucleophiles or electron-rich reagents is frequently used to introduce strong acceptor moieties, for example, 1,1,4,4-tetracyanobuta-1,3-diene (TCBD), into organic molecules [27, 28]. The cycloaddition/retroelectrocyclization reaction mechanism between TCNE and electron-rich alkynes activated by an electron-donating group (EDG) is illustrated in **Figure 1**. By leveraging the same chemistry, TCNQ can also react with electron-donating group substituted alkynes to exclusively yield the thermodynamically stable *Z*-isomer, as demonstrated in **Figure 2** [29].

Over the past decade, this “click” chemistry of cycloaddition/retroelectrocyclization reaction has been extensively used to synthesize electron donor-acceptor type organic molecules or dendrimers, which exhibit many interesting electrical, electrochemical, or nonlinear optical properties [30–33]. Very recently, this synthetic protocol has been generalized into macromolecular systems through step-growth polymerization or postfunctionalization due to the high reactivity of this reaction [12]. In particular, most of these polymers were realized by the postfunctionalization reaction of precursor polymers containing activated alkynes with TCNE or TCNQ. These electron donor-acceptor polymers can be classified into two major categories, namely, main chain and side chain, depending on the location of electron donor-acceptor chromophores in the macromolecular chain. For main-chain electron donor-acceptor conjugated polymers, the precursor polyene polymers often contain electron-donating moieties such as ferrocene [34], carbazole [35], thiophene [36], and metal acetylide [37]. However, only partial adduction of TCNE or TCNQ occurred, which was attributed to the low electron-donating property of electron donors as well as the high steric hindrance in the main chain [38]. To address this challenge, Huang [38] synthesized a poly(arylene ethynylene)

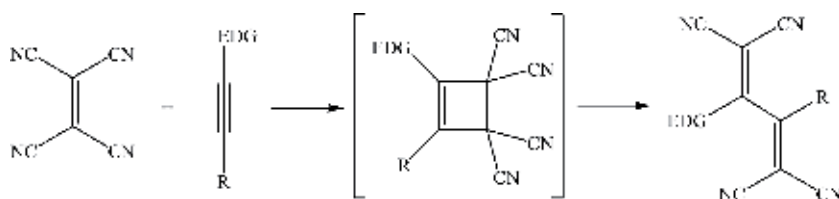


Figure 1. Cycloaddition/retroelectrocyclization reaction mechanism between tetracyanoethylene and electron-rich alkynes activated by an electron-donating group (EDG).

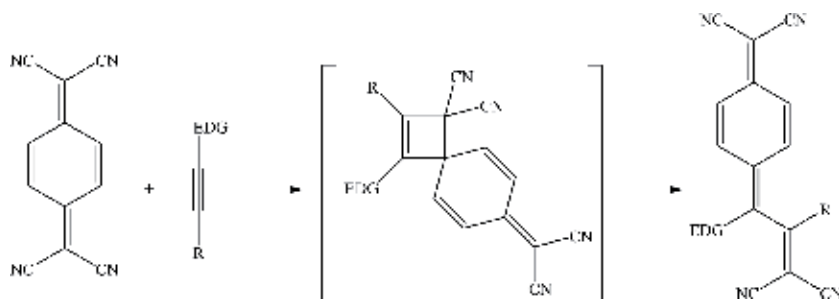


Figure 2. Cycloaddition/retroelectrocyclization reaction mechanism between 7,7,8,8-tetracyanoquinodimethane and electron-rich alkynes activated by an electron-donating group (EDG).

having dialkylanilino groups in the para-position relative to the ethynyl groups, which possess the strongest electron-donating effect on alkynes and thus enable the complete reaction of all alkynes in the main chain with TCNE to afford alternating electron donor-acceptor main-chain polymers. On the other hand, main-chain donor-acceptor nonconjugated polymers often involve a TCNQ-containing molecule and an aniline-activated alkyne molecule by cycloaddition/retroelectrocyclization reaction [39]. Furthermore, side-chain electron donor-acceptor polymers were generally synthesized from precursor polymers bearing dialkylaniline-substituted alkyne side chains [40, 41]. In contrast to main-chain alkynes, side-chain alkynes showed reactivity as high as the corresponding small molecules, probably due to the lowered steric hindrance [40]. Thus, the full TCNE (or TCNQ) addition to the polymer side chains could be achieved.

One of the striking features of cycloaddition/retroelectrocyclization reaction is that it does not involve any metal catalysts, and this reaction typically proceeds rapidly under mild conditions with very good yields [28]. Furthermore, the resulting molecular structure shows not only tunable redox activities in both the cathodic and anodic directions but also strong charge-transfer bands in the visible absorption region [39]. The TCNQ adducts exhibited a more bathochromically shifted absorption (usually a green color) as compared to the counter TCNE adducts (usually a red color) because of the extended π -conjugation [39, 42, 43]. The characteristics of click chemistry meet all the prerequisites required by the polymer synthesis. A very high yield of cycloaddition/retroelectrocyclization reaction is one of the essential parameters to obtain high-molecular-weight polymers by the step-growth polymerization [42]. In addition, a lack of side products for cycloaddition/retroelectrocyclization reaction is desirable. Generally, the synthesis of small molecules can be purified by distillation or chromatography techniques. Unfortunately, it is rather difficult to separate undesired subunits from polymers caused by side reactions. These donor-acceptor polymers display an enhanced thermal stability compared with the precursor polymer, which was attributed to the reinforced intermolecular interactions caused by the cyano groups [38].

The low bandgap energy of π -conjugated polymers is vital for their applications in many emerging areas such as organic photovoltaic devices, light-emitting diodes, and nonlinear optical devices [41]. The bandgap energy (E_g) of π -conjugated polymers may be defined by $E_g = E_{LUMO} - E_{HOMO}$ [44, 45], in which E_{HOMO} is the highest occupied molecular orbital (HOMO) energy and E_{LUMO} is the lowest unoccupied molecular orbital (LUMO) energy. E_g can be effectively reduced by enhancing the strength of electron donors and/or acceptors through the intramolecular charge-transfer interactions. As a result, the E_{HOMO} level of the donor and the E_{LUMO} level of the acceptor are closer than those in pristine systems, leading to narrower E_g [41]. In order to achieve a lower E_g of conjugated polymers, the strength of both electron-donating and electron-accepting units must be further improved, which can be accomplished by employing stronger electron-donating groups like dialkylamine on the donor to raise the E_{HOMO} as well as stronger electron-withdrawing groups such as $-\text{CN}$ group on the acceptor to reduce the E_{LUMO} [44, 45].

Furthermore, another important application of electron donor-acceptor polymers synthesized by cycloaddition/retroelectrocyclization reaction is for the use as colorimetric ion sensors, although their detection limits are usually inferior to those of fluorescent ion sensors. The nonplanar donor-acceptor chromophores in these polymers displayed the selective recognition of certain ions such as Fe^{3+} , Fe^{2+} , Sn^{2+} , and Ag^+ ions for the TCNE adducts and Fe^{3+} , Cu^{2+} , Ti^{4+} , Sc^{3+} , and Ag^+ ions for the TCNQ adducts [46, 47]. The recognition usually occurs at the aniline nitrogen, resulting in a decrease in the charge-transfer bands accompanied by visual color changes.

This chapter aims to provide an overview of the state-of-the-art development of electron donor-acceptor organic polymers synthesized by the “click” type cycloaddition/retroelectrocyclization reaction, thereby elaborating on the synthetic approaches for both main-chain and side-chain polymers as well as their applications.

2. Synthesis of electron donor-acceptor organic polymers

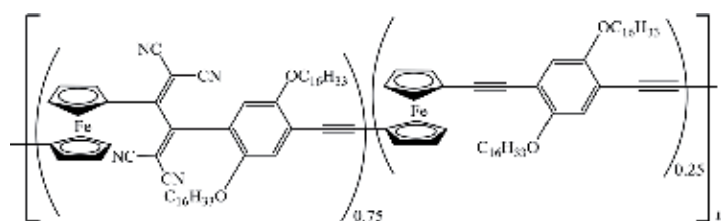
Over the past decade, a wide variety of functional polymers have been synthesized by cycloaddition/retroelectrocyclization reaction [48]. Among the synthetic protocols, postfunctionalization of precursor polymers bearing electron-rich alkynes with a strong electron acceptor is the most extensively employed technique for preparing electron donor-acceptor polymers because of the high reactivity and high yield of cycloaddition/retroelectrocyclization reaction [12].

2.1 Main-chain electron donor-acceptor organic polymers

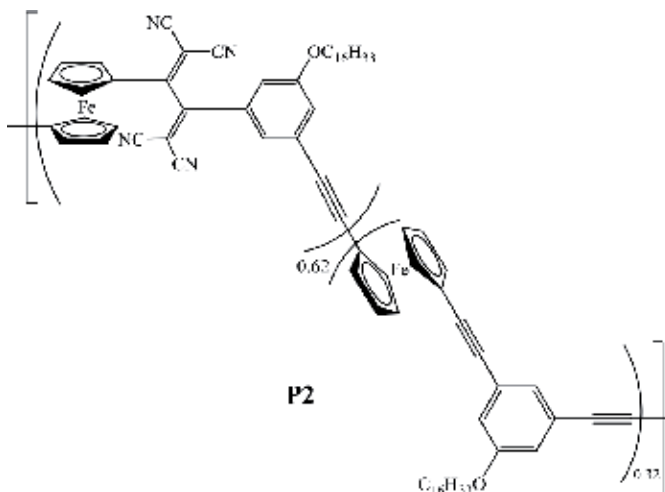
2.1.1 Main-chain electron donor-acceptor conjugated polymers

Low bandgaps of conjugated polymers are highly preferred for many important applications such as solar cells, light-emitting diodes, field-effect transistors, and supercapacitors [49–53]. The bandgap energy of conjugated polymers can be effectively reduced by introducing electron donor-acceptor chromophores into these polymers, primarily arising from the intramolecular charge-transfer interactions between electron donor and acceptor [44, 45]. TCNE and TCNQ are among the strongest electron acceptors [54], but they are sparsely employed for synthesizing donor-acceptor type conjugated polymers. The underlying reason lies in the difficulty in synthesizing TCNE or TCNQ derivatives that are suitable for polymerization. In addition, many conventional approaches for synthesizing conjugated polymers, especially those involved with the use of metal ion catalysts (e.g., palladium or nickel), are not appropriate for the use in synthesizing polymers having TCNE or TCNQ derivatives, because these TCNE or TCNQ derivatives would always form strong complexes with these metal ion catalysts leading to the reduction in their catalytic performance [55]. As a result, electron donor-acceptor conjugated polymers involving TCNE and TCNQ must be done by the postfunctionalization approach.

The postfunctionalization approach was first explored by Michinobu for ferrocene-containing poly(aryleneethynylene)s [34]. Slow heating to 120°C for 3 h was required to facilitate the cycloaddition/retroelectrocyclization reaction between ferrocene-containing poly(aryleneethynylene)s and TCNE, and the completion of reaction was evidenced by the color change of the reaction solution from orange to green. However, only partial adduction of TCNE occurred, for example, the TCNE addition amounted to 0.75 and 0.62 for **P1** and **P2**, respectively. This was attributed to the decreased electron-donating power of the ferrocene donor substituted by the TCBD acceptor as well as the high steric hindrance in the main chain. The excess of TCNE did not cause any undesired side reactions and was removed by sublimation or reprecipitation. Both **P1** and **P2** featured well-defined intramolecular charge-transfer absorption bands and redox activities in both anodic and cathodic directions.

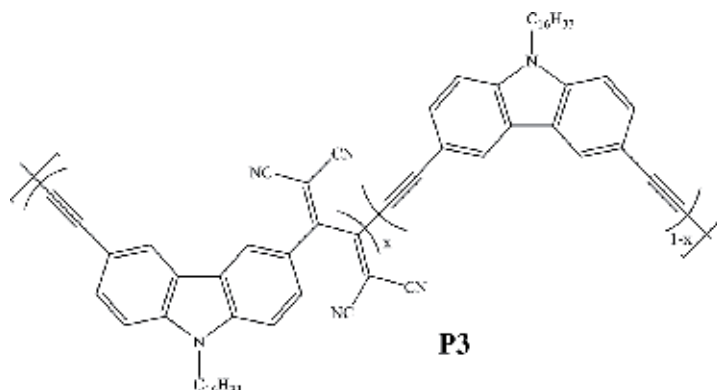


P1



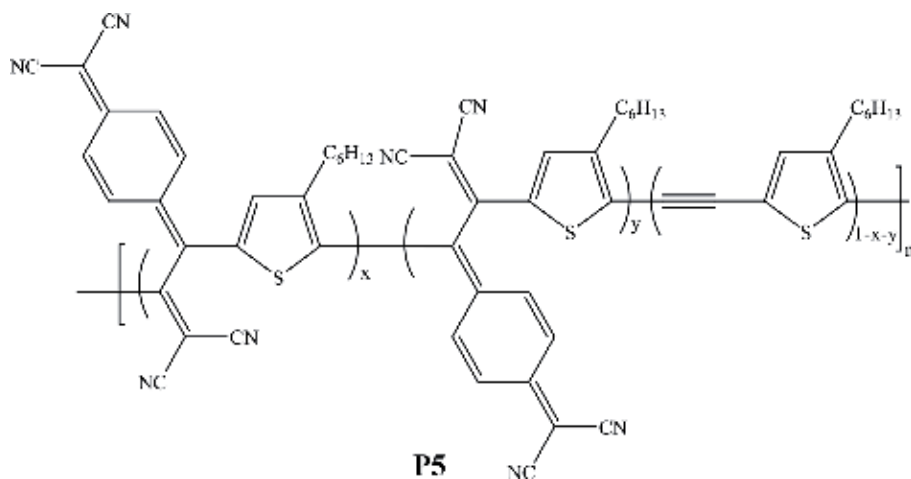
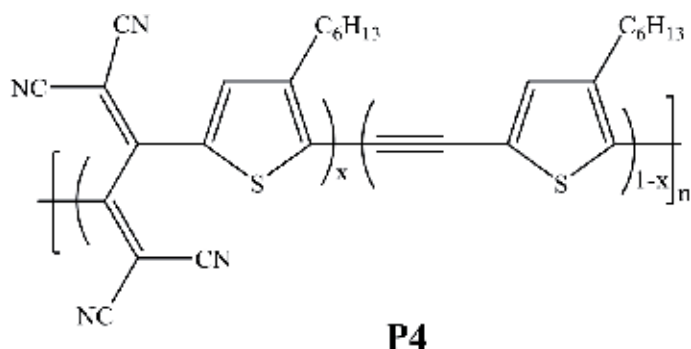
P2

Furthermore, carbazole was selected as an electron-donating group, and the corresponding poly(arylenebutadiynylene)s were prepared by the acetylenic oxidative polymerization [56]. The substitution pattern of carbazole had a significant influence in the efficiency of the cycloaddition/retroelectrocyclization reaction. For example, 3,6-carbazole-based poly(arylenebutadiynylene) was successfully converted into the donor-acceptor type conjugated polymer, whereas the 2,7-carbazole-based counterpart polymer did not react with TCNE due to the insufficient activation of alkyne moieties. Upon the optimization of reaction conditions, 0.75–0.8 equiv. of TCNE was successfully reacted with main-chain alkynes of 3,6-carbazole-based poly(arylenebutadiynylene), resulting in the donor-acceptor conjugated polymer, **P3**. This conjugated polymer showed strong intramolecular charge-transfer interactions as well as higher thermal stability having a thermal degradation temperature above 350°C.

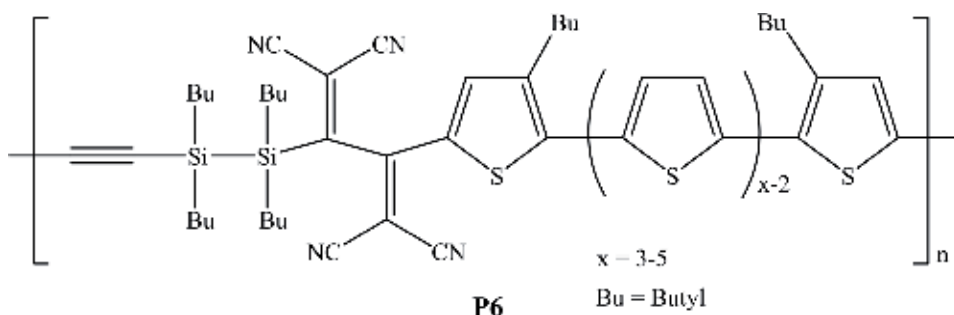


P3

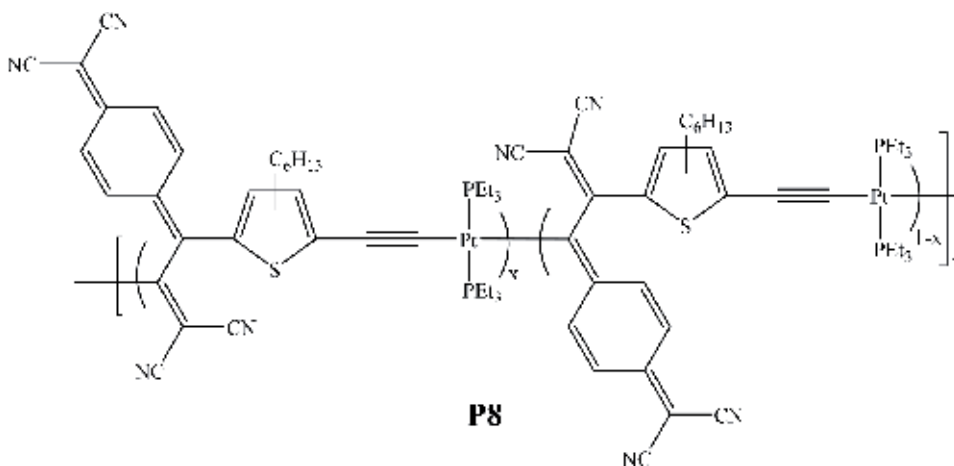
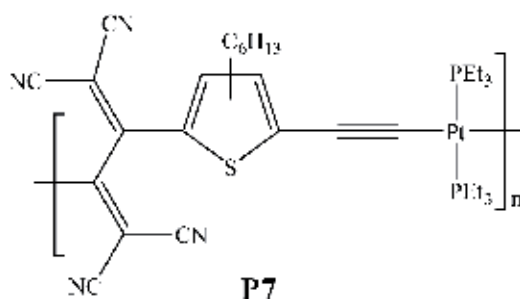
Thiophene is another important electron-donating moiety, and it has been incorporated into poly(thienyleneethynylene) by the Sonogashira polycondensation of 2-bromo-5-ethynyl-3-hexylthiophene [36, 56]. TCNE and TCNQ were employed to react with poly(thienyleneethynylene) in the presence of microwave irradiation to afford **P4** and **P5**, respectively. These two donor-acceptor conjugated polymers displayed an enhanced thermal stability as compared with the precursor polymer, arising from the reinforced intermolecular interactions caused by the cyano groups. UV-Vis-NIR spectroscopy revealed charge-transfer bands in the low-energy region, while electrochemistry confirmed the narrower bandgaps with the elevated HOMO and lower LUMO levels relative to the precursor polymer. After doping, these polymers showed room temperature conductivities of as high as 4.5×10^{-5} S/cm, which was about ten times greater than that of the precursor polymer.

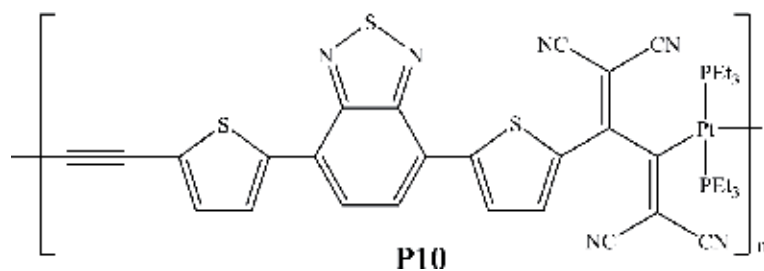
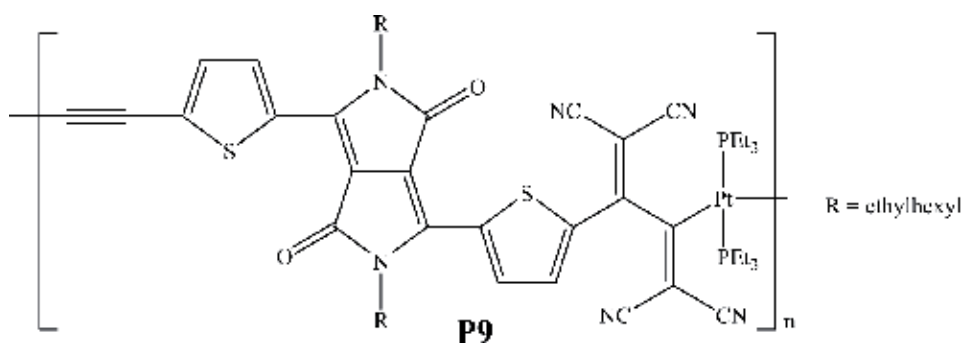


Ohshita et al. [57] reported the reaction of poly(disilanyleneethynyleneoligothienyleneethynylene)s with TCNE to yield new donor-acceptor type organosilicon polymers (**P6**) bearing oligothiénylene and tetracyanobutadienylenes units as the donor and acceptor units, respectively. These polymers exhibited red-shifted absorption bands at $\lambda_{\text{max}} = 513\text{--}565$ nm in UV-Vis spectrum, whose edges reached approximately 800 nm, indicative of the strong charge-transfer interaction between electron donor and acceptor in the macromolecular backbone. These polymers also displayed solvatochromic behaviors. Specifically, the UV-Vis absorption maxima moved to the longer wavelengths with increasing solvent polarity. **P6** was photoactive because irradiation of TiO_2 electrodes in the polymer solutions resulted in the attachment of the polymer onto the TiO_2 surface via the formation of Si—O—Ti anchor bonds.

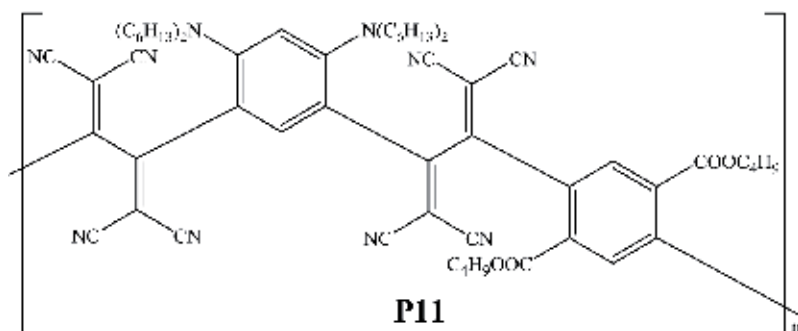


The cycloaddition/retroelectrocyclization reaction was first demonstrated in metal acetylide compounds [11], and thus metal-polyacetylene polymers may also be good candidates for the cycloaddition/retroelectrocyclization postfunctionalization to synthesize metal-containing donor-acceptor conjugated polymers. Yuan and Michinobu [37] synthesized a main-chain thiophene-based platinum-polyacetylene conjugated polymer, which was further reacted with TCNE to yield electron donor-acceptor polymer **P7**. The use of the thiophene and platinum (II) donors in the precursor polymer efficiently improved the reactivity of main-chain alkynes. As a result, **P7** was obtained under mild heating at 70°C. Moreover, this thiophene-based platinum (II)-polyacetylene precursor polymer was explored to react with TCNQ to afford **P8**. **P8** displayed stronger electron-accepting feature than **P7**, as revealed by the more bathochromically shifted charge-transfer band and the lower first reduction potential. In order to enhance the electron-withdrawing property of electron donor-acceptor polymers, diketopyrrolopyrrole and benzothiadiazole were incorporated into **P9** and **P10**, respectively [58]. The LUMO levels decreased significantly to about -4.2 to -4.5 eV after postfunctionalization with TCNE.



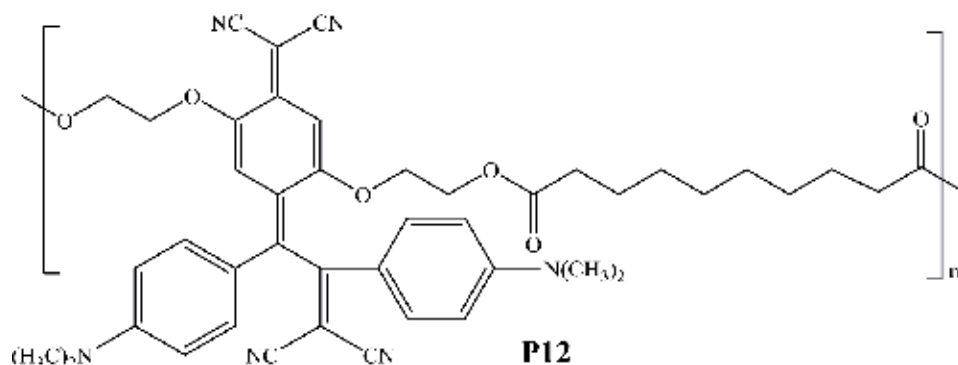


Huang [38] reported a facile synthetic route for synthesizing a main-chain donor-acceptor type polymer containing strong electron-donating dialkylamino groups and strong electron-accepting 1,1,4,4-tetracyanobuta-1,3-diene (TCBD) units. The precursor polymer has a dialkylanilino group in the para-position on each main-chain alkyne, affording the strongest electron-donating effect for promoting the highest reactivity between TCNE and main-chain alkynes [36]. This molecular design overcomes difficulty in successfully implementing the postfunctionalization of main-chain ethynyl groups along the macromolecular chain in a complete manner. Specifically, an electron-donating monomer 4,6-diethynyl-N,N,N,N-tetrahexylbenzene-1,3-diamine was successfully synthesized by converting two carbaldehyde groups in the corresponding monomer into acetylene groups using lithium trimethylsilyldiazomethane via a Colvin rearrangement. This electron-donating monomer was then polymerized with a carbonyl-activated diiodide monomer to afford an electron-donating π -conjugated precursor polymer with a reasonably high molecular weight, which was further reacted with TCNE via cycloaddition/retroelectrocyclization reaction under mild conditions to afford the target polymer (**P11**). **P11** shows a very low bandgap energy ($E_g^{opt} = 1.40$ eV and $E_g^{CV} = 1.10$ eV), because of strong intramolecular charge-transfer interactions between electron donors and acceptors along the macromolecular chain.

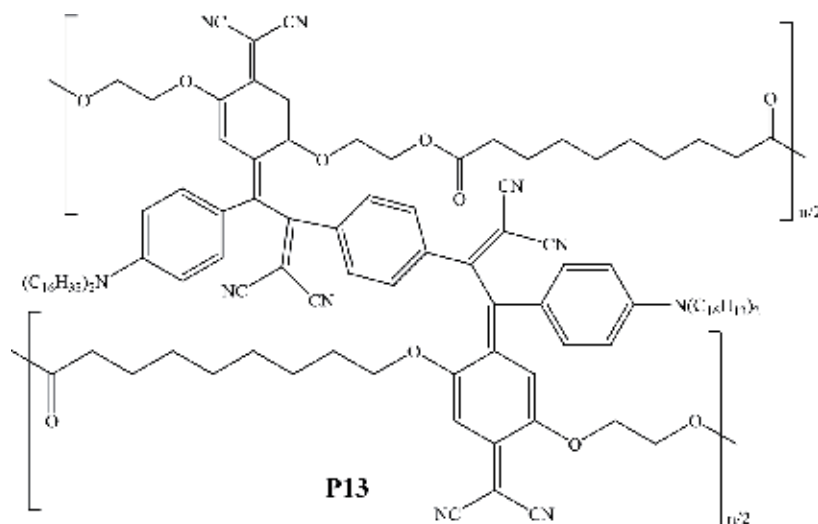


2.1.2 Main-chain electron donor-acceptor nonconjugated polymers

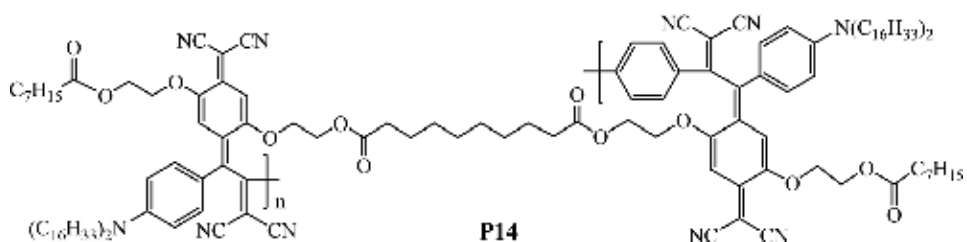
Washio and Michinobu et al. [39] reported postfunctionalization of TCNQ-containing polyester by cycloaddition/retroelectrocyclization reaction with a small-molecule aniline-activated alkyne to yield a polyester containing electron donor-acceptor chromophores (**P12**). **P12** possessed the colorimetric chemosensor ability, as evidenced by well-defined color changes of the charge-transfer band) due to the recognition of Ag^+ and Fe^{3+} ions. In contrast, the precursor TCNQ-containing polyester did not show any spectral changes upon the addition of Ag^+ and Fe^{3+} ions. Specifically, the Ag^+ ion was recognized by the cyano nitrogen atoms as a result of the effective multivalent coordination, leading to a bathochromic shift in the charge-transfer band. On the other hand, the Fe^{3+} ion was recognized by the aniline nitrogen atoms, as evidenced by the disappearance of the charge-transfer band.



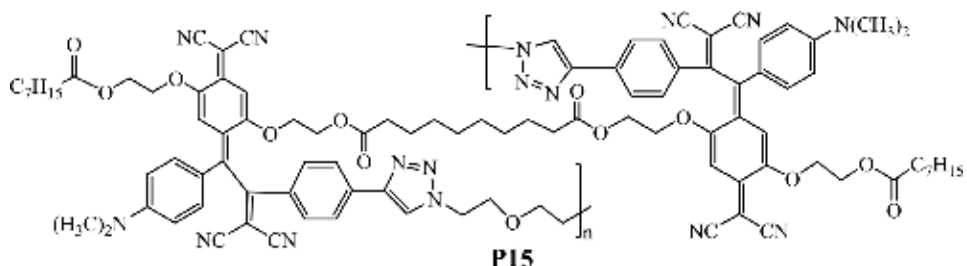
By using a similar method to the synthesis of **P12**, polymeric electro-optic materials (**P13**) were synthesized by simple heating of a mixed thin film of TCNQ-containing polyester and an aniline-activated dialkyne molecule to 140°C under electric poling [59]. A thermal addition reaction between electron-rich alkynes and TCNQ moieties enabled the formation of donor-acceptor chromophores as well as cross-linking networks throughout the polymer film to effectively fix the dipolar orientation induced by electrical poling. It took about 13 h to complete the reaction, and the electro-optic coefficient (d_{eff}) showed the maximum value of 0.609 pm/V after 2.5 h.



Washino and Michinobu [42] described the polyaddition polymerization between electron-rich alkynes and a TCNQ-containing molecule to yield electron donor-acceptor non-conjugated polymers (**P14**). The electron-donating monomer possesses two dialkylaniline-substituted alkynes, while the electron-accepting monomer contains two TCNQ moieties. The aforementioned two monomers were then reacted in 1,2-dichloroethane under mild heating conditions to produce the desired linear polymers with high molecular weights. It was reported that high molecular weight polymers were preferentially formed at high monomer concentrations; however, cyclic compounds dominated when the monomer concentration was low. In both cases, the degree of reaction could be readily monitored by observing the shift of the charge-transfer band in UV-Vis spectra. The presence of terminal groups in the polymers were determined by the cyclic voltammetry, demonstrating the linear polymer structures of **P14**. **P14** showed an excellent thermal stability with the decomposition temperature exceeding 300°C. It also exhibited strong charge-transfer bands and redox activities due to the produced donor-acceptor moieties.



Furthermore, Washino and Michinobu [60] synthesized sequence-regulated linear polymers by multiple click chemistry reactions, which could include cycloaddition/retroelectrocyclization reaction along with other click chemistry reactions such as copper (I)-catalyzed alkyne-azide cycloaddition (CuAAC) and Diels-Alder cycloaddition to create electron donor-acceptor polymers. The orthogonality with CuAAC was explored by investigating the reaction orders. It was only possible to complete the metal-free double click reactions in the order of the Diels-Alder cycloaddition followed by the alkyne-TCNQ addition. The resulting donor-acceptor chromophores in **P15** gave rise to optical metal ion sensing, a colorimetric chemosensor behavior toward the Ag⁺ ion and electrochemical properties.

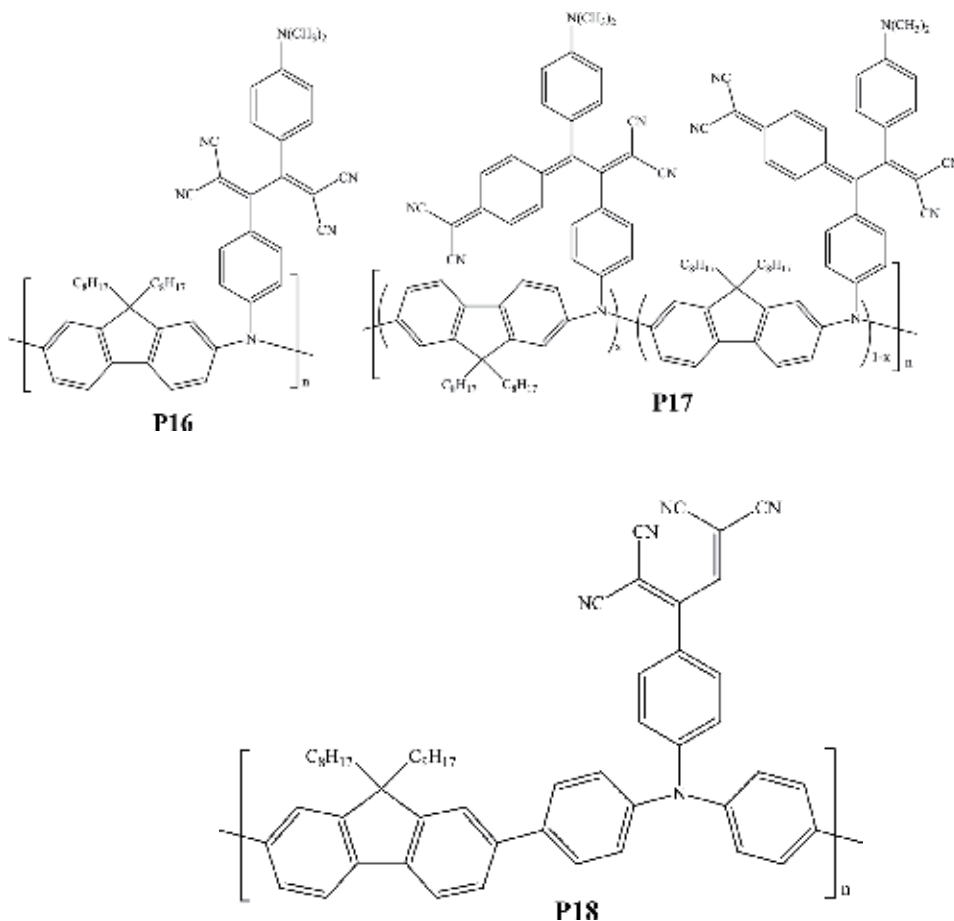


2.2 Side-chain electron donor-acceptor organic polymers

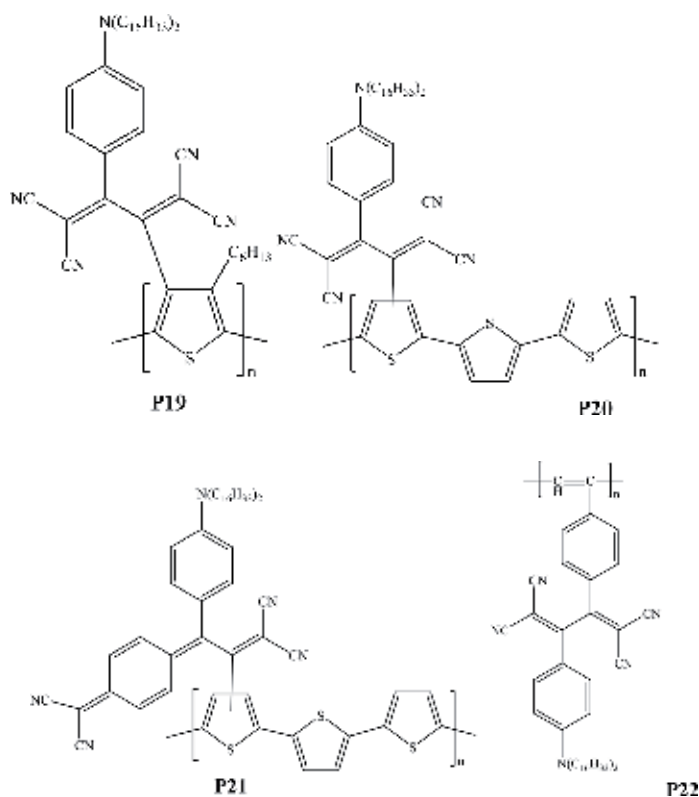
In contrast to main-chain alkynes, side-chain alkynes showed a reactivity as high as the corresponding small molecules, probably due to the lowered steric hindrance. Thus, the full TCNE addition to the polymer side chains could be achieved. Since click postfunctionalization does not require any tedious purification process, such as column chromatography and reprecipitation, a series of side-chain electron donor-acceptor polymers have been synthesized by this approach [40, 41, 61].

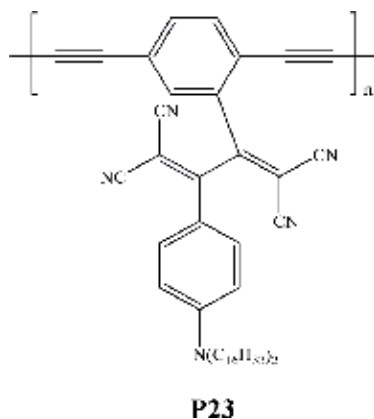
2.2.1 Side-chain electron donor-acceptor conjugated polymers

Michinobu [40] first synthesized a precursor polyamine bearing the electron-rich alkynes in the side chain, which was subsequently reacted with TCNE and TCNQ to give side-chain electron donor-acceptor conjugated polymers, **P16** and **P17**, respectively [62]. The successful addition of TCNE or TCNQ to the precursor polyamine was confirmed by the matrix-assisted laser desorption/ionization with time-of-flight (MALDI-TOF) mass spectra and the absence of the acetylene peak signals in the ^{13}C NMR spectrum. The π -conjugation length of **P16** and **P17** was enhanced in the presence of electron-accepting moieties, thus leading to red shifts in their absorption spectra and significant reduction in their bandgaps. As the TCNE or TCNQ addition increased, both glass transition temperature and thermal decomposition temperature of the polyamines gradually increased. For example, the increment in the glass transition temperature was 27°C , while the increase in the thermal degradation temperature was 118°C for **P16**. These authors successfully fabricated thin film transistors based on **P16** and **P17** and established a clear correlation between the polymer energy levels and hole mobilities [63]. By using a similar strategy, a triphenylamine-based conjugated polymer (**P18**) with cyano-containing chromophore in the side chain was synthesized and used for probing Hg^{2+} ion. Specifically, fluorescence of **P18** solution in tetrahydrofuran was specifically quenched by the introduction of I^- , accompanied by the change of its apparent color from pale brown to light yellow. In the presence of Hg^{2+} ion, the fluorescence of **P18/I** $^-$ complex recovered very quickly and even exceeded the initial intensity of pristine **P18** [64].

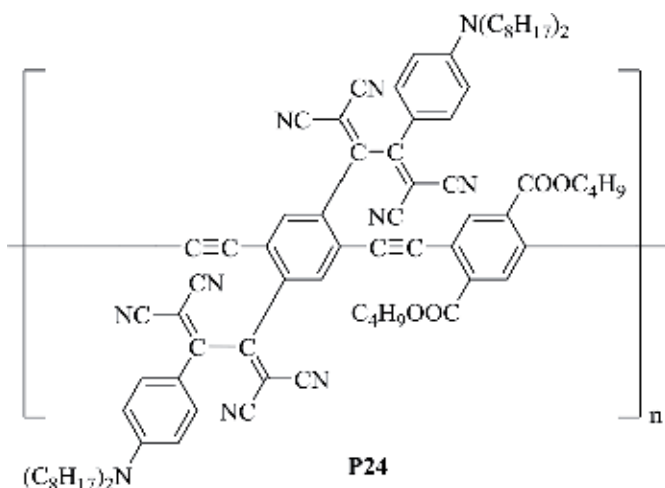


The click postfunctionalization of side-chain donor-acceptor conjugated polymers has been leveraged to other conjugated polymer systems, such as polythiophene, poly(p-phenyleneethynylene), and poly(phenylacetylene) derivatives. Yuan et al. [61] reported the synthesis of a polythiophene electron donor-acceptor polymer **P19**. The reaction started from the highly region-regular poly(3-hexylthiophene) prepared by the Grignard metathesis polymerization, bromination at the 4-position of the thiophene ring, and Stille coupling reaction, to TCNE addition to the side-chain alkynes. Chemical and electrochemical n-doping of the TCBD moieties of **P19** resulted in the formation of poly(radical anion)s and poly(dianion)s. The temperature-dependent magnetic measurements were used to characterize the high spin state of the poly(radical anion)s, because regioregular polythiophene is classified as a non-Kekule and non-disjoint connectivity [61]. Furthermore, a regio-irregular polythiophene derivative with dialkylanilino-substituted alkyne side chains was synthesized by the Suzuki polycondensation, and then it was reacted with TCNE and TCNQ to afford **P20** and **P21**, respectively [65]. The study on the poly(phenylacetylene)-based electron donor-acceptor polymers (**P22**) indicated that the click postfunctionalization had a significant impact on the intermolecular interactions [29, 66]. Upon the completion of cycloaddition/retroelectrocyclization click postfunctionalization of the precursor polymer with TCNE, the film morphology changed from an unstructured homogeneous surface to fibrous nanostructures. As a result, the diffusion coefficients of O₂ and N₂ were dramatically reduced, which was attributed to the decrease in the void spaces. Wang et al. [67] synthesized a series of poly(p-phenylenebutadiynylene) electron donor-acceptor polymers (**P23**), which were prepared by homocoupling polymerization of asymmetric bifunctional monomers, followed by the “click” chemistry with TCNE to introduce donor-acceptor chromophores in the side chain. The energy level and bandgap could be precisely controlled by the addition of acceptor molecules, as evidenced by the optical and electrochemical characterizations.





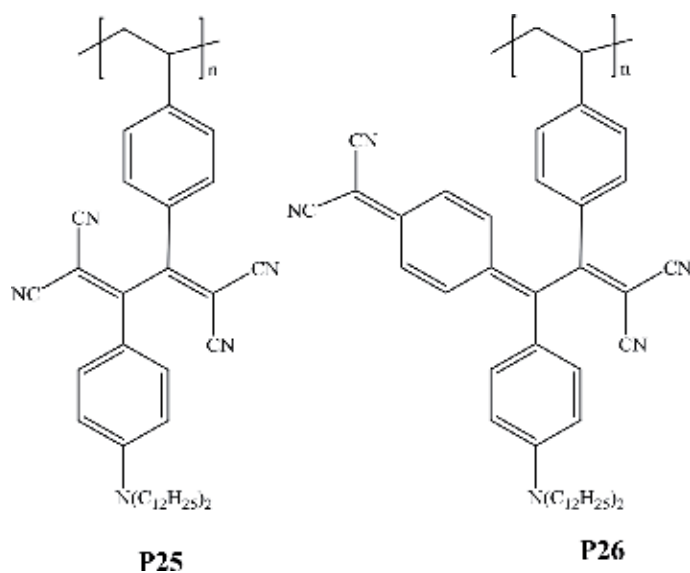
Huang and Chen [41] developed an effective approach to synthesizing a low bandgap poly(arylene ethynylene) (**P24**) having donor-acceptor type chromophores in both side chains. Specifically, a diacetylene monomer and a carbonyl-activated diiodide monomer were synthesized and then polymerized by palladium-catalyzed cross-coupling reaction to afford a π -conjugated precursor polymer, which has approximately 50 repeat units of alternating arylene and ethynylene. The dioctylanilino-activated alkynes in the side chains of the precursor polymer were able to selectively react with TCNE by click-type [2+2] cycloadditions and the subsequent retroelectrocyclization to form the donor-acceptor type chromophores. The deactivated alkynes in the main chain of the precursor polymer remained intact so that the unique features of poly(arylene ethynylene)s such as excellent thermal stability and photostability could be kept in the target polymer. This unique polymer exhibited strong intramolecular charge-transfer interactions as evidenced by UV-Vis spectroscopy and cyclic voltammometry. As a result, **P24** has a low bandgap energy ($E_g^{opt} = 1.59$ eV and $E_g^{CV} = 1.35$ eV) and enhanced thermal stability.



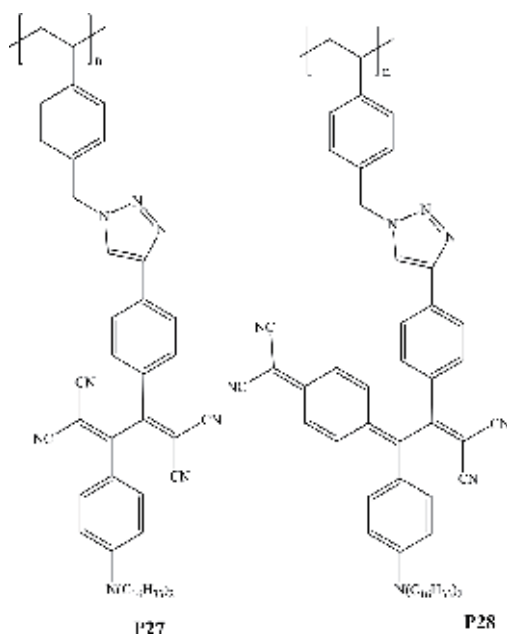
2.2.2 Side-chain electron donor-acceptor nonconjugated polymers

Polystyrene-based polymers bearing dialkylanilino-substituted alkynes in the side chain are an important family of precursors for synthesizing electron donor-acceptor nonconjugated polymers by cycloaddition/retroelectrocyclization reaction. The “click” type reaction of TCNE and TCNQ with these

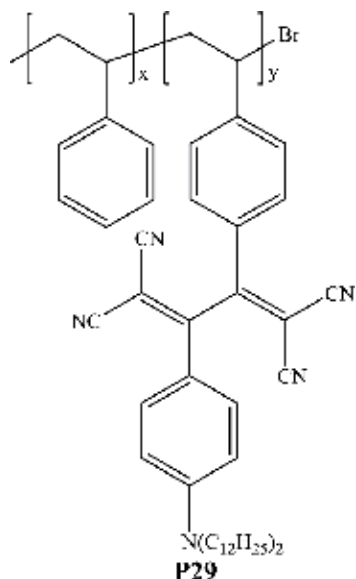
polystyrene-based precursors afforded the corresponding new materials (**P25** and **P26**) bearing electron donor-acceptor moiety in the side chain [46, 47]. Both **P25** and **P26** displayed well-defined charge-transfer bands in the visible region at ca. 480 and 730 nm, respectively, which enabled the visual detection of analytes. Specifically, **P25** selectively detected Fe^{3+} , Sn^{2+} , and Fe^{2+} ions, while **P26** preferred Fe^{3+} , Sc^{3+} , Ti^{4+} , and Cu^{2+} ions. The decrease in the charge-transfer band in the visible–near-infrared region was a result of the recognition of these metal ions by anilino nitrogen atoms in the side chain of **P25** and **P26**, and thus discoloration was a sign for visual recognition. On the other hand, only the Ag^+ ion could interact with the cyano groups in the side chains of polymers through the multivalent coordination. As a result of this interaction, a bathochromic shift occurred in the charge-transfer bands, leading to the change of the visual colors.



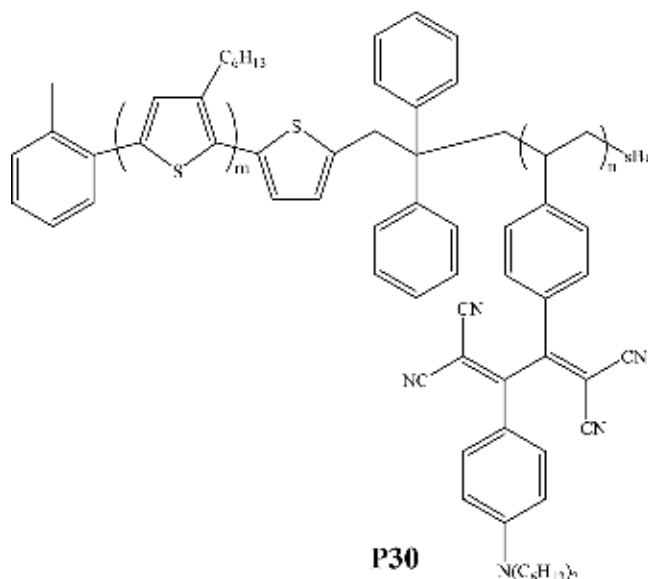
The orthogonal reactivity is one of the key features of click reactions. In order to illustrate the orthogonal reactivity of the cycloaddition/retroelectrocyclization reaction, double click postfunctionalization of poly(4-azidomethylstyrene) was conducted by CuAAC, followed by a cycloaddition/retroelectrocyclization reaction with TCNE or TCNQ to yield polymers, **P27** and **P28**, respectively [64, 68–72]. It should be noted that both click reactions proceeded rapidly without any side reactions, and carrying out the reactions in the reverse order also gave the same products. Upon the completion of electric poling, the second-order nonlinear optical responses of the polymer films were observed. Furthermore, all these polystyrene-based electron donor-acceptor nonconjugated polymers exhibited very specific colorimetric ion sensing behaviors [73–76]. The hard basic anilino nitrogen atoms preferred to interact with hard acidic metal ions like Fe^{3+} , leading to the decrease in the charge-transfer absorption band and thereby resulting in decolorization. On the other hand, soft basic cyano nitrogen atoms selectively captured the soft acidic Ag^+ metal ion, which caused a bathochromic shift of the charge-transfer band wavelength, thus leading to well-defined color changes. Nevertheless, the recognition of Ag^+ ions by the cyano groups was not possible for the corresponding monomeric electron donor-acceptor molecule, which was attributed to the fact that multiple cyano coordinations were essential for the selective recognition of the Ag^+ ions.



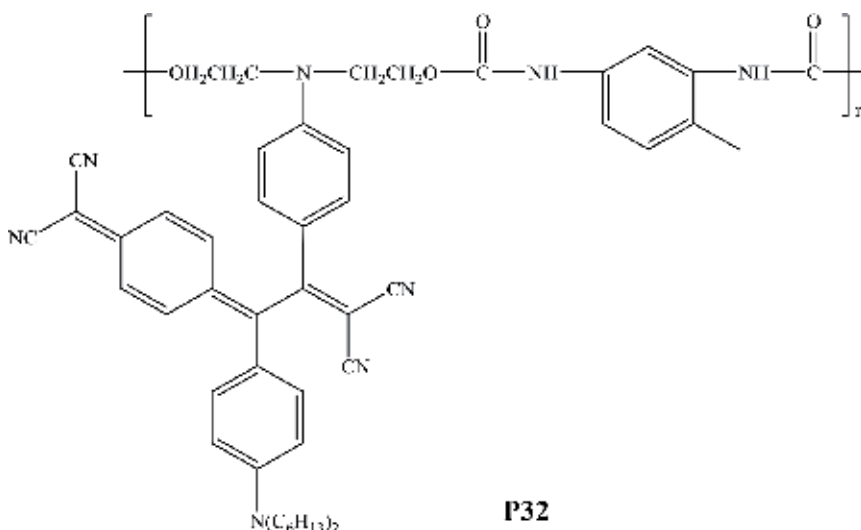
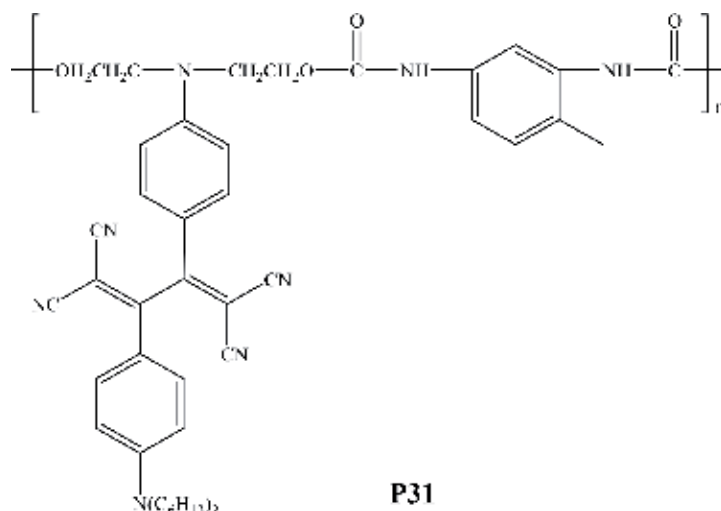
Atom transfer radical polymerization (ATRP) of *N,N*-didodecyl-4-[(4-vinylphenyl)ethynyl]aniline was conducted with bromine-terminated polystyrene to synthesize block copolymers composed of unsubstituted polystyrene and electron-rich alkyne functionalized polystyrene segments. These block copolymers were then reacted with TCNE to introduce electron donor-acceptor chromophores into the side chains of polymers to produce TCNE-adducted polymers (P29). P29 exhibited intense charge-transfer bands, well-defined redox activities, and good thermal stability. In addition, polymer thin films based on P29 were prepared by spin coating on a glass slide. The second harmonic generation (SHG) of these thin films was measured before and after electric poling. The results showed that the SHG coefficient (d_{33}) of the poled thin film was as high as 3.0 pm/V [70].



Fujita et al. reported the synthesis of a block copolymer (**P30**) by combining living polymerization techniques and cycloaddition/retroelectrocyclization reaction [77, 78]. This block copolymer contains a poly(3-hexylthiophene) block and a polystyrene block with an electron donor-acceptor chromophore. **P30** was used as an interfacial compatibilizer for P3HT/PCBM (herein, P3HT = poly(3-hexylthiophene), and PCBM = phenyl-C61-butyric acid methyl ester) bulk-heterojunction organic photovoltaic cells in order to facilitate the nanophase separation of each semiconducting domain. The TCBD moiety in polystyrene block of **P30** had higher affinity to the n-type semiconducting domain, while poly(3-hexylthiophene) block in **P30** had good compatibility with poly(3-hexylthiophene) p-type polymer. Under the optimized blend ratio of the block copolymer, the power conversion efficiency was enhanced, which was attributed to the increased short-circuit current and fill factor. Also, the crystallinity of poly(3-hexylthiophene) polymer was improved upon the addition of **P30**. The efficient compatibilizing performance of **P30** at the interface of P3HT/PCBM enlarged and fixed the interfacial area and in turn suppressed the recombination of the generated carriers.



The combination of cycloaddition/retroelectrocyclization “click” chemistry and specific Ag^+ ion recognition was later leveraged to create multicolored polyurethanes [79]. Specifically, a colorless polyurethane derivative having electron-rich alkynes substituted by dialkylaniline donors at both sides was synthesized by polyaddition between a diol monomer and tolylene-2,4-diisocyanate. The side-chain alkynes in the precursor polyurethane were then reacted with TCNE and TCNQ to yield orange-colored and green-colored polymers, **P31** and **P32**, respectively. **P31** and **P32** exhibited the intramolecular charge-transfer bands centered at 476 nm and 698 nm in CH_2Cl_2 , respectively. After complexation of Ag^+ ion with cyano groups in the side chains of **P31** and **P32**, the colors of the postfunctionalized polyurethanes were further changed. This was related to the change of the strengths of the intramolecular donor-acceptor interactions. For example, the solution color of **P31** changed to magenta and that of **P32** to a yellowish-green upon the Ag^+ ion addition. Furthermore, the electrochemical oxidation of the precursor polyurethane at $> +0.25$ V (versus Ag/AgCl in MeCN) gave a blue polymer. This color change was attributed to the formation of aromatic amine-based radical cations.



3. Summary and perspectives

This chapter gives an overview of electron donor-acceptor organic polymers synthesized by the “click” type cycloaddition/retroelectrocyclization reaction between electron donor-activated alkynes and olefinic acceptors such as TCNE and TCNQ. This “click” chemistry has many unique characteristics including high yields, short reaction times, and without the need for a catalyst or even a solvent. The salient features of the resulting electron donor-acceptor polymers encompass strong intramolecular charge-transfer interactions with tunable electronic absorptions that extend into the near-infrared region, active redox behavior, potent electron acceptor characteristics, high third-order nonlinear optical properties, high thermal stability, good solubility, and sublimation without decomposition, thereby enabling the preparation of thin films by vapor deposition. These electron donor-acceptor moieties have been integrated into the main chain or the side chain of polymers. In particular, the narrower bandgap and unique electrochemical properties of the resulting electron donor-acceptor conjugated polymers showed great potential in various applications such as nonlinear optical devices, organic photovoltaic devices, and light-emitting diodes.

This “click” chemistry was also effective for the synthesis of functional polymers with beautiful colors and successfully furnished the ion sensing abilities by the nonplanar donor-acceptor chromophores. Chemosensors are mainly classified as colorimetric and fluorometric sensors. However, chemosensors with a dual detection ability are very rare. Nonconjugated polymers bearing side-chain electron donor-acceptor chromophores composed of dialkylanilino donor and cyano-based acceptor groups have demonstrated the dual colorimetric detection behavior of several metal ions based on the specific interactions with different nitrogen atoms. Hard to borderline metal ions, such as Fe^{3+} , Fe^{2+} , and Sn^{2+} , are always recognized by the dialkylanilino nitrogen atom, resulting in a decrease in the charge-transfer band intensity of the donor-acceptor chromophores. On the other hand, the recognition site of a soft metal ion of Ag^+ is the cyano nitrogen atom due to the readily formed multivalent coordination which produces formed multivalent coordination leading to the bathochromic shift of the charge-transfer band. Chemosensors that can detect specific metal ions based on ligand-metal interactions have attracted increasing attention because of their high selectivity and low cost compared to other precise analytical techniques, such as atomic absorption spectroscopy and mass spectrometry.

The successful stories of electron donor-acceptor polymers enabled by the cycloaddition/retroelectrocyclization “click” chemistry open up a new avenue toward the synthesis of advanced polymers such as low bandgap polymers, intrinsically molecule-based conductive and/or magnetic polymers, organic photovoltaics, molecular batteries, and many other future applications.


Author details

Wenyi Huang

E.I. du Pont de Nemours and Company, Midland, MI, USA

*Address all correspondence to: wenyi.huang@dupont.com

IntechOpen

© 2019 The Author(s). Licensee IntechOpen. This chapter is distributed under the terms of the Creative Commons Attribution License (<http://creativecommons.org/licenses/by/3.0>), which permits unrestricted use, distribution, and reproduction in any medium, provided the original work is properly cited. 

References

- [1] Kolb HC, Finn MG, Sharpless KB. Click chemistry: Diverse chemical function from a few good reactions. *Angewandte Chemie International Edition*. 2001;**40**(11):2004-2021
- [2] Qin A, Lam JWY, Tang BZ. Click polymerization: Progresses, challenges, and opportunities. *Macromolecules*. 2010;**43**(21):8693-8702
- [3] Tasdelen MA. Diels–Alder “click” reactions: Recent applications in polymer and material science. *Polymer Chemistry*. 2011;**2**(10):2133-2145
- [4] Hoyle CE, Bowman CN. Thiol–Ene click chemistry. *Angewandte Chemie International Edition*. 2010;**49**(9):1540-1573
- [5] Hoyle CE, Lowe AB, Bowman CN. Thiol-click chemistry: A multifaceted toolbox for small molecule and polymer synthesis. *Chemical Society Reviews*. 2010;**39**(4):1355-1387
- [6] Golas PL, Matyjaszewski K. Marrying click chemistry with polymerization: Expanding the scope of polymeric materials. *Chemical Society Reviews*. 2010;**39**(4):1338-1354
- [7] Rutjes F, Fokin VV, Sharpless KB. *Click Chemistry*. Weinheim, Germany: Wiley-VCH; 2014
- [8] Chandrasekaran S. *Click Reactions in Organic Synthesis*. Weinheim, Germany: Wiley-VCH; 2016
- [9] Yu C, Rui TZ. *Click Chemistry: Approaches, Applications, and Challenges*. New York: Nova Science Publishers, Incorporated; 2017
- [10] Nulwala HB; University of California, S. B. *Highly Efficient Monomer and Polymer Synthesis Using Click Chemistry*. Santa Barbara: University of California; 2009
- [11] Bruce MI, Rodgers JR, Snow MR, Swincer AG. Cyclopentadienyl-ruthenium and -osmium chemistry. Cleavage of tetracyanoethylene under mild conditions: X-ray crystal structures of [Ru{ η^3 -C(CN)₂CPh·C(CN)₂}(PPh₃)(η -C₅H₅)] and [Ru{C[·C(CN)₂]CPh·C(CN)₂}(CNBut)(PPh₃)(η -C₅H₅)]. *Journal of the Chemical Society, Chemical Communications*. 1981;(6):271-272
- [12] Michinobu T. Click synthesis of donor–acceptor-type aromatic polymers. *Pure and Applied Chemistry*. 2010;**82**:1001
- [13] Kivala M, Diederich F. Conjugation and optoelectronic properties of acetylenic scaffolds and charge-transfer chromophores. *Pure and Applied Chemistry*. 2008;**80**(3):411-427
- [14] Kivala M, Diederich F. Acetylene-derived strong organic acceptors for planar and nonplanar push-pull chromophores. *Accounts of Chemical Research*. 2009;**42**(2):235-248
- [15] Xu J, Liu X, Lv J, Zhu M, Huang C, Zhou W, et al. Morphology transition and aggregation-induced emission of an intramolecular charge-transfer compound. *Langmuir*. 2008;**24**(8):4231-4237
- [16] Zhou W, Xu J, Zheng H, Yin X, Zuo Z, Liu H, et al. Distinct nanostructures from a molecular shuttle: Effects of shuttling movement on nanostructural morphologies. *Advanced Functional Materials*. 2009;**19**(1):141-149
- [17] Mochida T, Yamazaki S. Mono- and diferrocenyl complexes with electron-accepting moieties formed by the reaction of ferrocenylalkynes with tetracyanoethylene. *Journal of the Chemical Society, Dalton Transactions*. 2002;(18):3559-3564

- [18] Kato S-i, Kivala M, Schweizer WB, Boudon C, Gisselbrecht J-P, Diederich F. Origin of intense intramolecular charge-transfer interactions in nonplanar push-pull chromophores. *Chemistry—A European Journal*. 2009;**15**(35):8687-8691
- [19] Shoji T, Ito S, Toyota K, Iwamoto T, Yasunami M, Morita N. Reactions between 1-ethynylazulenes and 7,7,8,8-tetracyanoquinodimethane (TCNQ): Preparation, properties, and redox behavior of novel azulene-substituted redox-active chromophores. *European Journal of Organic Chemistry*. 2009;**2009**(25):4316-4324
- [20] Shoji T, Ito S, Toyota K, Yasunami M, Morita N. Synthesis, properties, and redox behavior of mono-, bis-, and tris[1,1,4,4,-tetracyano-2-(1-azulenyl)-3-butadienyl] chromophores binding with benzene and thiophene cores. *Chemistry—A European Journal*. 2008;**14**(27):8398-8408
- [21] Kivala M, Boudon C, Gisselbrecht J-P, Seiler P, Gross M, Diederich F. A novel reaction of 7,7,8,8-tetracyanoquinodimethane (TCNQ): Charge-transfer chromophores by [2 + 2] cycloaddition with alkynes. *Chemical Communications (Cambridge, U. K.)*. 2007;(45):4731-4733
- [22] Reutenauer P, Kivala M, Jarowski PD, Boudon C, Gisselbrecht J-P, Gross M, et al. New strong organic acceptors by cycloaddition of TCNE and TCNQ to donor-substituted cyanoalkynes. *Chemical Communications (Cambridge, U. K.)*. 2007;(46):4898-4900
- [23] Zhou W, Xu J, Zheng H, Liu H, Li Y, Zhu D. Charge transfer chromophore-stopped [2]rotaxane through [2 + 2] cycloaddition. *The Journal of Organic Chemistry*. 2008;**73**(19):7702-7709
- [24] Kivala M, Boudon C, Gisselbrecht J-P, Enko B, Seiler P, Müller Imke B, et al. Organic super-acceptors with efficient intramolecular charge-transfer interactions by [2+2] cycloadditions of TCNE, TCNQ, and F4-TCNQ to donor-substituted cyanoalkynes. *Chemistry—A European Journal*. 2009;**15**(16):4111-4123
- [25] Jarowski PD, Wu Y-L, Boudon C, Gisselbrecht J-P, Gross M, Schweizer WB, et al. New donor-acceptor chromophores by formal [2+2] cycloaddition of donor-substituted alkynes to dicyanovinyl derivatives. *Organic & Biomolecular Chemistry*. 2009;**7**(7):1312-1322
- [26] Andersson AS, Diederich F, Nielsen MB. Acetylenic tetrathiafulvalene-dicyanovinyl donor-acceptor chromophores. *Organic & Biomolecular Chemistry*. 2009;**7**(17):3474-3480
- [27] Fatiadi AJ. New applications of tetracyanoethylene in organic chemistry. *Synthesis*. 1986;**1986**(04):249-284
- [28] Webster OW. Cyanocarbons: A classic example of discovery-driven research. *Journal of Polymer Science Part A: Polymer Chemistry*. 2002;**40**(2):210-221
- [29] Li Y, Fujita H, Hyakutake T, Michinobu T. Side-chain engineering of polyphenylacetylene derivatives for tuning the self-assembly and gas permeability properties. *Journal of Fiber Science and Technology*. 2017;**73**(4):82-86
- [30] Kivala M, Stanoeva T, Michinobu T, Frank B, Gescheidt G, Diederich F. One-electron-reduced and -oxidized stages of donor-substituted 1,1,4,4-tetracyanobuta-1,3-dienes of different molecular architectures. *Chemistry—A European Journal*. 2008;**14**:7638-7647
- [31] Kivala M, Boudon C, Gisselbrecht J-P, Seiler P, Gross M, Diederich F.

Charge-transfer chromophores by cycloaddition-retroelectrocyclization: Multivalent systems and cascade reactions. *Angewandte Chemie, International Edition*. 2007;**46**:6357-6360

[32] Michinobu T, May JC, Lim JH, Boudon C, Gisselbrecht J-P, Seiler P, et al. A new class of organic donor-acceptor molecules with large third-order optical nonlinearities. *Chemical Communications*. 2005:737-739

[33] Michinobu T, Boudon C, Gisselbrecht J-P, Seiler P, Frank B, Moonen NNP, et al. Donor-substituted 1,1,4,4-tetracyanobutadienes (TCBDs): new chromophores with efficient intramolecular charge-transfer interactions by atom-economic synthesis. *Chemistry—A European Journal*. 2006;**12**:1889-1905

[34] Michinobu T, Kumazawa H, Noguchi K, Shigehara K. One-step synthesis of donor-acceptor type conjugated polymers from ferrocene-containing poly(aryleneethynylene)s. *Macromolecules*. 2009;**42**:5903-5905

[35] Yuan Y, Michinobu T, Ashizawa M, Mori T. Microwave-assisted TCNE/TCNQ addition to poly(thienyleneethynylene) derivative for construction of donor-acceptor chromophores. *Journal of Polymer Science Part A: Polymer Chemistry*. 2011;**49**(4):1013-1020

[36] Fujita H, Tsuboi K, Michinobu T. High-yielding alkyne-tetracyanoethylene addition reactions: A powerful tool for analyzing alkyne-linked conjugated polymer structures. *Macromolecular Chemistry and Physics*. 2011;**212**(16):1758-1766

[37] Yuan Y, Michinobu T. Construction of donor-acceptor chromophores in platinum polyyne polymer by [2 + 2] cycloaddition of organic acceptors.

Macromolecular Chemistry and Physics. 2012;**213**(20):2114-2119

[38] Huang W. Synthesis and characterization of a main-chain donor-acceptor type low-bandgap polymer by post-functionalization of a poly(arylene ethynylene). *Reactive and Functional Polymers*. 2014;**83**:42-48

[39] Washio Y, Michinobu T. Emergence of colorimetric chemosensor ability of metal ions in TCNQ polyester by postfunctionalization. *Journal of Photopolymer Science and Technology*. 2012;**25**(3):267-270

[40] Michinobu T. Click-type reaction of aromatic polyamines for improvement of thermal and optoelectronic properties. *Journal of the American Chemical Society*. 2008;**130**(43):14074-14075

[41] Huang W, Chen H. Synthesis and characterization of a low-bandgap poly(arylene ethynylene) having donor-acceptor type chromophores in the side chain. *Macromolecules*. 2013;**46**(5):2032-2037

[42] Washino Y, Michinobu T. Application of alkyne-TCNQ addition reaction to polymerization. *Macromolecular Rapid Communications*. 2011;**32**(8):644-648

[43] Washino Y, Murata K, Michinobu T. Postfunctionalization of aromatic polyamine by [2+2] cycloaddition of 7,7,8,8-tetracyanoquinodimethane with side chain alkynes. *Polymer Bulletin*. 2012;**69**(2):137-147

[44] Ajayaghosh A. Donor-acceptor type low band gap polymers: Polysquaraines and related systems. *Chemical Society Reviews*. 2003;**32**:181-191

[45] Roncali J. Synthetic principles for bandgap control in linear π -conjugated systems. *Chemical Reviews*. 1997;**97**:173-205

- [46] Li Y, Ashizawa M, Uchida S, Michinobu T. A novel polymeric chemosensor: Dual colorimetric detection of metal ions through click synthesis. *Macromolecular Rapid Communications*. 2011;**32**(22):1804-1808
- [47] Li Y, Ashizawa M, Uchida S, Michinobu T. Colorimetric sensing of cations and anions by clicked polystyrenes bearing side chain donor-acceptor chromophores. *Polymer Chemistry*. 2012;**3**(8):1996-2005
- [48] Michinobu T, Diederich F. The [2+2] cycloaddition-retroelectrocyclization (CA-RE) click reaction: Facile access to molecular and polymeric push-pull chromophores. *Angewandte Chemie International Edition*. 2018;**57**(14):3552-3577
- [49] Winder C, Sariciftci NS. Low bandgap polymers for photon harvesting in bulk heterojunction solar cells. *Journal of Materials Chemistry*. 2004;**14**:1077-1086
- [50] Bundgaard E, Krebs FC. Low band gap polymers for organic photovoltaics. *Solar Energy Materials & Solar Cells*. 2007;**91**:954-985
- [51] Kulkarni AP, Tonzola CJ, Babel A, Jenekhe SA. Electron transport materials for organic light-emitting diodes. *Chemistry of Materials*. 2004;**16**:4556-4573
- [52] Chen M, Crispin X, Perzon E, Andersson MR, Pullerits T, Andersson M, et al. High carrier mobility in low band gap polymer-based field-effect transistors. *Applied Physics Letters*. 2005;**87**:252105
- [53] Soudan P, Lucas P, Ho HA, Jobin D, Breaux L, Bélanger D. Synthesis, chemical polymerization and electrochemical properties of low band gap conducting polymers for use in supercapacitors. *Journal of Materials Chemistry*. 2001;**11**:773-782
- [54] Miller JS. Tetracyanoethylene (TCNE): The characteristic geometries and vibrational absorptions of its numerous structures. *Angewandte Chemie, International Edition*. 2006;**45**:2508-2525
- [55] Huang W, Han CD. Synthesis and intramolecular charge-transfer interactions of a donor-acceptor type polymer containing ferrocene and TCNAQ moieties. *Macromolecules*. 2012;**45**:4425-4428
- [56] Michinobu T, Fujita H. Postfunctionalization of alkyne-linked conjugated carbazole polymer by thermal addition reaction of tetracyanoethylene. *Materials*. 2010;**3**(10):4773
- [57] Ohshita J, Kajihara T, Tanaka D, Ooyama Y. Preparation of poly(disilanylenetetra-cyanobutadienyleneoligothienylene)s as new donor-acceptor type organosilicon polymers. *Journal of Organometallic Chemistry*. 2014;**749**:255-260
- [58] Yuan Y, Michinobu T, Oguma J, Kato T, Miyake K. Attempted inversion of semiconducting features of platinum polyyne polymers: A new approach for all-polymer solar cells. *Macromolecular Chemistry and Physics*. 2013;**214**(13):1465-1472
- [59] Washino Y, Tsuboi K, Michinobu T. Simultaneous formation of donor-acceptor chromophores and cross-linking for electro-optic polymer materials. *Journal of Photopolymer Science and Technology*. 2011;**24**(3):305-309
- [60] Washino Y, Michinobu T. Sequence-regulated linear polymers with ion-sensing charge-transfer chromophores by the multiple click approach. *Macromolecular Chemistry and Physics*. 2014;**215**(15):1485-1490
- [61] Yuan Y, Choi W, Nishide H, Michinobu T. Sequential and click-type

- postfunctionalization of regioregular poly(3-hexylthiophene) for realization of n-doped multiplet state. *Chemical Science*. 2013;**4**(1):345-350
- [62] Ko Y-G, Kim DM, Kim K, Jung S, Wi D, Michinobu T, et al. Digital memory versatility of fully π -conjugated donor-acceptor hybrid polymers. *ACS Applied Materials & Interfaces*. 2014;**6**(11):8415-8425
- [63] Michinobu T, Seo C, Noguchi K, Mori T. Effects of click postfunctionalization on thermal stability and field effect transistor performances of aromatic polyamines. *Polymer Chemistry*. 2012;**3**(6):1427-1435
- [64] Shi W, Ma F, Hui Y, Mi H, Tian Y, Lei Y, et al. TCNE-decorated triphenylamine-based conjugated polymer: Click synthesis and efficient turn-on fluorescent probing for Hg^{2+} . *Dyes and Pigments*. 2014;**104**:1-7
- [65] Yuan Y, Michinobu T. Energy level tuning of polythiophene derivative by click chemistry-type postfunctionalization of side-chain alkynes. *Journal of Polymer Science Part A: Polymer Chemistry*. 2010;**49**(1):225-233
- [66] Yongrong L, Tsuyoshi H, Tsuyoshi M. Oxygen permeability change of polyphenylacetylene derivatives by postfunctional TCNE addition. *Chemistry Letters*. 2011;**40**(6):570-572
- [67] Wang D, Zhang R, Gao H, Wang X, Wang H, Yang Z, et al. Energy-level tuning of poly(p-phenylenebutadiynylene) derivatives by click chemistry-type postfunctionalization of side-chain alkynes. *Reactive and Functional Polymers*. 2016;**105**:114-121
- [68] Li Y, Michinobu T. Sequential double click reactions: A highly efficient post-functionalization method for optoelectronic polymers. *Polymer Chemistry*. 2010;**1**(1):72-74
- [69] Li Y, Tsuboi K, Michinobu T. Double click synthesis and second-order nonlinearities of polystyrenes bearing donor-acceptor chromophores. *Macromolecules*. 2010;**43**(12):5277-5286
- [70] Li Y, Tsuboi Y-K, Michinobu T, Ishida Y, Hirai T, Hayakawa T, et al. Efficient synthesis of block copolymers bearing donor-acceptor chromophores for second-order nonlinear optical applications. *Journal of Photopolymer Science and Technology*. 2010;**23**(3):337-342
- [71] Song S, Ko Y-G, Lee H, Wi D, Ree BJ, Li Y, et al. High-performance triazole-containing brush polymers via azide-alkyne click chemistry: A new functional polymer platform for electrical memory devices. *NPG Asia Materials*. 2015;**7**:e228
- [72] Grigoras M, Ivan T, Vacareanu L, Catargiu AM, Tigoianu R. Synthesis and optoelectronic characterization of some triphenylamine-based compounds containing strong acceptor substituents. *Journal of Luminescence*. 2014;**153**:5-11
- [73] Michinobu T, Li Y, Hyakutake T. Polymeric ion sensors with multiple detection modes achieved by a new type of click chemistry reaction. *Physical Chemistry Chemical Physics*. 2013;**15**(8):2623-2631
- [74] Wang Y, Michinobu T. Polymeric chemosensors: A conventional platform with new click chemistry. *Bulletin of the Chemical Society of Japan*. 2017;**90**(12):1388-1400
- [75] Li Y, Washino Y, Hyakutake T, Michinobu T. Colorimetric ion sensors based on polystyrenes bearing side chain triazole and donor-acceptor chromophores. *Analytical Sciences*. 2017;**33**(5):599-604

[76] Tang X, Liu W, Wu J, Zhao W, Zhang H, Wang P. A colorimetric chemosensor for fast detection of thiols based on intramolecular charge transfer. *Tetrahedron Letters*. 2011;52(40):5136-5139

[77] Fujita H, Michinobu T, Tokita M, Ueda M, Higashihara T. Synthesis and postfunctionalization of rod-coil diblock and coil-rod-coil triblock copolymers composed of poly(3-hexylthiophene) and poly(4-(4'-N,N-dihexylaminophenylethynyl)styrene) Segments. *Macromolecules*. 2012;45(24):9643-9656

[78] Fujita H, Michinobu T, Fukuta S, Koganezawa T, Higashihara T. Sequentially different ab diblock and aba triblock copolymers as P3HT:PCBM interfacial compatibilizers for bulk-heterojunction photovoltaics. *ACS Applied Materials & Interfaces*. 2016;8(8):5484-5492

[79] Li Y, Michinobu T. Multi-coloration of polyurethane derivatives through click postfunctionalization, electrochemical oxidation, and Ag⁺ ion complexation. *Journal of Materials Chemistry*. 2012;22(19):9513-9521

Application of Organic Coagulants in Water and Wastewater Treatment

Emmanuel Kweinor Tetteh and Sudesh Rathilal

Abstract

Coagulation is an essential mechanism that occurs in most conventional water and wastewater treatment plants. This occurs in a physical purification unit involving transport processes and the addition of coagulants for chemical reactions, charge neutralization, and formation of smaller flocs to agglomerate into larger flocs. This enhances the effective removal of recalcitrant contaminants by downstream processes. However, poor treatment of wastewater might have a high negative impact on biodiversity and the environment in general. This chapter seeks to address the limitation of employing inorganic coagulants by evaluating the efficiency of organic coagulants and exploring the factors and mechanism governing coagulation in a physiochemical treatment process of water and wastewater resources. The effect of pH, coagulant type and dosage to ease the high sludge production and discharge of residual metals into the downstream waters is addressed. The emerging of organic coagulants and technology to mitigate the performance and recovery of mineral coagulants from wastewater treatment residual is been proposed.

Keywords: coagulation, organic polymers, water and wastewater, purification

1. Introduction

The deterioration of the natural source of fresh water supply correlates with the increase in global social economic growth and activities, which generates wastewater with a high content of pollutants [1, 2]. Due to the detrimental effects of pollution in wastewater, water-related technologies and materials development have become the utmost priority in most of the wastewater industrials [2, 3]. Among the numerous purification methods, integrating coagulation along with filtration [2–4], sedimentation or flotation [5, 6] have been well-known pre-treatment techniques in water and wastewater settings where water quality is cardinal [7]. However, a variation of inflow water quality and lack of optimized treatment facilities result in decreasing the treatability efficiency with the incurred cost of production [8, 9]. Chemical purification process, well known as coagulation, even though it's essential in wastewater settings, sometimes is seen to be an expensive technology due to the cause of cost of chemical usage involved [10–12]. This method involves the precipitation of the soluble metal ions by using coagulants. Subsequently, the long-term application of metal-based coagulants (aluminum and iron) [11] has raised concerns associated with sludge generation and heavy metal residuals which are potentially toxic

to the ecosystem [10–12]. This has resulted in most effluent not complying with the stringent Environmental Protection Agency's standards for regulating the quality of effluent plants [8].

In a typical wastewater treatment plant (**Figure 1**), a mixture of inorganic and organic polymer additives are usually employed as a heterocoagulation technique [14, 15]. This is to accelerate the agglomeration and coalescing of weighted particles to be separated from the water either by sedimentation or flotation techniques [5, 6]. However, most of the industrial wastewaters from the oil refinery, food, and the agricultural processing industries contain organics, suspended and emulsified oil and grease that prefer to float than settle [10, 15, 16]. Also, to enhance dewatering and advanced treatment of sewage which includes the removal of phosphorus, the utilization of polymers has become a very common practice [14, 17, 18]. Although, coagulant chemicals and its derivatives are very resourceful in wastewater treatment settings, they may alter the characteristics of the effluents in terms of its physiochemical properties [11, 17]. Also, the problem related to disposal of huge sludge and metals in the effluents, for instance in the application of hydroxide precipitation [4, 13, 19], requires a technique to recover the valuable or toxic metals from the sludge [20, 21]. In response to this, Donnan membrane technology which requires a lower operating pressure than others has been one of the fields tested technique in the wastewater treatment settings. However, the cost of the membrane is one of the setbacks [20–22].

As some of the limitations associated with inorganic based coagulants are being mentioned, this study focuses on the option for the natural and composite inorganic-organic polymer to maximize the treatability performance in the wastewater settings. Therefore, the goal is to evaluate the efficiency of organic polymers as coagulant agents for the treatment of water and wastewater and also to provide an alternative option to metal salts for the chemical purification process. This is done by exploring the use of organic polymer coagulant techniques as compared to metal-based salt coagulants in existing conventional treatment methods on the basis of effectiveness. Furthermore, to identify some of the operating conditions that affect chemical purification process.

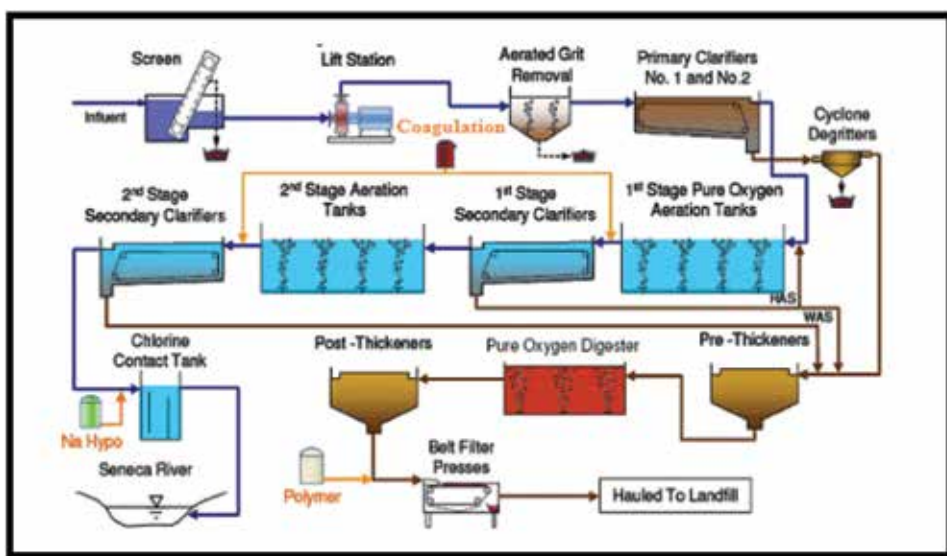


Figure 1. Schematic flow chart of a typical sewage treatment plant adapted from [13].

2. Chemical purification process

Chemical treatment using metal salts of iron and aluminum is widely applied in several wastewater treatment industries as primary treatments for the removal of particulate and organic matter effectively [23]. **Figure 2** shows a typical chemical treatment process for both wastewater and drinking water settings, which usually consists of coagulation, flocculation, and sedimentation or flotation [24]. Coagulation is an indispensable mechanism that promotes the aggregation of the suspended solids, which are mostly responsible for turbidity, color, and taste and odor removal [24–26]. The flocculation facilitates the agglomeration of the coagulated particles to form larger flocs, thereby hastening the gravitational settling or flotation process for the removal of contaminants [24]. The spontaneous forming of flocs in suspension is term as flocculation. This is usually applicable in water purification and sewage treatment. The cationic polyelectrolytes have been the most viable flocculants. Their low charge density makes not to reverse the surface charge and hence they are less prone to induce destabilization.

Also, agglomeration of particles to form large and stable flocs involve mixing of the coagulants with the wastewaters usually monitored via Jar test. However, there are several types of coagulants which show the different potential application in treating drinking water or wastewater [11, 17, 27]. Due to the detrimental effects of discharging untreated wastewater, it is essential for purification systems to be well established and optimized [28, 29]. Ideally, the suitable operation conditions required depends on the characteristics of the wastewater and the coagulants, as well as the physical properties as shown in **Table 1**.

2.1 Types of chemical treatment processes

2.1.1 Coagulation and sedimentation

Coagulation, flocculation and sedimentation processes in water and wastewater treatment are crucial. The first stage in most chemical water treatment processes is coagulation, whose performance is dependent on coagulant concentration and the water chemistry [12, 14]. Essentially, there are four coagulation mechanisms for aggregation of particles to occur, namely (1) double layer compression;

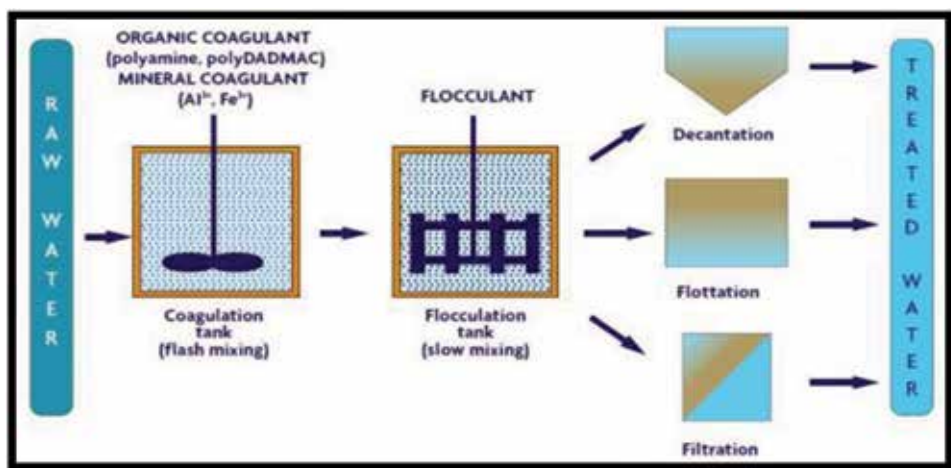


Figure 2.
Physicochemical treatment process [24].

Coagulant characteristics	MOW characteristics	Physical characteristics
Coagulant type	Water quality	Flotation/settling time
Coagulant dosage	Suspended solids	Mixing intensity
Coagulant quality	Temperature	Coagulant dosage end point
Coagulant lifespan	pH	Chemical stability during storage
Proper solution makeup and dilution	Alkalinity	
	Ionic constituents	

Table 1.
Factors that affect the chemical purification process [17].

(2) sweep flocculation; (3) adsorption and charge neutralization; and (4) adsorption and interparticle bridging [13, 17–24]. This involves the reaction between the colloids and the added coagulant to destabilize and neutralize the electric charges in the particles, whereas the flocculation facilitates the agglomerated flocs in the colloidal suspension.

For instance (**Figure 3**), the addition of the coagulant is accountable for the creation of small scattered particles which come together into larger and more stable particle flocs. These then make the flocs heavier than the water, which settle as sediments and can be removed. This results in the removal of about 90% of the suspended matter [1, 2]. Furthermore, the coagulation step depends on conditions of time and agitation whereby the particles coalesced to form larger flocs could be eliminated by sedimentation.

2.1.2 Coagulation and flotation

Conventionally, flotation is a concentration process in which selective hydrophobic materials are separated from hydrophilic materials by a gravity separation process [30]. In a typical flotation process (**Figure 4**), the coagulated particles adhere to air bubbles lowering the apparent density below that of the water, which then allows the flocs to float to the surface. To cause a change in the separation phase

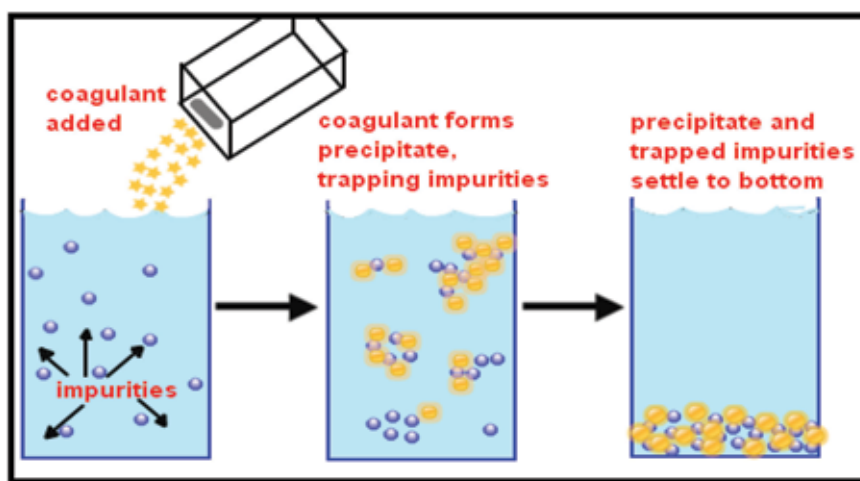


Figure 3.
Process of coagulation, flocculation, and sedimentation [24].

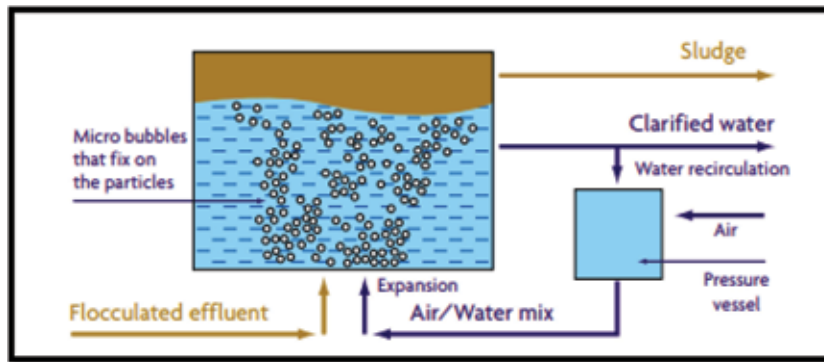


Figure 4.
Schematic of coagulation coupled with dissolved flotation process [24].

depends on four mechanisms such as (1) air bubble generation, (2) contact between air bubble and the particulates, (3) attachment of gas bubbles to particulates, and (4) rising up of the combined air bubble- particulate [31, 32].

The addition of the coagulant enhances the air bubbles and organic matter to form robust flocs that can resist breakage in the flotation zone [33]. However, this process is somehow complicated because it requires the hydrodynamics and surface chemistry interaction via the means of bubble attachment, where the bubbles are generated as a result of compressed air released into the flotation zone. Therefore, to obtain good performance, studies have shown that coagulation chemistry has a strong influence on flotation performance [34], such that the chemical reaction between the coagulants and the organic matter results in forming larger oil flocs, whereas, the flotation process facilitates separation [35, 36]. This allows the coagulated flocs to float on the surface as sludge, whereas clear water moves to the bottom of the floatation tank to the sewer as treated water.

2.2 Parameters affecting coagulation treatment efficiency

There are several operating factors that have an impact on the parallel and sequential reactions that occur when a coagulant is added to the wastewater. To promote the interparticle bridging and floc formation, there are a series of transportation mechanisms which occurs including Brownian diffusion and fluid motion. All these influence the efficiency and effectiveness of the coagulation process for wastewater treatment.

2.2.1 Effects of polymer molecular weight and charge density

Polymer molecular weight (MW) and charge density (CD) affects the interparticle bridging and electrostatic force mechanism which contributes to the coagulation efficiency [37, 38], such that an increase in molecular weight improves agglomeration and floc formation. Although anionic charge on the polymer can obstruct adsorption onto an undesirable surface, it promotes the polymer chain via mutual charge repulsion between polymer molecules [39]. Organic polymer concentration originates to be free of molecular weight but reliant on ionic strength. The CD is generally expressed as a percentage of ionic groups (both those that are charged, irrespective of pH and those that can become charged under certain pH conditions) relative to all the groups in the polymer. The CD is expressed in terms of length (qL), area (qA) and volume (qV) as shown in (1)–(3) as a function of the amount of ionic charge (qQ) per length (L), area (A) or volume (V) respectively.

$$q_l = \frac{d_Q}{L} \quad (1)$$

$$q_A = \frac{d_Q}{A} \quad (2)$$

$$q_V = \frac{d_Q}{V} \quad (3)$$

2.2.2 Temperature

Temperature serves as the driving force for chemical reaction. This affects the coalescence and the physical properties of the polymer including viscosity, mobility, collision, and solubility, density, rising or settling velocity of the flocs. Thus, higher temperature hastens the rate of chemical reactions, whereas low temperatures stabilize the colloidal surfaces to reduce the hydrolysis reactions [38, 40]. This might affect the free movement of the particles and higher solubility as well as higher reaction kinetics of the polymer applied, which in turn decreases the coagulation efficiency.

2.2.3 Effects of mixing conditions

The degree of coagulation completion for effective treatment can be related to coagulant dosage and mixing conditions. Sequentially, destabilization and agglomeration of coagulated flocs occur through two mixing regimes, viz. rapid mixing and slow mixing as shown in **Figure 5**. The rapid or fast mixing occurs after the addition of the coagulants, which requires turbulent mixing to form a homogeneous solution [24, 25, 29]. Lack of rapid mixing might cause poor performance of the coagulants due to under dose or overdose. On the other hand, slow mixing comes soon after rapid mixing, and is intended to increase the particle entrapment and growth of the flocs.

Furthermore, consistent slow mixing accelerates the rate floc aggregation and entrapment of the particles in suspension to enhance separation. Slow mixing provides a velocity gradient for particles with similar size that can be larger than 1 μm . Such that the relation between the aggregation of a given size and the polymer MW can enhance the bridging or breaking forces of the flocs to either settle or float [33, 36, 38]. In practice (**Figure 5**), this is achieved by a suspension being stirred at a high rate (250 rpm) to cause floc breakage, and after the breakages, the slow mixing (30 rpm) is initiated to increase the floc size [24, 27]. In flotation principle, a lower dosage of the polymer can be used because the agitation creates a well-established suspension of smaller flocs to agglomerate to float [33, 41].

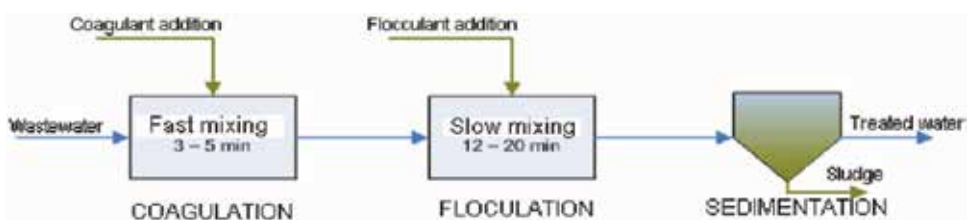


Figure 5. Schematic steps of mixing in coagulation process.

2.2.4 Effects of pH

The pH plays a dominant role in coagulant-particle interaction for effective neutralization and agglomeration of the flocs. In addition, the solubility of metal hydroxide species can be affected by pH (4–8) [36, 41]. Therefore pH adjustment prior to coagulant addition is very important to influence the chain reactions that will occur. The effective species of inorganic coagulants or polymers being a metal-based ion can affect the floc formation through a double-layer compression [24, 38]. With an increase in pH, these species become charged resulting in a change in mechanism. For instance, when the colloids are hydrophilic, e.g. acids, the pH will affect the protonation.

2.2.5 Coagulant type and dosage

There are various types of coagulants used in wastewater settings, such as inorganic and organic polymers. However, polymers are generally more costly than inorganic coagulants. This depends on the type and quantity of chemical the coagulant might contain. Selection of the suitable coagulant for wastewater treatment is very important, which also depends on the water chemistry, the hydrodynamics and operating conditions of the processing system [4, 41]. Coagulant dosage is an energetic factor in finding how the metal ions react with the organic matter in wastewater to enhance its clarity.

Organic polymers by nature are very viscous solutions, which sometimes becomes problematic to be distributed homogeneously in a medium [15, 17]. However, they are very attractive towards particle surfaces, which is irreversible when attached. So uneven distribution of polymers in polluted wastewater might contribute to inefficiency and cost of the treatment process [17, 18, 24]. Thus, the dosage needs to be stepped up in order to compensate for the loss of the polymer.

2.2.6 Ionic strength

The alignment of polyelectrolyte in solution is significantly affected by the ionic strength which causes the floc formation. The metal ions hinders the hydrolysis activity when a metal-based coagulant is added to a solution [24, 38, 40]. In contrast, like-charges of a polymer chain tend to expand when there is a mutual repulsion. This is directed to an increase in viscosity of a polyelectrolyte solution as ionic strength decreases. Also, an increase in ionic strength shields the charged site of the polymer which then affects its hydrodynamic volume expansion by decreasing the viscosity of the solution [39, 40]. This causes a double layer compression to be formed around the floc surface area where there might be oppositely charged ions.

3. Coagulants

There are several types of coagulants which are applicable to water and wastewater treatment settings [42]. These can either be chemical, non-chemical, synthetic material or natural coagulants. However, each type of coagulant has its own unique properties with positive ions which will entrap the negative charge of the organic matter in the water that causes turbidity.

3.1 Inorganic coagulants

Aluminum and iron salts are the most commonly used inorganic coagulants in the wastewater treatment settings. These include based aluminum metals (aluminum

chloride, aluminum sulfate, sodium aluminate) and iron based metals (ferrous sulfate, ferric sulfate, ferric chloride) [13, 17, 18]. The addition of these coagulants to wastewater undergo a series of reactions with the hydroxyl ions (OH^-) producing monomeric and polynuclear species. These results in dissociation of their metal salts to release their trivalent ions, which hydrates to give complex water molecules of Al (H_2O) $_6^{3+}$ and Fe (H_2O) $_6^{3+}$ for aluminum and iron respectively [26, 37, 39, 43]. This results in the replacement of the water molecules (H_2O) by OH^- ions to form soluble Al (OH) $_2^+$ and Fe (OH) $_2^+$ which increases the coagulation performance by the trivalent ions being strongly adsorbed onto the negative surface of the colloids [26, 29].

Consequently, metal-based coagulants are most widely used due to their low cost and availability; however, there are some drawbacks [17, 18]. These include high dosage dependence, a high requirement on pH, weakness to temperature disparity and high sludge generation. Some of these inorganic coagulants with their merits and demerits are presented in **Table 2**. Furthermore, an overdose of aluminum and iron in effluent poses a threat to both the ecosystem and human health such as intestinal constipation, abdomen colic and spasms. In addition, Ferric-based coagulants are very caustic and produce highly visible rust-colored stains associated with chemical spills and leaks [25, 33]. Therefore, there is great interest in improving inorganic coagulants by employing polymeric organic and natural coagulants for the treatment of wastewater.

3.2 Organic coagulants

Organic coagulants are generally synthesized monomers of aluminum and iron-based coagulants, applicable in the wastewater settings as coagulant aids or floc builders [15, 17]. **Table 3** shows some of the organic coagulants which are usually employed in potable and wastewater treatment after the addition of inorganic

Name	Advantages	Disadvantages
Aluminum sulfate (Alum) $\text{Al}_2(\text{SO}_4)_3 \cdot 18\text{H}_2\text{O}$	Easy to handle and apply; most commonly used; produces less sludge than lime; most effective between pH 6.5 and 7.5	Adds dissolved solids (salts) to water; effective over a limited pH range
Sodium aluminate $\text{Na}_2\text{Al}_2\text{O}_4$	Effective in hard waters; small dosage usually needed	Often used with alum; high cost; ineffective in soft waters
Polyaluminium chloride (PAC) $\text{Al}_{13}(\text{OH})_{20}(\text{SO})_4\text{Cl}_{15}$	In some applications, Floc, formed is denser and faster settling than alum	Not commonly used; little full-scale data compared to other aluminum derivatives
Ferric sulfate $\text{Fe}_2(\text{SO}_4)_3$	Effective between pH 4–6 and 8.8–9.2	Adds dissolved solids (salts) to water; usually, need to add alkalinity
Ferric chloride $\text{FeCl}_3 \cdot 6\text{H}_2\text{O}$	Effective between pH 4 and 11	Adds dissolved solids (salts) to water; consumes twice as much alkalinity as alum
Ferrous sulfate $\text{FeSO}_4 \cdot 7\text{H}_2\text{O}$	Not as pH sensitive as lime	Adds dissolved solids (salts) to water; usually need to add alkalinity
Lime $\text{Ca}(\text{OH})_2$	Commonly used; very effective; may not add salts to effluent	pH-dependent; produces large quantities of sludge; overdose can result in poor effluent quality

Table 2. Advantage and disadvantage of inorganic coagulants [18, 33, 41].

Name	Formula	Typical properties	Uses
Polyaluminium chlorohydrate (ACH) $Al_2(OH)_5Cl$	PAC 23	* 23–24% Al_2O_3	Used in lieu of alum where raw water has low pH & alkalinity. Has little impact on pH
	MEGAPAC 23	or 40–41% w/w ACH	
	ALCHLOR AC	* SG 1.33	
		* 83–84% basicity	
	PROFLOC A23	* 8.5% w/w Cl *535 g/l	
Polyaluminium chloride (PACl) $Al_2(OH)_3Cl_3$	PAC-10 LB	* 10–11% Al_2O_3	Used in lieu of alum where raw water has low pH & alkalinity. Has greater impact on pH than ACH
	MEGAPAC 10	or 20–23% w/w PACl	
		* SG 1.18	
		* 50% basicity	
		* 10.5% w/w Cl * 245 g/l	
Polyaluminium silicosulphate $Al_2(OH)_{3.24}Si_{0.1}(SO_4)_{1.58}$	PASS [®]	* 10% Al_2O_3 or 5.3% w/w Al	Forms flocs easily
		* SG 1.34	
		* 54% basicity	
Polyferric sulfate $Fe_2(OH)_{0.6}(SO_4)_{2.7}$	PFS [®]	* 12.2% w/w Fe(III) or 43.7% w/w $Fe_2(SO_4)_3$	Mostly used for oil emulsified wastewater
		* SG 1.54	
		* 10% basicity	
		* 673 g/l	

Table 3. *Examples of organic polymer coagulants for water and wastewater treatment [16, 24].*

coagulants to enhance its treatment efficiency [15]. There are various types of organic coagulants, which have different covalent charges and bonds of their polymeric molecules. These include the charge or ionic polymers (polyelectrolytes) and no charge or non-ionic polymers [15, 25]. In respect to the charge polymers, those with a positive charge are termed as cationic polymers, whereas those with negative charges are called anionic polymers.

4. General characteristics of coagulants

There are two characteristics of polymers that defines them to be used as coagulant or flocculant aids [15, 17]. These include (1) they have a very high charge density to neutralize the negative charges present on the surface of the colloidal material, and (2) they have a relatively low molecular weight (MW) which allows good diffusion of the cationic charges around the particles. This enhances good distribution of the coagulant in the effluent, when not concentrated at low viscosity of less than 2×10^3 centipoises, and when concentrated at a high viscosity of 20×10^3 centipoises [14, 15, 24]. Organic polymers have long chain molecular weights, which consists of repeating chemical units called monomers. This makes them be classified as low with MW less than 10^5 , and medium and high when they are between 10^5 and 10^6 and more than 10^6 respectively [14, 15, 17].

4.1 Methods of polymerization

Organic polymer coagulants can exist in different forms which is due to the method of polymerization such as liquid, beads, powder, emulsion, and dispersion [15, 24].

- (a) Powders: The polymerized monomers are obtained in a gel form, which is then grounded and dried.
- (b) Beads: The monomers are polymerized by adding a solvent to be made to be a suspension. The solvent is later evaporated to obtain microspheres. This prevents dust and enhances rapid dissolution.
- (c) Emulsions: The monomers are emulsified in a solvent before being polymerized. Afterwards, a surfactant is added to make it dissolvable in water.
- (d) Liquids: The monomers are polymerized at low concentration in aqueous solutions, making it effortless to use.
- (e) Dispersions: In this case, the monomers are usually dispersed in brine before being polymerized. This is done as direct feed inline without any solvent or surfactant and aging time. These are applicable in the flotation process, making it a cost-effective process for the treatment of oil refinery wastewater. **Figure 6** shows the dissociation of the ionic charge of the polymer when introduced into a receiving medium (emulsion of oil-water).

4.2 Types of polymeric coagulants

Hydrophobic organic coagulants adapted from inorganic coagulants have gained attention in application due to their unique characteristics. Organic polymers, in general, are classified as natural and synthetic polymers [14, 15, 17]. Natural polymers are hydrophilic compounds which carry natural characteristics as being nontoxic to humans, readily available and environmentally friendly. However, the use of natural polymers only might not be effective in all cases in wastewater

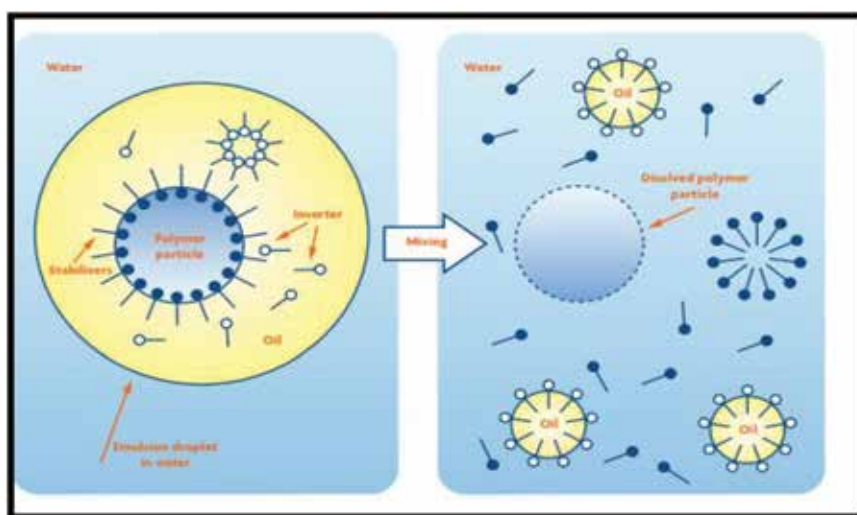


Figure 6. Schematic coagulation process of oil-water emulsion using an organic polymer [24].

treatment settings. This might be due to their properties which cannot be modified (e.g. Chitosan, tannin, starch, *Moringa oleifera*). Natural polymers are usually mixed with inorganic coagulants to enhance their treatability efficiency, although synthetic polymers can at times be toxic to humans [11, 14, 44].

Organic polymers can easily be modified and optimized during the manufacturing process for wider application. Several polymers are produced with polymer chains of the linear, branched or cross-linked form of structures [11, 18]. For instance, **Figure 7** shows the chemical structure of poly diallyl dimethyl ammonium chloride (pDADMAC), epichlorohydrin/dimethylamine polymers (ECH/DMA) and cationic polyacrylamides (CPAMs) are examples of cationic synthetic polymers while chitosan is an example of the cationic natural polymer [15, 17, 24].

4.2.1 Anionic polymers

Anionic polymers are amphoteric polymers, which gets a negative charge when their ionic groups dissociate in a medium [15, 17]. Their polymerization is very sensitive, involving a change in molecular weight, charge groups and density as well their structure being linear or branched as shown in **Figure 8**. This is usually instigated by using either active anionic species like sodium, nitrile, hydroxide or cationic species such as hydrochloric acid, sulfuric acid, and phosphoric acid. Subsequent hydrolysis of the polyacrylamide under basic pH conditions produces a polymer with anionic charges. **Table 4** shows the molecular formulas of anionic APAMs or PAMs, containing changing proportions of acrylamide co-monomers in terms of charge density (mol%) and a theoretical basis in meq/g of polymer.

4.2.2 Cationic polymers

Cationic polymers are positively charged natural or synthetic based organic coagulants. Some of these polymers have charge ammonium groups making them strong electrolytes irrespective of their pH variation [15, 17]. For instance, pDADMAC, ECH/DMA and CPAMs are synthetic cationic polymers while Chitosan is a

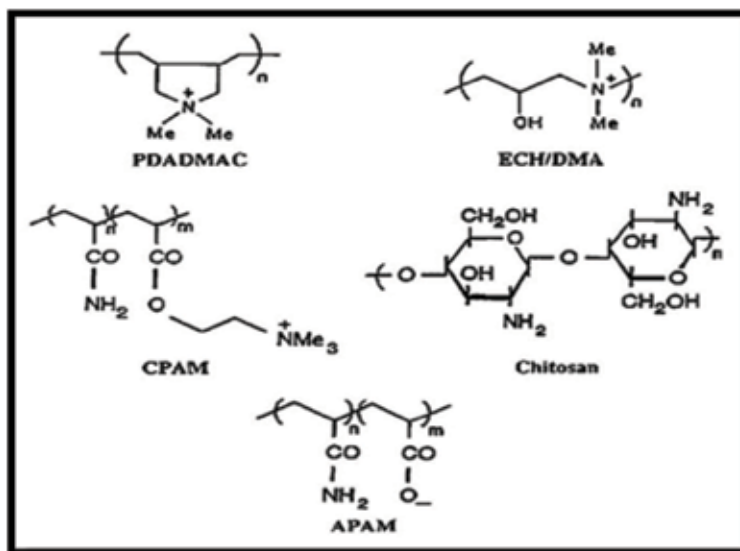


Figure 7. Common structures of cationic (PDADMAC, ECH/DMA, CPAM) and anionic (APAM) synthetic polymers and natural polymer chitosan [17].

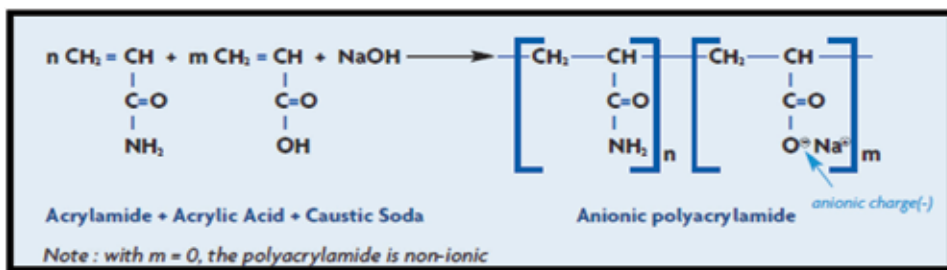


Figure 8.

Copolymers of acrylamide and acrylic acid to form anionic polyacrylamides [24].

natural cationic polymer as mentioned previously. The hydrolysis of the ester groups and consequent loss of cationic charge is CD and pH dependent. **Table 5** outlines the CD of various cationic polymers in mol% and meq/g of polymer. The higher charge density shows that the polymer has a greater loop which enhances interparticle bridging and effective destabilization of the medium. **Figure 9** shows the cationic polymer structure, denoting polymerization of acrylamide followed by partial hydrolysis.

4.2.3 Natural or non-ionic polymers

There are several naturally-occurring polymers that have inherent cationic properties, which can be modified to yield a cationic polyelectrolyte to be used for solid-liquid separations as flocculants [11]. Non-ionic polymers vary in structure, molecular weight and degradability. Some examples include polyacrylamides (PAMs), Chitosan, starch without substitutions, cellulose derivative, and glues [17, 38, 44]. Chitosan, like most natural polymers, is toxic free which makes them generally acceptable on health grounds. The use of chitosan in water purification applications has been referenced to decolorizing dye house effluents, the treatment of food-processing wastes, metal ion removal and sludge conditioning.

Subsequently, organoclay which are by-products from natural or synthetic materials are being used as adsorbents for water treatment. They are generally known as low-cost adsorbents which are readily available. These include ball clay, bentonite and kaolin. Organoclay is also a result of merging sodium montmorillonite clay with a cationic quaternary amine salt which interchanges the adsorbed sodium through ion exchange [17, 25].

Furthermore, plants and minerals are a cardinal source of natural polymers. Some examples includes: *Nirmali* seeds, *Moringa oleifera*, Tannin, eggplant seed and radish seed which are locally available from vegetables for treatment [14, 15, 44]. These coagulants are nontoxic, renewable, produce lower sludge, biodegradable and relatively cost-effective. Moreover, natural coagulants have a wide range of effective

Molecular formula	CD (mol %)	CD (meq/g)
$\text{C}_3\text{H}_3 \text{O}_2\text{Na}$	100	10.2
$(\text{C}_3\text{H}_3 \text{O}_2\text{Na})_{0.75}(\text{C}_3\text{H}_5 \text{ON})_{0.25}$	75	8.5
$(\text{C}_3\text{H}_3 \text{O}_2\text{Na})_{0.50}(\text{C}_3\text{H}_5 \text{ON})_{0.50}$	50	6.1
$(\text{C}_3\text{H}_3 \text{O}_2\text{Na})_{0.25}(\text{C}_3\text{H}_5 \text{ON})_{0.75}$	25	3.3
$(\text{C}_3\text{H}_3 \text{O}_2\text{Na})_{0.1}(\text{C}_3\text{H}_5 \text{ON})_{0.9}$	10	1.4

Table 4.

Charge densities of anionic polyacrylamides [17].

Polymer	Molecular formula	CD (mol %)	CD (meq/g)
PDADMAC	$C_8H_{16}NCl$	100	6.2
ECH/DMA	$C_5H_{12}ONCl$	100	7.3
CPAM	$C_8H_{16}O_2NCl$	100	5.2
CPAM	$(C_8H_{16}O_2NCl)_{0.5}(C_3H_5ON)_{0.5}$	50	3.8
CPAM	$(C_8H_{16}O_2NCl)_{0.25}(C_3H_5ON)_{0.75}$	25	2.5
CPAM	$(C_8H_{16}O_2NCl)_{0.1}(C_3H_5ON)_{0.9}$	10	1.2
Chitosan	$C_6H_{11}O_4N.HCl$	100	5.2

Table 5.
 Charge densities of cationic polyelectrolytes [17].

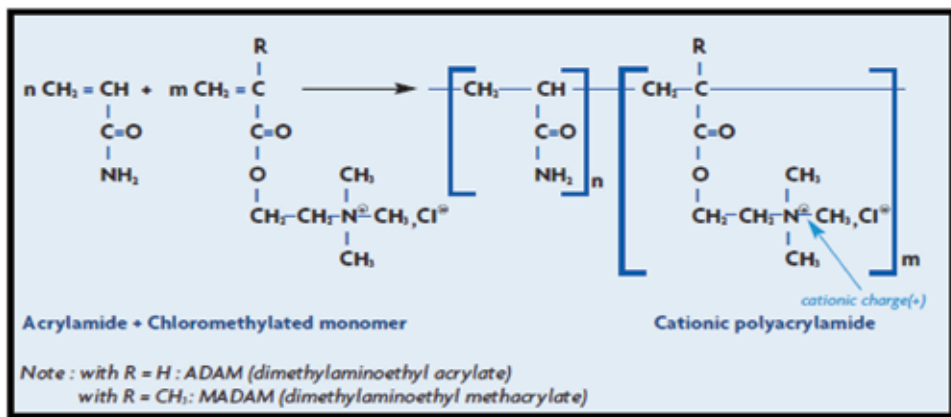


Figure 9.
 Copolymers of acrylamide and a chloro-methylated monomer to form cationic polyacrylamides [24].

dosage and do not change the value of pH for the treated water. Another example of a plant-based coagulant using unexploded waste is cassava peel. Fresh cassava peels have three main efficiencies: spread very rapidly, contain phytates, and huge amounts of cyanogenic glycosides [3, 44].

4.2.4 Application of organic polymers

Organic polymers and inorganic coagulants over the years have been used in chemical treatment and purification of water and wastewater [41]. These are used in chemical treatment to assist sedimentation of sewage solids to enhance the removal of suspended matter. Coagulation used ahead of gravity settling may be expected to yield suspended solid removals of about 90% as compared to without coagulation [1, 11]. This concept is also applicable to primary coagulation of industrial wastewaters where the separation may be based on flotation, as in examples from the leather, steel, wool scouring, cosmetic, detergent, plastics, dyehouse, paper, food processing, and brewing industries. The cationic polymer which is hydrophobically modified is significant in the case of soap, oil and grease removal. **Table 6** shows some examples for the application of organic polymers for the treatment of wastewater.

Their many advantages associated with organic polymers been used as primary coagulants, however, it is sometimes quite challenging selecting the suitable one for specific water treatment. The selection of the right polymer to use under the

Industries	Coagulant	Dosing	Performance	Reference
Pulp and paper	Poly-aluminum-silicate-chloride	40 mg/l	93.13% COD 91.12% turbidity	[45]
Textile industry	PAC	25 mg/l	90.17% COD, 74.09% TDS and 93.47% turbidity	[37]
Dye wastewater	Polyferric chlorides (PFCs)	30 mg/l	55% reduction	[46]
Vegetable tannery wastewater	PACl (poly aluminum chloride)	60 mg/l	45%TSS, 20% COD and 80% turbidity	[47]
Palm oil effluent	PAC	0.5 g/l, 8.0 and 60 g/l	99% SOG	[48]

Table 6.
Application of organic polymers in wastewater settings.

circumstances in question depends on their molecular weight, charge density, and structure, dose, mixing condition, amount and type of impurities found in the water and pH dependency. However, to achieve optimum stabilization and agglomerating of flocs requires optimum dosage, which is inversely dependent on the size of the particles in suspension [39, 40].

5. Conclusion

Coagulation is one of the simplest methods for the treatment of water and wastewater, especially for non-settleable solids, turbidity, and color from effluents. Application of coagulation is expected to enhance the gravity system for the removal of suspended solids of about 90% as compared to a system without coagulation. Thus, the issue of sludge sedimentation which must be floated is relatively low to flotation systems utilizing organic polymers rather than inorganic coagulants. This chapter addresses the limitation associated with coagulation using inorganic coagulants, by highlighting some of the eco-friendly organic coagulants and operating parameters of coagulation for water and wastewater treatment. Also, composite polymerization and impregnation of organic polymers with inorganic coagulants as a research area should be focused for commercialization and industrialization.

Acknowledgements


The authors wish to thank the Durban University of Technology and National Research Foundation South Africa for their support.

Author details

Emmanuel Kweinor Tetteh* and Sudesh Rathilal
Faculty of Engineering and the Built Environment, Department of Chemical
Engineering, Durban University of Technology, Durban, South Africa

*Address all correspondence to: ektetteh34@gmail.com

IntechOpen

© 2019 The Author(s). Licensee IntechOpen. This chapter is distributed under the terms of the Creative Commons Attribution License (<http://creativecommons.org/licenses/by/3.0>), which permits unrestricted use, distribution, and reproduction in any medium, provided the original work is properly cited. 

References

- [1] Choy SY, Prasad KMN, Wu TY, Raghunandan ME, Ramanan RN. Utilization of plant-based natural coagulants as future alternatives towards sustainable water clarification. *Journal of Environmental Sciences*. 2014;**26**(11):2178-2189
- [2] Jones DL, Freeman C, Sánchez-Rodríguez AR. Waste water treatment. In: *Encyclopedia of Applied Plant Sciences*. UK: Academic Press; 2016
- [3] Yin CY. Emerging usage of plant-based coagulants for water and wastewater treatment. *Process Biochemistry*. 2010;**45**(9):1437-1444
- [4] Konieczny K, Sakol D, Płonka J, Rajca M, Bodzek M. Coagulation-ultrafiltration system for river water treatment. *Desalination*. 2009;**240**(1-3):151-159
- [5] de Sena RF, Tambosi JL, Genena AK, Moreira R d FPM, Schröder HF, José HJ. Treatment of meat industry wastewater using dissolved air flotation and advanced oxidation processes monitored by GC-MS and LC-MS. *Chemical Engineering Journal*. 2009;**152**(1):151-157
- [6] Amaral Filho J, Azevedo A, Etchepare R, Rubio J. Removal of sulfate ions by dissolved air flotation (DAF) following precipitation and flocculation. *International Journal of Mineral Processing*. 2016;**149**(2016):1-8
- [7] WHO, WHO Guidelines for Drinking-Water Quality. 4th ed; 2011
- [8] Tyagi S, Sharma B. Water quality assessment in terms of water quality index. *American Journal of Water Resources*. 2013, 2014;**1**(3):34-38
- [9] The Environmental and Protection Agency. Parameters of water quality. *Environmental Protection*. 2002
- [10] Yu L, Han M, He F. A review of treating oily wastewater. *Arabian Journal of Chemistry*. 2017;**10**:S1913-S1922
- [11] Sillanpää M, Ncibi MC, Matilainen A, Vepsäläinen M. Removal of natural organic matter in drinking water treatment by coagulation: A comprehensive review. *Chemosphere*. 2018;**190**:54-71
- [12] Teh CY, Budiman PM, Shak KPY, Wu TY. Recent advancement of coagulation-flocculation and its application in wastewater treatment. *Industrial and Engineering Chemistry Research*. 2016;**55**(16):4363-4389
- [13] Gebbie P. Using Polyaluminium Coagulants in Water Treatment. 2001. Available from: <https://mysullys.com/flow-chart-of-complete-sewage-treatment-plant/onondaga-county-department-water-environment-protection/#content> [Accessed: 28 December 2018]
- [14] Kango S, Kalia S, Celli A, Njuguna J, Habibi Y, Kumar R. Surface modification of inorganic nanoparticles for development of organic-inorganic nanocomposites—A review. *Progress in Polymer Science*. 2013;**38**(8):1232-1261
- [15] V. Chandrasekhar, *Inorganic and Organometallic Polymers*. Berlin: Springer; 2005:108-112
- [16] Santander M, Rodrigues RT, Rubio J. Modified jet flotation in oil (petroleum) emulsion/water separations. *Colloids and Surfaces A: Physicochemical and Engineering Aspects*. 2011;**375**(1-3):237-244
- [17] Bolto B, Gregory J. Organic polyelectrolytes in water treatment. *Water Research*. 2007;**41**(11):2301-2324
- [18] Zachmann HG. Advances in polymer science. *Zeitschrift*

für Physikalische Chemie.
1976;255(8):729-734

[19] Konieczny K, Bodzek M, Rajca M. A coagulation-MF system for water treatment using ceramic membranes. *Desalination*. 2006

[20] Lightfoot EN. Membrane separations technology: Principles and applications. *Chemical Engineering Science*. 1996

[21] Sarkar S, Sengupta AK, Prakash P. The Donnan membrane principle: Opportunities for sustainable engineered processes and materials. *Environmental Science and Technology*. 2010

[22] Cumbal L, Sengupta AK. Arsenic removal using polymer-supported hydrated iron(III) oxide nanoparticles: Role of Donnan membrane effect. *Environmental Science and Technology*. 2005;39(17):6508-6515

[23] Tetteh EK, Rathilal S. Effects of a polymeric organic coagulant for industrial mineral oil wastewater treatment using response surface methodology (Rsm). *Water SA*. 2018;44(2):155-161

[24] SNF Floerger. Coagulation-Flocculation. Vol. 1. ZAC de Milieux; 2003

[25] Duan J, Gregory J. Coagulation by hydrolysing metal salts. *Advances in Colloid and Interface Science*. 2003;100:475-502

[26] Tzoupanos ND, Zouboulis AI. Coagulation-flocculation processes in water/wastewater treatment : The application of new generation of chemical reagents. In: 6th IASME/WSEAS International Conference on Heat Transfer, Thermal Engineering and Environment. 2008

[27] Rajasulochana P, Preethy V. Comparison on efficiency of various techniques in treatment of waste and

sewage water—A comprehensive review. *Resource-Efficient Technologies*. 2016;2(4):175-184

[28] Sahu OP, Chaudhari PK. Review on chemical treatment of industrial waste water review on chemical treatment. *Journal of Applied Sciences and Environmental Management*. 2013;17(2):241-257

[29] Gupta VK, Ali I, Saleh TA, Nayak A, Agarwal S. Chemical treatment technologies for waste-water recycling—An overview. *RSC Advances*. 2012;2(16):6380-6388

[30] Edzwald JK. Dissolved air flotation and me. *Water Research*. 2010;44(7):2077-2106

[31] Sim TS, Goh A, Becker EW. Comparison of centrifugation, dissolved air flotation and drum filtration techniques for harvesting sewage-grown algae. *Biomass*. 1988;16(1):51-62

[32] Edzwald JK. Principles and applications of dissolved air flotation. *Water Science and Technology*. 1995;31(3-4):1-23

[33] Kyzas GZ, Matis KA. Electroflotation process: A review. *Journal of Molecular Liquids*. 2016;220:657-664

[34] Tetteh EK, Rathilal S, Chollom MN. Treatment of industrial mineral oil wastewater—Optimisation of coagulation flotation process using response surface methodology (RSM). *International Journal of Applied Engineering Research*. 2017;12(23):13084-13091

[35] Behin J, Bahrami S. Modeling an industrial dissolved air flotation tank used for separating oil from wastewater. *Chemical Engineering and Processing: Process Intensification*. 2012;59:1-8

- [36] Zouboulis AI, Avranas A. Treatment of oil-in-water emulsions by coagulation and dissolved-air flotation. *Colloids and Surfaces A: Physicochemical and Engineering Aspects*. 2000;**172**(1-3):153-161
- [37] Verma AK, Dash RR, Bhunia P. A review on chemical coagulation/flocculation technologies for removal of colour from textile wastewaters. *Journal of Environmental Management*. 2012;**93**(1):154-168
- [38] Scholz M, Scholz M. Chapter 7—Coagulation and flocculation. In: *Wetlands for Water Pollution Control*. 2016
- [39] Lee CS, Robinson J, Chong MF. A review on application of flocculants in wastewater treatment. *Process Safety and Environment Protection*. 2014
- [40] Watanabe Y. Flocculation and me. *Water Research*. 2017;**114**:88-103
- [41] Wei H, Gao B, Ren J, Li A, Yang H. Coagulation/flocculation in dewatering of sludge: A review. *Water Research*. 2018
- [42] Tetteh EK, Rathilal S, Robinson K. Treatment of industrial mineral oil wastewater—Effects of coagulant type and dosage. *Water Practice Technology*. 2017;**12**(1):139-145
- [43] Yang R, Li H, Huang M, Yang H, Li A. A review on chitosan-based flocculants and their applications in water treatment. *Water Research*. 2016;**95**:59-89
- [44] Ndabigengesere A, Subba Narasiah K. Quality of water treated by coagulation using *Moringa oleifera* seeds. *Water Research*. 1998;**32**(3):781-791
- [45] Rodrigues AC, Boroski M, Shimada NS, Garcia JC, Nozaki J, Hioka N. Treatment of paper pulp and paper mill wastewater by coagulation-flocculation followed by heterogeneous photocatalysis. *Journal of Photochemistry and Photobiology A: Chemistry*. 2008;**194**(1):1-10
- [46] Wang Z, Xue M, Huang K, Liu Z. Textile dyeing wastewater treatment. In: *Advances in Treating Textile Effluent*. UK: IntechOpen press; 2011
- [47] Panizza M, Cerisola G. Electrochemical oxidation as a final treatment of synthetic tannery wastewater. *Environmental Science and Technology*. 2004;**38**(20):5470-5475
- [48] El-Naas MH, Alhajja MA, Al-Zuhair S. Evaluation of a three-step process for the treatment of petroleum refinery wastewater. *Journal of Environmental Chemical Engineering*. 2014;**2**(1):56-62

Directed Self-Assembly of Block Copolymers Based on the Heterogeneous Nucleation Process

Rui Lu, Xiaobing Qu, Lu Zhang, Nana Zhu and Tao Yang

Abstract

By introducing the heterogeneous nucleation concept to directed self-assembly of block copolymers, the ordering of dynamical process and defect pattern design in thin films of binary blend, AB diblock/C homopolymer (AB/C), are investigated by the time-dependent Ginzburg-Landau theory and simulated by the cell dynamics simulations. The detailed annealing process of a few isolated defects occurring in AB/C blend under triangular and hexagonal confinements is presented, and it indicates that angle-matched confinement of triangular and hexagonal potential well is favorable conditions for generating defect-free ordered structures. Meanwhile, we gave a model which composed of many double-spot potentials with controllable position and orientation to investigate the relationship between defect spacing and mismatched angle, and we found the relationship is similar to hard crystals. Additionally, as an example, the design of defect pattern of “NXU” for abbreviation of Ningxia University is proposed and tested. In this chapter, the feasibility of directed self-assembly of block copolymers based on the heterogeneous nucleation process is systematically confirmed.

Keywords: block copolymer, directed self-assembly, heterogeneous nucleation, defect pattern, ordered pattern

1. Introduction

Moore's law is the observation that the number of transistors in a dense integrated circuit doubles approximately every 2 years [1, 2]. It means the semiconductor industry continuously pursues approaches to fabricating nanostructures with higher resolution and higher throughput at lower cost. As an important manufacturing process of semiconductor, conventional lithography is approaching its physical limit for fabricating large-scale defect-free geometrically simple patterns or device-orientated, irregular structures with sub-10 nm node [3–5]. New strategy of fabricating large-scale perfectly ordered patterns and device-orientated, interesting defect patterns via directed self-assembly of block copolymers becomes the most realistic and possible technology that is feasible to fabricate nanoimprint template to manufacture integrated circuits of semiconductor industry [6–10]. Block copolymers, a kind of macromolecules which is jointed via covalent bonds by two or more homopolymers, can self-assemble into nanoscale periodic morphologies (5–100 nm). However, the structure self-assembled by block copolymers in

bulk or in thin films on a uniform substrate is difficult to form the desired structures [11–14]. The reason is that block copolymers are typical system of soft matter; it is often interfered by thermal fluctuations resulting in the formation of uncontrollable defective morphologies. Theoretically, the defective morphologies are metastable states, and the defects would be removed as the annealing process that proceeds in a long time [15, 16]. The system would transform from metastable (disordered) state into a more stable state (ordered), that is, the system ends up in thermodynamic equilibrium state. But in fact, those defective morphologies are long-lived relative to experimentally accessible time, and the annealing time is so long that it is rare to obtain the target structure in the experiment [17–20]. Note that the system would be readily trapped kinetically into one of the many possible metastable defective states, so this process is more studied from the perspective of dynamic evolution [15, 16, 18, 21–24]. Therefore, how to overcome these shortcomings and obtain the desired target structure via self-assembly of block copolymers has become a hot topic in this field. Among the many ideas proposed by researchers, directed self-assembly (DSA) of block copolymers [6–9, 11, 12, 15, 16, 23, 24] is the most attractive scheme which has been intensively studied, and it is also regarded as a promising new-generation lithography technique [3–5, 10].

DSA is one of the most effective methods to form long-range desired patterns of block copolymer domains. The basic idea of DSA is that the small-scale pattern information is encoded into the molecular structure of block copolymers. Then, the short-range guiding patterns on the substrate from the chemical (chemoepitaxy) or topographical (graphoepitaxy) field [14, 19, 20, 25–28] could direct the orientation on long-range order and control the registration of block copolymer structures with external boundaries. Based on this concept, different geometrically confined systems, and various topographical or chemical guiding patterns on the substrate, have been devised to guide the self-assembly of block copolymers to form the desired nanostructures. For example, in AB diblock copolymer, as the macromolecular architecture changes from symmetric to asymmetric, the minor component can self-assemble into several ordered structures, such as lamellar, gyroid, fddd network, and hexagonally arranged cylindrical, and body-centered cubic (bcc) spherical phases in the bulk [29–31]. Among those order structures, the hexagonally arranged cylindrical and lamellar phases are extensively used to prepare the samples of standing cylinders arranged in triangular lattice and geometrically stripe with line and space patterns, respectively [12, 19, 21–26, 32, 33]. Clearly, the guiding patterns must be sparse and have similar symmetries and integer multiple of periods to the domain period of the bulk phase. The density multiplication (DM) is introduced to evaluate the directing efficiency, which is defined as the ratio between the number of self-assembled domains and the number of directing substrate domains in a given area or volume of the sample. Intuitively, the sparser the guiding pattern, the lower the manufacturing cost. However, it has been proved that there exists the bottleneck in directing efficiency. The upper limit of DM in experiment for hexagonally arranged cylinders/spheres is small than 25 in the literature [12, 21, 22]. This means that the patterns on substrate could not greatly increase DM. Therefore, it remains a challenge to satisfy the rigorous demands on defect concentration and precise control required by the fabrication of integrated circuits.

Theoretically, the reason for efficiency limit is that the phase separation kinetics are spinodal microphase separation or spontaneous nucleation [34, 35]. It has an extremely high nucleation rate which induces nucleated domain grains with random positions and orientations [23]. With every domain area that grows and merges each other, the system leads to a large number of clustered defects derived from the incommensurate orientations between neighboring domain areas [15, 16].

In other words, structures formed via spinodal microphase separation cannot keep long-range order because thermal fluctuations at any locations simultaneously produce multiple grains that do not have coherent locations and orientations. Once the defects are formed, the system enters into the metastable state. As we have known, the transition from the metastable state to the stable state in block copolymer system is an extremely long process. In order to eliminate this disadvantage and increase the DM, a new DSA method, the heterogeneous nucleation, was proposed to suppress the spinodal decomposition and precisely control the domain location and orientation [15, 16, 23, 24], that is, the thermodynamics of the system must be regulated, such that the phase separation kinetics is dictated by a controlled nucleation process. These characteristics are very similar as crystals [36], so the classical nucleation theory may also be valid in block copolymers.

According to classical nucleation theory, the edges and corners of a confining system and the external nuclei can serve as heterogeneous nucleation sites with different nucleation rate [23, 35–37]. Defining the nucleation rate p , which expressed the probability of nucleation events in a unit volume per unit time, is proportional to the exponential term $\exp(-\Delta F_b/k_B T)$, where ΔF_b is energy barrier which represents the free energy difference between certain disordered metastable phase and ordered stable phase during the first-order phase transition, k_B is the Boltzmann constant, and T is the temperature. Obviously, by controlling the nucleation rate p , the desired target structure could be obtained. Meanwhile, there are a number of promising applications in two directions with this method: (i) large-scale perfectly ordered structure by reducing homogeneous nucleation rate and controlling the location and orientation of the induced ordered domains and (ii) interesting defect patterns by optimizing the nucleation rate and programing the location and orientation of nucleation agents. The former one, which is preparation for large-scale perfectly ordered structure, has been extensively studied. Therefore, in this chapter, we only express several details of the ordering process. The latter is the main focus of our research in this chapter. We will study the properties of different defects and program the desired defect patterns by means of heterogeneous nucleation strategy, that is, designing the positions and shapes of external nuclei.

In this chapter, we select frequently used model which is thin films of binary blend, AB diblock copolymer and C homopolymer (AB/C) [15, 16, 23, 24], with a lateral confinement and neutral top and bottom surfaces. In this way, the hexagonally packed cylindrical A domains are aligned perpendicular to the substrate. Homopolymer C is often added into block copolymers to regulate the segregation degree and the domain spacing. In other words, homopolymer can adjust the homogeneous nucleation rate effectively. The kinetics of micro-/macrophase separation in this system can be described by the time-dependent Ginzburg-Landau (TDGL) theory. According to previous work, we adopt cell dynamics simulation (CDS) to solve the equations of TDGL model [15, 16, 23, 24, 38, 39].

2. Model and theory

In this system, AB/C blend, a number of parameters such as the chain lengths and interaction parameters are expressed as a series of phenomenological parameters. The volume fraction of C homopolymer is defined as $\bar{\phi}_C$, and the block ratio of the A block is f in the AB diblock copolymer. Two independent order parameters are introduced to denote the phase separation of this three-component system, $\varphi(\mathbf{r}) = \varphi_A(\mathbf{r}) - \varphi_B(\mathbf{r})$ and $\eta(\mathbf{r}) = \varphi_A(\mathbf{r}) + \varphi_B(\mathbf{r}) - \Psi_C(\mathbf{r})$, where $\varphi_A(\mathbf{r})$ and $\varphi_B(\mathbf{r})$ are the local volume fractions of A and B component at any position \mathbf{r} , respectively. $\Psi_C(\mathbf{r})$ is a constant that used to modulate the macrophase separation. Based on the

Ohta-Kawasaki model [38, 39] for AB/C blend, the free energy can be described as a functional of the two-order parameters,

$$F[\phi(\mathbf{r}), \eta(\mathbf{r})] = F_S[\phi(\mathbf{r}), \eta(\mathbf{r})] + F_L[\phi(\mathbf{r}), \eta(\mathbf{r})] + \int d\mathbf{r} H_{\text{ext}}(\mathbf{r})\phi(\mathbf{r}) \quad (1)$$

where F_S is the short-range interaction that is derived from the ordinary standard Ginzburg-Landau free energy; it is written as

$$F_S[\phi, \eta] = \int d\mathbf{r} \left\{ \frac{D_1}{2} [\nabla\phi(\mathbf{r})]^2 + \frac{D_2}{2} [\nabla\eta(\mathbf{r})]^2 + f_\phi[\phi] + f_\eta[\eta] + f_{\text{int}}[\phi, \eta] \right\} \quad (2)$$

Here D_1 and D_2 are two positive constants related to the interfacial properties between the three immiscible components. The derivatives of energy density terms $f_\phi[\phi]$ and $f_\eta[\eta]$ are given by $\frac{df_\phi[\phi]}{d\phi} = -A_\phi \tan \phi + \phi$ and $\frac{df_\eta[\eta]}{d\eta} = -A_\eta \tan \eta + \eta$ with $A_\phi > 1$ and $A_\eta > 1$ to tune the micro-/macrophase separation degree. The last term is expressed as $f_{\text{int}} = b_1\eta\phi - \frac{b_2\eta\phi^2}{2} - b_3(\eta\phi^3 + \eta^2\phi + \eta^3\phi) + \frac{b_4\eta^2\phi^2}{2}$, where the phenomenological coefficients b_i ($i = 1, 2, 3, 4$) is constant with unambiguous physical meaning as proposed by Ohta and Ito.

The long-range interaction term F_L is expressed as

$$F_L[\phi, \eta] = \int d\mathbf{r} \int d\mathbf{r}' G(\mathbf{r}, \mathbf{r}') \left[\frac{\alpha\delta\phi(\mathbf{r})\delta\phi(\mathbf{r}')}{2} + \beta\delta\phi(\mathbf{r})\delta\eta(\mathbf{r}') + \frac{\gamma\delta\eta(\mathbf{r})\delta\eta(\mathbf{r}')}{2} \right] \quad (3)$$

where $\delta\phi(\mathbf{r}) = \phi(\mathbf{r}) - \bar{\phi}$ and $\delta\eta(\mathbf{r}) = \eta(\mathbf{r}) - \bar{\eta}$ and $\bar{\phi}, \bar{\eta}$ are average values in full space for $\phi(\mathbf{r})$ and $\eta(\mathbf{r})$, respectively. The coefficients α, β and γ are related to the polymerization degrees of AB and C, which obey the relationship of $\frac{\beta}{\alpha} = \frac{\gamma}{\beta}$. The Green function of $G(\mathbf{r}, \mathbf{r}')$ is with a Coulomb interaction form that denotes the long-range feature of the chain connectivity of the diblock copolymer. In the last term of free energy in Eq. (1), $H_{\text{ext}}(\mathbf{r})$ is a potential field imposed on nucleation agent whose explicit expression will be given in the following sections for different models.

The phase separation kinetics of AB/C blend is dominated by following two conserved Cahn-Hilliard equations:

$$\frac{\partial\phi}{\partial t} = \frac{M_1\nabla^2\delta F[\phi, \eta]}{\delta\phi} + \xi_\phi(\mathbf{r}, t) \quad (4)$$

$$\frac{\partial\eta}{\partial t} = \frac{M_2\nabla^2\delta F[\phi, \eta]}{\delta\eta} + \xi_\eta(\mathbf{r}, t) \quad (5)$$

where M_1, M_2 are two mobility coefficients and ξ_ϕ, ξ_η are the random noise terms that satisfy the fluctuation dissipation theorem. For the sake of discussion, the parameters of system are set as $f = 0.4, D_1 = 0.5, D_2 = 1, M_1 = M_2 = 1, A_\phi = 1.26, A_\eta = 1.10, b_1 = -0.05, b_2 = 0.05, b_3 = 0.01, b_4 = 0.10, \Psi_C = 0.20$, and $\bar{\phi}_C$ is fixed as $\bar{\phi}_C = 0.025$. All spatial lengths in the following calculations are expressed in terms of the cylinder-to-cylinder distance L_0 in AB/C blend. Because this model is the thin films of binary blend, the system is simplified to be two-dimensional; hence the hexagonally packed cylindrical A domains would align perpendicular to the substrate. The kinetic equations can be solved numerically by standard discretization scheme of CDS. Based on CDS, the two-dimensional substrate is divided into $N_x \times N_y$ squares with length of its sides $\Delta x = \Delta y = \Delta = 0.5$, and the Laplace operator is written as

$$\nabla^2 X = \left(\frac{1}{6} \sum_{nn} X_i + \frac{1}{12} \sum_{nnn} X_i - X \right) / \Delta^2 \quad (6)$$

where “nn” denotes nearest neighbors and “nnn” next-nearest neighbors.

3. Results and discussion

3.1 Phase-ordering process

It has been proved that the large-scale perfectly ordered hexagonal patterns can be obtained by many block copolymer systems with different DM. Early experiments and theories indicated that the maximum DM would not exceed 25 [12, 21, 22], and later it was increased to 34 confirmed by self-consistent mean field theory [40]. Recently, a very innovative idea has been proposed by Xie et al. [23], which greatly improves the directing efficiency. The idea is based on the concept of heterogeneous nucleation. By careful adjustment of the sparse periodic array of several pairs of potential wells in AB/C blend, it realized perfect hexagonal pattern with DM values of at least 128. However, this scheme has serious shortcomings in manufacture process because the nucleation agent unit size is as small as the lattice constant L_0 . Thus, other nucleation agents are needed. Inspired by the classical nucleation theory, the six corners of lateral hexagonal confinement would be an ideal choice [24]. Corner-induced domain grains grow and integrate into an ordered hexagonal pattern filling in whole substrate. Because the corner angle is 120° , which is commensurate in hexagonal pattern, this method is high-efficient. Because this method is ready to implement, Ho et al. [41] realized a defect-free hexagonal pattern by self-assembly of star-block PS-PDMS based on heterogeneous nucleation. Although the hexagonal confinement is not difficult to produce technically, there is a better choice, such as rectangular confinement. Yang et al. [15] demonstrated the heterogeneous nucleation process in rectangular confinement and still acquired the defect-free hexagonal pattern.

Most of the above work focuses on the implementation of perfectly ordered hexagonal patterns and rarely gives the ordering process after growth time t_{fill} which denotes the moment when domains grow up to fill in the entire sample. However, the ordering process is very important in the sample preparation of lithography techniques. The size and shape of confinements, the position and orientation of nucleation agents, the strength and range of chemical potential, and so on all severely affect the path of phase-ordering kinetics from a metastable disordered phase to ordered phase. Here we will give this process in detail. Considering the angle-matched confinement that will lead to ordered structure, we choose lateral, triangular, and hexagonal confinements to demonstrate the process.

Since AB/C blend is laterally confined in triangular and hexagonal well, an external field, $H_{\text{ext}}(\mathbf{r})$ is imposed on each sidewall to denote the preferential interaction on A or B block; and thus the sidewalls are acted as nucleation agents. The form of field is set as

$$H_{\text{ext}}(\mathbf{r}) = \frac{1}{2} \Lambda_0 \left\{ \tanh \left[\frac{\sigma - d(\mathbf{r})}{\epsilon} \right] + 1 \right\} \quad (7)$$

where the shortest distance of the position \mathbf{r} to any sidewall is $d(\mathbf{r}) < 2\sigma$. In Eq. (7), Λ_0 is the field strength, 2σ is the interaction distance, and ϵ is the potential steepness, respectively. For convenience, here we fixed $\sigma = 0.15L_0$, $\epsilon = 0.5L_0$ in following calculations, and more details can be found elsewhere [15, 24].

It is worth noting that in the process on DSA of block copolymer, the defects are inevitable. When angle-matched confinement is introduced, a number of isolated dislocations (or five-seven defect pairs) are occurred due to the thermal fluctuations. In theory and experiment, the dislocations would be annihilated in long time. In **Figure 1**, the defect annealing process which started as the growth time t_{fill} under triangular confinement is presented.

As can be seen from **Figure 1a**, there are five dislocations when the phase separation just finished and the domains were filled in the sample at $t = t_{\text{fill}} = 3.5 \times 10^5$. With the continuous evolution process, all defects gradually moved in the direction of their nearest side and at $t = 1.0 \times 10^6$; the defect in the lower left corner has disappeared, which is shown in **Figure 1b**. Obviously, all defects are constantly moving outward in order to transform into a more steady state. In **Figure 1c**, the defect on the right side is eliminated by annealing at $t = 3.0 \times 10^6$, and at this stage, only three five-seven defect pairs remain in whole substrate. Until $t = 1.0 \times 10^7$ in **Figure 1d**, the number of defects did not decrease, but the distance between them increased, and all defects are closer to the sides. This annealing process also shows that the relaxation time of soft matter system is extremely long.

Additionally, we also considered the long-time annealing behavior under the hexagonal confinement. In **Figure 2a**, there are four isolate five-seven dislocations and four isolate seven disclinations in sample. When the domain nucleated from each angle and the domain area expanded and intersected each other at the center of the edge, the distance between the cylinders is more than one time of L_0 , so a disclination may be formed at four sides. The two defects that are closer to the top and the bottom sides are different from the other four disclinations at sides, which may derive from the algorithm and we will discuss later. After a long time, in **Figure 2b**, by adjusting its period, even if it is slightly larger than L_0 , the system gradually evolves to a steady state, thus the four disclinations are eliminated. In **Figure 2c**, the two five-seven dislocations in the center of the sample, because they

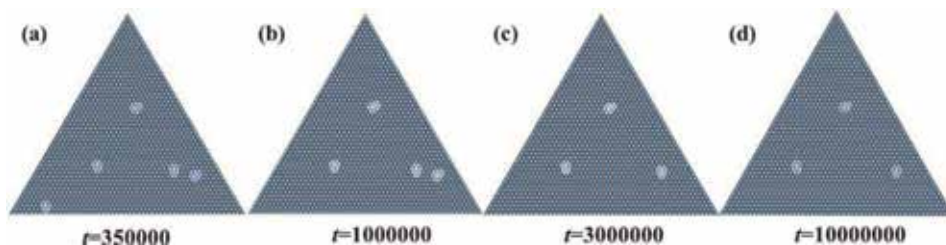


Figure 1. Snapshots of a few side-induced five-seven dislocations observed during the annealing process (a)–(d) formed in triangular confinement with field strength $\Lambda_0 = 0.005$ and a side length $L = 50.5L_0$.

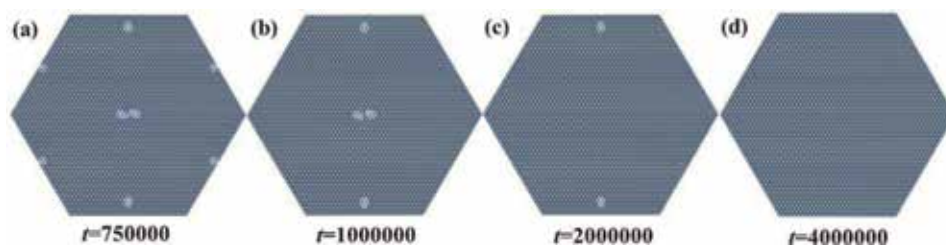


Figure 2. Snapshots of a few side-induced five-seven dislocations observed during the annealing process (a)–(d) formed in hexagonal confinement with field strength $\Lambda_0 = 0.003$ and a side length $L = 30.5L_0$.

have nearly opposite Burgers vectors, move toward each other and finally cancel each other. Similarly, the two remaining defects move in the direction of sides and are annihilated. Finally, a defect-free pattern is obtained in **Figure 2d**.

It is worth noting that the phase-ordering kinetics given in **Figures 1 and 2** describes the process from a disordered metastable state to an ordered stable state. On the one hand, from the perspective of energy, the defect annealing process is also the process of releasing stress energy and reducing free energy of the system [42, 43]. On the other hand, the angle-matched confinement with triangular and hexagonal well is favorable conditions for generating defect-free ordered structures.

The other one is worth noting that the size commensurability or size tolerance of the directing effect to the confinement is very important. In general, the spacing of domains self-assembled by the block copolymer with a certain confinement is adjusted itself within a limited range to obtain ordered structure. However, when the size is incommensurate with the domain spacing, it is very difficult to form defect-free structure. The defect concentration is introduced to evaluate the direct efficiency, which is defined as $f_{DF} = \frac{n_{DF}}{n_{domain}} \times 100\%$, where n_{domain} is the total number of domains and n_{DF} the number of five-seven dislocations in the sample.

In previous work, it has been proved that there is a size tolerance window for manufacture of large-scale ordered structures via the heterogeneous nucleation process in the hexagonal and rectangle confinements. In other words, the directing effect is dependent on the geometric confinement size, even for the angle-matched hexagonal confinement. But it is amazing that there is no size dependent for regular triangular confinement systems when nucleation is corner-induced with a weak field $\Lambda_0 = 0.002$. In **Figure 3**, the average concentrations $\langle f_{DF} \rangle$ calculated by averaging 10 independent runs are shown. When the system is corner-induced ($\Lambda_0 = 0.002$), the defect concentrations $\langle f_{DF} \rangle$ keep zero with the size length from $10L_0$ to $55L_0$. While the size length L increases to $55L_0$, more than 1300 cylinder domains are contained in the sample, and the system has reached the μm scale. This intriguing feature contrasts with existing work and would have potential

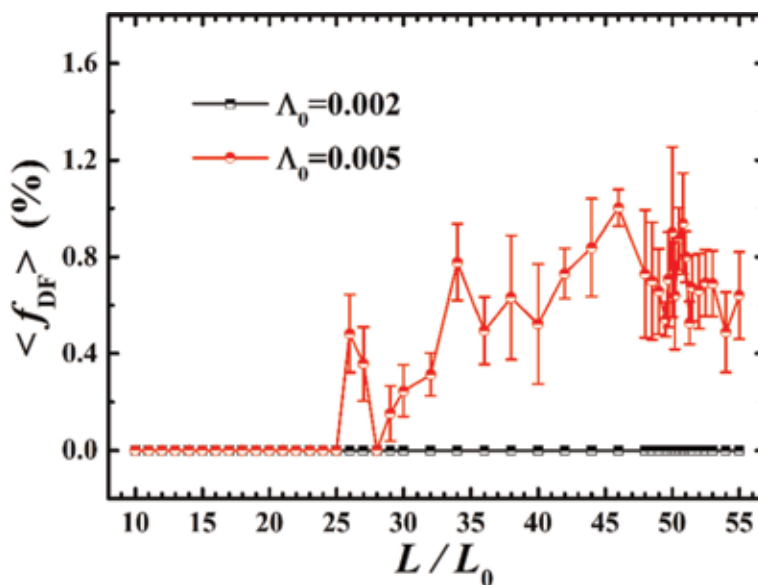


Figure 3. Average defect concentration of the hexagonal pattern $\langle f_{DF} \rangle$ as a function of side length L for field strength $\Lambda_0 = 0.002$ and 0.005 . The point value and its standard deviations are obtained by averaging the data on 10 independent simulation samples.

applications in the manufacture of integrated circuits. Under a slightly stronger field, $\Lambda_0 = 0.005$, the defect concentration $\langle f_{DF} \rangle$ is zero at small size sample and is with a small fluctuation amplitude within $0 \leq \langle f_{DF} \rangle \leq 1.2\%$ at larger size because of high probability of defects that still has no obvious limit to the size. As is known, the mismatched angle between neighboring domain grains is multiples of 60° ; the two grains may merge into a single crystalline grain. Here the regular triangular system is just the smallest multiples of 60° ; compared to hexagonal system, 120° , it has strong confining effect and thus has higher tolerance to the size incommensurability.

3.2 Spacing of dislocations

Based on the concept of heterogeneous nucleation [36], different boundary conditions acted as nucleating agents and can be introduced, such as the corners and sides of different geometric confinements. The defect-free hexagonal patterns can be realized. However, due to the common irregular structures in the semiconductor industry, the same attention should be paid to the defect as to ordered structures in block copolymers.

The large-scale regular/irregular soft crystal structures formed from DSA of block copolymers are fundamentally different from those conventional crystals. The defects or dislocations in this soft crystal may have distinctive features as to those in hard crystals. But we might study and understand some property of soft matter with the help of classical nucleation theory. According to classical nucleation theory, the average distance between dislocations is related to the mismatched angle between neighboring domain grains. As shown in **Figure 4a**, taking two hexagons, the axis of one hexagon is horizontal, and the other one is tilted θ relative to the horizontal axis. In this way, the two domain grains are at a mismatched angle of θ , resulting in defects when θ is not multiples of 60° . Intuitively, different angles correspond to different overlap areas of two hexagons; thus we first investigate the overlapping area for convenience. In **Figure 4a**, the shaded area APRQA is one-sixth of the whole overlap areas, and the area is expressed as

$$S_{OL} = 6S_1 = 6 \left(\int_0^{x_{Q_1}} y_{AQ} dx + \int_{x_{Q_1}}^{x_{R_1}} y_{CD} dx + \int_{x_{R_1}}^{x_{P_1}} y_{BE} dx - \int_{x_{P_1}}^0 y_{AP} dx \right) \quad (8)$$

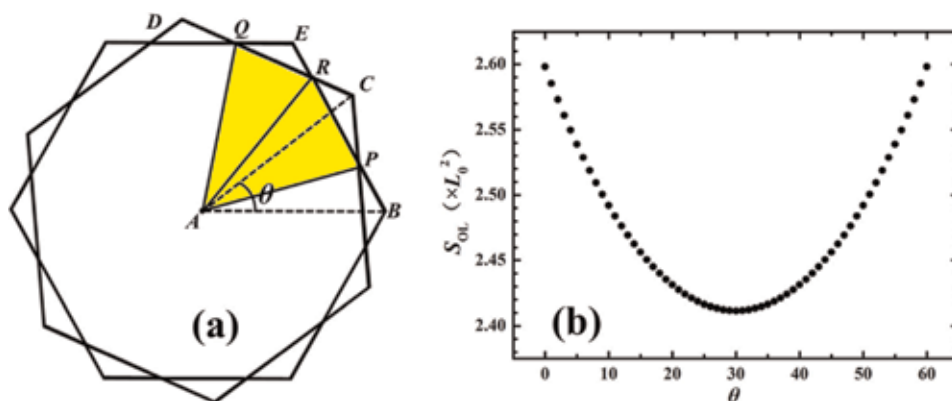


Figure 4. (a) Schematic representation of overlapping region of two hexagons. The axis of one hexagon is horizontal, and the other is tilted θ relative to the horizontal axis, and the shaded area marks one-sixth of the overlap area. (b) The overlap area varies with mismatched angle θ of the two hexagons.

where y_{AQ} , y_{CD} , y_{BE} , y_{AP} are functional expressions for line AQ, CD, BE, and AP in coordinate system. The coordinate system is established as follows: the center of the hexagons is the origin, the horizontal right direction is the positive direction of the x -axis, and the vertical upward direction is the positive direction of the y -axis. Specifically, $y_{AQ} = 3[\sec(\frac{\pi}{6} + \theta) - \tan(\frac{\pi}{6} + \theta)]x$, $y_{CD} = -\cot(\frac{\pi}{6} + \theta)x + \sin\theta + \cot(\frac{\pi}{6} + \theta)\cos\theta$, $y_{BE} = -\sqrt{3}x + \sqrt{3}$, $y_{AP} = (2 - \sqrt{3})x$, and the side length of hexagons is formally fixed as L_0 . The results are shown in **Figure 4b**.

Figure 4b shows the relationship between the overlap area and mismatched angle. When $\theta \rightarrow 0$, the two hexagons coincide each other, so the overlap area is maximized. In another words, the mismatch degree is zero at $\theta \rightarrow 0$, so there are no defects in sample. As θ increases, the overlap area gradually decreases, and the minimum value is reached when $\theta = 30^\circ$. In this process, the mismatch degree increases gradually and finally reaches the maximum, which means that the number of defects also increase, that is, the dislocations arrange from sparse distribution to the closest arrangement. In contrast, the overlap area increases again after $\theta = 30^\circ$, until $\theta = 60^\circ$. This law is similar to that of the distance between defects in hard crystals.

In order to validate this relationship, we propose a model in which two domain grains are induced by two pairs of double-spot potential. The schematic is shown in **Figure 5**. Using the double-spot potential as the nucleation agents, the domain grain with definite orientation can be produced. In **Figure 5**, each pair of the double well is tilted $\frac{\theta}{2}$ relative to the horizontal axis; thus the angle between the two domain grains induced by them is θ . The two grains start to grow from double well and will meet in the middle of the two wells ($y = \frac{L_y}{2}$) and finally get a number of five-seven dislocations if the mismatched angle will not be multiples of 60° . By examining the distance of dislocations produced by this model, the relationship between mismatched angle θ and average spacing of dislocations d_{DL} will be calculated quantitatively. The morphological snapshots of five-seven dislocations at different mismatched angle θ are presented in **Figure 6**.

As a nucleation agent, the double-spot potential spaced at equal distance L_0 as shown in **Figure 5** can orient the induced ordered domains. Therefore, we put a potential field with the following form around double spots [23]:

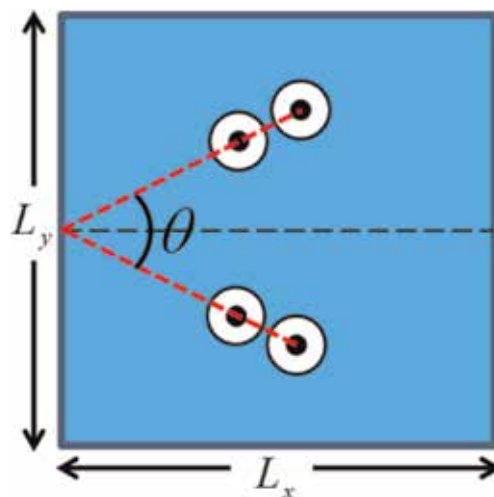


Figure 5. Schematic of the setup for preparation of two domain grains. The nucleation agent is composed of two pairs of double-well potentials, of which each pair is tilted $\frac{\theta}{2}$ relative to the horizontal axis.

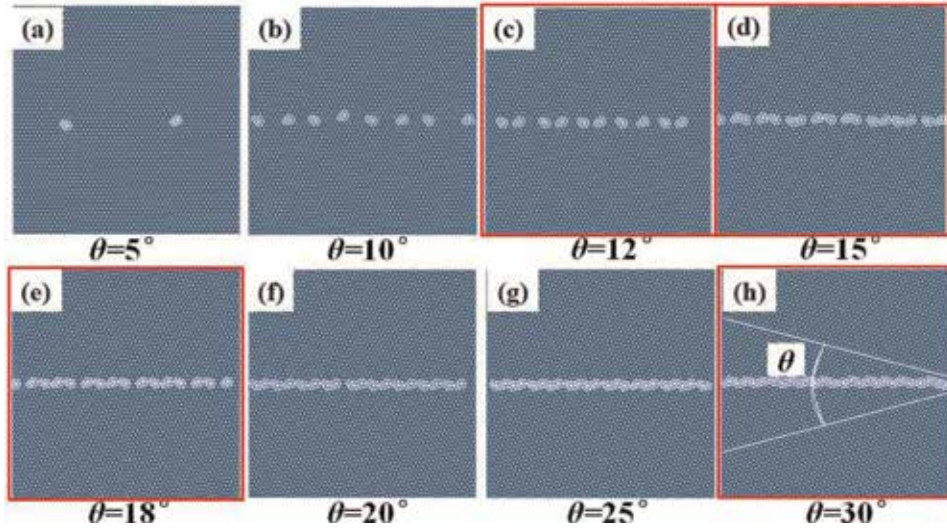


Figure 6.

Morphological snapshots of five-seven defect pattern at different mismatched angle θ of two domain grains. From (a) to (h), $\theta = 5, 10, 12, 15, 18, 20, 25, 30^\circ$. We fixed the size of sample $50L_0 \times 50L_0$ and the position of the two double-spot wells that are selected at $(\frac{L_x}{2}, \frac{L_y}{6})$ and $(\frac{L_x}{2}, \frac{5L_y}{6})$, respectively. The marked in red (c), (e), (d), and (h) represent that AB/C blend is under the regular pentagonal (corner- and side-induced), octagonal, and square confinements.

$$H_{\text{ext}}(\mathbf{r}) = -\frac{V_0}{2} \left\{ \tanh \left[\frac{-|\mathbf{r} - \mathbf{R}_n| + \sigma}{\lambda} \right] + 1 \right\} \quad (9)$$

for $|\mathbf{r} - \mathbf{R}_n| \leq 2\sigma$ and otherwise $H_{\text{ext}}(\mathbf{r}) = 0$. The strength of field $V_0 = 0.04$ denotes that the spot potential is preferential to minor component A block. \mathbf{R}_n indicates the coordinate of spot potential n , and $\sigma = 0.15L_0$ is the radial size of well, and $\lambda = 0.5$ gives the steepness of potential well.

In **Figure 6**, we select square confinement with fixed boundary conditions, and the size of sample is $50L_0 \times 50L_0$. The centers of two double-spot potentials are set at center in the x direction, symmetric with respect to $= \frac{L_y}{2}$, that is, $(\frac{L_x}{2}, \frac{L_y}{6})$ and $(\frac{L_x}{2}, \frac{5L_y}{6})$; thus they can induce two pieces of ordered domain grains which meet at $\frac{L_y}{2}$ due to the symmetry. When the two grains have different orientations, a few five-seven dislocations are formed at $\frac{L_y}{2}$.

Because the above setup can be used to investigate the defect distribution under continuous change of mismatched angles, we only give eight typical morphological snapshots of five-seven dislocations at $\theta = 5, 10, 12, 15, 18, 20, 25, 30^\circ$ in **Figure 6a-h**. It is worthy noted that when $\theta = 0^\circ$, an ordered structure is obtained because of same orientations for two grains induced by the two double-spot potentials. It also indicates the spacing of dislocations $d_{\text{DL}} \rightarrow \infty$ when $\theta = 0^\circ$. With the increase of the mismatched angle θ , more and more dislocations are formed where the domain grains meet. Accordingly, the spacing of dislocations is decreasing, and the dislocations are arranged more and more closely, as shown in **Figure 6a-g**. When $\theta = 30^\circ$, the distance of dislocations is minimized, and the five-seven dislocations are end-to-end (**Figure 6h**). This result is consistent with that of **Figure 4**. So, the relationship for spacing of dislocations in hard materials may hold for this system whose units are soft deformable domains and are very distinguishable from atoms. Here is the relationship between mismatched angle and distance of dislocations [16, 36, 42–45],

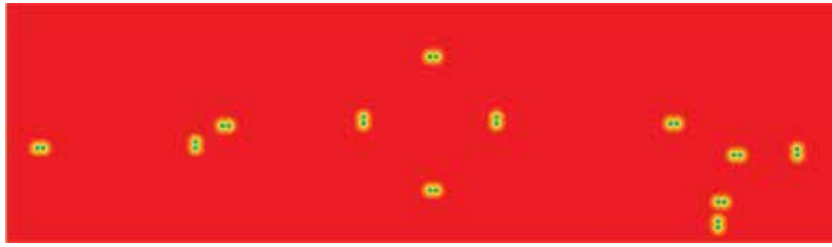


Figure 7. Snapshots of distribution of 12 nuclei which composed of the double-spot potential. The size of sample is $120L_0 \times 40L_0$.

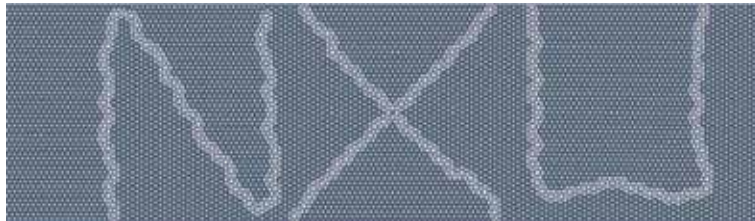


Figure 8. Snapshots of defect pattern “NXU” formed via heterogeneous nucleation process originated from **Figure 7**.

$$d_{DL} \propto \frac{a_0}{2 \sin\left(\frac{\theta}{2}\right)} \quad (10)$$

where a_0 is the lattice constant and in this soft crystal system $a_0 = L_0$.

Although the above discussions focus on the properties of dislocations, they also provide us with a new idea that dislocations are controllable with heterogeneous nucleation technique. One on hand, nucleation agents with desired positions and uniform orientation can make single-crystal pattern efficiently because of no defect occurring at this condition. On the other hand, by tailoring the positions and orientations of nucleation agents, we can program the defect patterns in soft crystals and obtain the devise-oriented irregular structures which might have potential applications in metamaterials, semiconductor industry, etc.

3.3 Defect patterns

As well as we known, a significant feature of soft matter is sensitively responsive to thermal fluctuations as well as external fields. In these systems, the contribution of entropy is not negligible and even more important than the contribution of enthalpy. Therefore, the probability of formation of defects increases dramatically because of the responsiveness to thermal fluctuations. Conversely, the opportunities to design soft crystals are offered, such as fabrication of large-scale order structures and devise-oriented irregular structures, because of their sensitive responsiveness to external fields.

In Section 3.2, we have already discussed the properties of dislocations in detail and have proposed a feasible technique to obtain the desired pattern by controlling the nucleation process. The technique is originated from the concept of heterogeneous nucleation. Using this method, we give a design scheme to implement a defect pattern of “NXU” which is abbreviation for Ningxia University.

We choose the size of the two-dimensional sample as $120L_0 \times 40L_0$ with fixed boundary conditions. Many nuclei composed of the double-spot potential are put in designed positions and orientations. The parameters are the same as in Section 3.2.

Specifically, the positions and orientations of nuclei are shown in **Figure 7**. For convenience, we only selected two double-spot orientations that were standing at 0° and 90° to the horizontal direction. This means that the grains induced by them either would be commensurate with each other ($\theta = 0$) and formed an ordered structure or produce the densest defects ($\theta = 30^\circ$) when they meet.

The final defect pattern induced by the nucleus agent distributed in **Figure 7** is shown in **Figure 8**. As we expected, the desired pattern “NXU” is obtained. It proves the feasibility of the technique for producing desired patterns via a heterogeneous nucleation process in block copolymers. In principle, most of the irregular patterns at the nanoscale can be obtained by this method.

4. Conclusions

In block copolymers, as a typical system of soft matter, the kinetic and thermodynamic behaviors are sensitively responsive to thermal fluctuations and external fields. The pattern self-assembled by block copolymers is inevitable to face this problem. In order to produce desired pattern, an effective technique of DSA via heterogeneous nucleation is adopted to investigate the behaviors of self-assembly. Two potential applications are considered by the method in this chapter. One is the phase-ordering process, and the other is the defect pattern design. The corresponding process of thin films of binary blend, AB diblock copolymer, and C homopolymer is simulated using the CDS based on the TDGL, demonstrating the feasibility and practicality of heterogeneous nucleation in fabrication of desired nanoscale patterns.

Because there are many factors that affect the self-assembly process, the phase-ordering process is very important in the sample preparation of lithography techniques. By adjusting the heterogeneous nucleation process, the path of phase-ordering kinetics from a metastable disordered phase to ordered phase is easier to achieve. We choose two angle-matched confinements, lateral triangular and hexagonal confinements, whose sides and corners are acted as nucleation agents, to demonstrate the phase-ordering process. Especially, the annealing process for a small number of defects was also recorded. It may be useful for the preparation of large-scale ordered structures.

On the contrary, irregular structures with various defect patterns in the semiconductor industry have received little attention. However, the study for defect in soft matter is of great significance both theoretically and experimentally, because of so many distinctive features for soft matter as to those in hard crystals. We gave a robust model which composed of many double-spot potentials with controllable position and orientation, to investigate the relationship between defect spacing and mismatched angle. Additionally, as an example, the design of defect pattern of “NXU” for abbreviation of Ningxia University is proposed.

With the development of DSA techniques via heterogeneous nucleation process, various defect-free patterns on large scales or irregular device-oriented structures are technically easy to implement. In order to obtain more complex structures or structures with smaller characteristic dimensions, more efforts should devote to optimizing the properties and extending the choice of materials in theory and experiment.

Acknowledgements

Rui Lu thanks the funding support by the National College Students' innovation and entrepreneurship training program (Grant No. 201810749005).

T.Y. thanks the funding support by the Natural Science Foundation of Ningxia (Grant No. NZ1640).

Conflict of interest

The authors have no conflict of interest to declare.

Author details

Rui Lu, Xiaobing Qu, Lu Zhang, Nana Zhu and Tao Yang*
Ningxia Key Laboratory of Information Sensing and Intelligent Desert, School of Physics and Electronic-Electrical Engineering, Ningxia University, Yinchuan, China

*Address all correspondence to: yang_tao@alumni.sjtu.edu.cn

IntechOpen

© 2019 The Author(s). Licensee IntechOpen. This chapter is distributed under the terms of the Creative Commons Attribution License (<http://creativecommons.org/licenses/by/3.0/>), which permits unrestricted use, distribution, and reproduction in any medium, provided the original work is properly cited. 

References

- [1] Moore GE. Cramming more components onto integrated circuits. *Proceedings of the IEEE*. 1998;**86**:82-85. DOI: 10.1109/JPROC.1998.658762
- [2] Gelsinger P. Moore's law—The genius lives on. *IEEE Solid-State Circuits Newsletter*. 2006;**20**:18-20. DOI: 10.1109/N-SSC.2006.4785855
- [3] Park M, Harrison C, Chaikin PM, Register RA, Adamson DH. Block copolymer lithography: Periodic arrays of ~1011 holes in 1 square centimeter. *Science*. 1997;**276**:1401-1404. DOI: 10.1126/science.276.5317.1401
- [4] Cheng JY, Ross CA, Thomas EL, Smith HI, Vancso GJ. Fabrication of nanostructures with long-range order using block copolymer lithography. *Applied Physics Letters*. 2002;**81**: 3657-3659. DOI: 10.1063/1.1519356
- [5] Stoykovich MP, Müller M, Kim SO, Solak HH, Edwards EW, de Pablo JJ, et al. Directed assembly of block copolymer blends into nonregular device-oriented structures. *Science*. 2005;**308**:1442-1446. DOI: 10.1126/science.1111041
- [6] Darling SB. Directing the self-assembly of block copolymers. *Progress in Polymer Science*. 2007;**32**:1152-1204. DOI: 10.1016/j.progpolymsci.2007.05.004
- [7] Herr DJC. Directed block copolymer self-assembly for nanoelectronics fabrication. *Journal of Materials Research*. 2011;**26**:122-139. DOI: 10.1557/jmr.2010.74
- [8] Luo M, Epps TH III. Directed block copolymer thin film self-assembled: Emerging trends in nanopattern fabrication. *Macromolecules*. 2013;**46**: 7567-7579. DOI: 10.1021/ma401112y
- [9] Hu H, Gopinadhan M, Osuji CO. Directed self-assembly of block copolymers: A tutorial review of strategies for enabling nanotechnology with soft matter. *Soft Matter*. 2014;**10**: 3867-3889. DOI: 10.1039/C3SM52607K
- [10] Bates CM, Maher MJ, Janes DW, Ellison CJ, Willson CG. Block copolymer lithography. *Macromolecules*. 2014;**47**: 2-12. DOI: 10.1021/ma401762n
- [11] Li WH, Müller M. Defects in the self-assembly of block copolymers and their relevance for directed self-assembly. *Annual Review of Chemical and Biomolecular Engineering*. 2015;**6**: 187-216. DOI: 10.1146/annurev-chembioeng-061114-123209
- [12] Bitá I, Yang JKW, Jung YS, Ross CA, Thomas EL, Berggren KK. Graphoepitaxy of self-assembled block copolymers on two-dimensional periodic patterned templates. *Science*. 2008;**321**:939-943. DOI: 10.1126/science.1159352
- [13] Campbell IP, Lau GJ, Feaver JL, Stoykovich MP. Network connectivity and long-range continuity of lamellar morphologies in block copolymer thin films. *Macromolecules*. 2012;**45**: 1587-1594. DOI: 10.1021/ma2025336
- [14] Ruiz R, Sandstrom RL, Black CT. Induced orientational order in symmetric diblock copolymer thin films. *Advanced Materials*. 2007;**19**: 587-591. DOI: 10.1002/adma.200600287
- [15] Yang T, Tian SW, Zhu Y, Li WH. Perfectly ordered patterns formed by a heterogeneous nucleation process of block copolymer self-assembly under rectangular confinement. *Langmuir*. 2016;**32**:13787-13794. DOI: 10.1021/acs.langmuir.6b03638
- [16] Yang T, Zhu Y, Xue HY, Li WH. Defect patterns from controlled heterogeneous nucleations by polygonal confinements. *Langmuir*. 2018;**34**:

5901-5909. DOI: 10.1021/acs.langmuir.8b00101

[17] Li WH, Müller M. Directed self-assembly of block copolymers by chemical or topographical guiding patterns: Optimizing molecular architecture, thin-film properties, and kinetics. *Progress in Polymer Science*. 2016;**54**–55:47-75. DOI: 10.1016/j.progpolymsci.2015.10.008

[18] Xu Y, Xie N, Li W, Qiu F, Shi AC. Phase behaviors and ordering dynamics of diblock copolymer self-assembly directed by lateral hexagonal confinement. *The Journal of Chemical Physics*. 2012;**137**:194905. DOI: 10.1063/1.4765098

[19] Cheng JY, Rettner CT, Sanders DP, Kim HC, Hinsberg WD. Dense self-assembly on sparse chemical patterns: Rectifying and multi-plying lithographic patterns using block copolymers. *Advanced Materials*. 2008;**20**:3155-3158. DOI: 10.1002/adma.200800826

[20] Tavakkoli AKG, Gotrik KW, Hannon AF, Alexander-Katz A, Ross CA, Berggren KK. Templating three-dimensional self-assembled structures in bilayer block copolymer films. *Science*. 2012;**336**:1294-1298. DOI: 10.1126/science.1218437

[21] Li WH, Qiu F, Yang YL, Shi AC. Ordering dynamics of directed self-assembly of block copolymers in periodic two-dimensional fields. *Macromolecules*. 2010;**43**:1644-1650. DOI: 10.1021/ma9023203

[22] Li WH, Xie N, Qiu F, Yang YL, Shi AC. Ordering kinetics of block copolymers directed by periodic two-dimensional rectangular fields. *The Journal of Chemical Physics*. 2011;**134**:144901. DOI: 10.1063/1.3572266

[23] Xie N, Li WH, Qiu F, Shi AC. New strategy of nanolithography via controlled block copolymer

self-assembly. *Soft Matter*. 2013;**9**:536-542. DOI: 10.1039/c2sm26833g

[24] Deng HL, Xie N, Li WH, Qiu F, Shi AC. Perfectly ordered patterns via corner-induced heterogeneous nucleation of self-assembling block copolymers confined in hexagonal potential wells. *Macromolecules*. 2015;**48**:4174-4182. DOI: 10.1021/acs.macromol.5b00681

[25] Kim SO, Solak HH, Stoykovich MP, Ferrier NJ, de Pablo JJ, Nealey PF. Epitaxial self-assembly of block copolymers on lithographically defined nanopatterned substrates. *Nature*. 2003;**424**:411-414. DOI: 10.1038/nature01775

[26] Ruiz R, Kang HM, Detcheverry FA, Dobisz E, Kercher DS, Albrecht TR, et al. Density multiplication and improved lithography by directed block copolymer assembly. *Science*. 2008;**321**:936-939. DOI: 10.1126/science.1157626

[27] Segalman RA, Yokoyama H, Kramer EJ. Graphoepitaxy of spherical domain block copolymer films. *Advanced Materials*. 2001;**13**:1152-1155. DOI: 10.1002/1521-4095(200108)13:15<1152::AID-ADMA1152>3.0.CO;2-5

[28] Cheng JY, Mayes AM, Ross CA. Nanostructure engineering by templated self-assembly of block copolymers. *Nature Materials*. 2004;**3**:823-828. DOI: 10.1038/nmat1211

[29] Matsen MW, Schick M. Stable and unstable phases of a diblock copolymer melt. *Physical Review Letters*. 1994;**72**:2660-2663. DOI: 10.1103/PhysRevLett.72.2660

[30] Matsen MW. The standard Gaussian model for block copolymer melts. *Journal of Physics. Condensed Matter*. 2002;**14**:R21-R47. DOI: 10.1088/0953-8984/14/2/201

[31] Tyler CA, Morse DC. Orthorhombic Fddd network in triblock and diblock

- copolymer melts. *Physical Review Letters*. 2005;**94**:208302. DOI: 10.1103/PhysRevLett.94.208302
- [32] Liu CC, Ramirez-Hernandez A, Han E, Craig GSW, Tada Y, Yoshida H, et al. Chemical patterns for directed self-assembly of lamellae-forming block copolymers with density multiplication of features. *Macromolecules*. 2013;**46**: 1415-1424. DOI: 10.1021/ma302464n
- [33] Tada Y, Akasaka S, Takenaka M, Yoshida H, Ruiz R, Dobisz E, et al. Nine-fold density multiplication of hcp lattice pattern by directed self-assembly of block copolymer. *Polymer*. 2009;**50**: 4250-4256. DOI: 10.1016/j.polymer.2009.06.039
- [34] Hashimoto T, Sakamoto N, Koga T. Nucleation and growth of anisotropic grain in block copolymers near order-disorder transition. *Physical Review E*. 1996;**54**:5832-5835. DOI: 10.1103/PhysRevE.54.5832
- [35] Wickham RA, Shi AC, Wang ZG. Nucleation of stable cylinders from a metastable lamellar phase in a diblock copolymer melt. *The Journal of Chemical Physics*. 2003;**118**: 10293-10305. DOI: 10.1063/1.1572461
- [36] Kalikmanov VI. Nucleation theory. *Lecture Notes in Physics*. 2012;**860**: 17-53. DOI: 10.1007/978-90-481-3643-8
- [37] Spencer RKW, Wickham RA. Simulation of nucleation dynamics at the cylinder-to-lamellar transition in a diblock copolymer melt. *Soft Matter*. 2013;**9**:3373-3382. DOI: 10.1039/C3SM27499C
- [38] Ohta T, Ito A. Dynamics of phase-separation in copolymer-homopolymer mixtures. *Physical Review E*. 1995;**52**: 5250-5260. DOI: 10.1103/PhysRevE.52.5250
- [39] Ohta T, Kawasaki K. Equilibrium morphology of block copolymer melts. *Macromolecules*. 1986;**19**:2621-2632. DOI: 10.1021/ma00164a028
- [40] Tang QY, Ma YQ. High density multiplication of graphoepitaxy directed block copolymer assembly on two-dimensional lattice template. *Soft Matter*. 2010;**6**:4460. DOI: 10.1039/c0sm00238k
- [41] Krishnan MR, Lu KY, Chiu WY, Chen IC, Lin JW, Lo TY, et al. Directed self-assembly of star-block copolymers by topographic nanopatterns through nucleation and growth mechanism. *Small*. 2018;**14**:1704005. DOI: 10.1002/sml.201704005
- [42] Harrison C, Angelescu DE, Trawick M, Cheng ZD, Huse DA, Chaikin PM, et al. Pattern coarsening in a 2D hexagonal system. *EPL*. 2004;**67**: 800-806. DOI: 10.1209/epl/i2004-10126-5
- [43] Vega DA, Harrison CK, Angelescu DE, Trawick ML, Huse DA, Chaikin PM, et al. Ordering mechanisms in two-dimensional sphere-forming block copolymers. *Physical Review E*. 2005;**71**: 061803. DOI: 10.1103/PhysRevE.71.061803
- [44] Gómez LR, Vallés EM, Vega DA. Lifshitz-Safran coarsening dynamics in a 2D hexagonal system. *Physical Review Letters*. 2006, 2006;**97**:188302. DOI: 10.1103/PhysRevLett.97.188302
- [45] Pezzutti AD, Vega DA, Villar MA. Dynamics of dislocations in a two-dimensional block copolymer system with hexagonal symmetry. *Philosophical Transactions. Series A, Mathematical, Physical, and Engineering Sciences*. 2011;**369**:335-350. DOI: 10.1098/rsta.2010.0269

New Methods in the Synthesis of (Meth)Acrylates

Cengiz Soykan

Abstract

Generally, the words “reactive polymers” and “functional polymers” mean the same thing and are used interchangeably in most studies and describe cross-linked (insoluble) bead-structured resins containing chemically reactive functional groups. In this way, reactive polymers are widely used as polymeric reagents or polymer supports in biochemical and chemical applications. Functional (meth)acrylates referred here to supply “functional esters” ruins as a general reactive group precursor. In other sense, the leaving (activating) groups of these monomers may easily react with the alcohols and amines carrying the desired reactive groups and therefore, in general, provide a single reaction step for the synthesis of reactive polymers. In this paper, we suggest new routes for a new (meth)acrylate-based monomers and polymers. Also, the synthesis of a serial new (meth)acrylate esters including amide, dioxolane, benzofuran, and chalcone groups is described.

Keywords: activated (meth)acrylates, α -chloro-N-aryl acetamides, dioxolane, benzofuran, chalcone, functional polymers

1. Introduction

Today, the term “functional polymers” is used to compare the specific properties such as chemical, physicochemical or biochemical functions of polymeric materials and to classify polymers in this field. For the preparation of different purpose polymers, new monomers are obtained by binding the functional group to the structure of certain monomers. Copolymers of commercial monomers and monomers with functional groups are prepared and their properties are investigated. In addition, chemical polymers are chemically modified and functional groups are bonded to produce chemical-reactive polymers in both the industry and polymer-based chemistry. The application of chemical modification to the polymers is used to prepare polymers which cannot be prepared by direct polymerization of the monomer.

There are two ways to synthesize a polymer with the planned pendant reactive group: (1) functionalization of a non-functional polymer by chemical modification; (2) binding of a reactive side group to the monomer and polymerization of this reactive group monomer by chain addition polymerization methods [1]. Both methods have been successfully applied to obtain vinyl polymers. The synthesis and studies on (meth)acrylate polymers have attracted the attention of various groups in recently [2–13]. Acrylate homopolymers along with their copolymers are used in various fields such as thin films, adsorption, fibers, filament coatings, lithography, lacquers, adhesives, printing inks, and binders [14–34].

There are some disadvantages in linking functional groups on polymers:

1. The distribution of bound functional groups on polymer molecules may not be regular.
2. The density of the bound reactive groups is generally low, and therefore, in such polymers, there may be no results in terms of reaction between the functional group and the polymer structure.
3. Polymer functionalization reactions should be carried out in temperate conditions and the efficiency of the reactions should be quantitative. Because it will be a part of the polymer chain in the undesirable groups that may occur by side reactions. Therefore, precautions should be taken in such a way that no side reactions occur as long as possible.
4. The activity of the groups to be bound on the polymer molecules may be different due to the surrounding of the macromolecule compared to similar small molecules. Therefore, more characteristic reaction conditions may be required for a satisfactory transformation.
5. Side reactions during the polymer functionalization reaction will produce impurities in the obtained polymer due to unreacted groups and other functional groups, which will reveal the problem of purification.
6. Due to undesirable side reactions, the chemical and physical properties of the polymer, such as dissolution, cross-linking, halogen and gas release, can be varied.
7. Since the functional groups allow for cross-linking during polymerization and the polymer will not dissolve, there may not be sufficient analytical methods to investigate the properties of the polymer.
8. In particular, where the polymer chain is susceptible to chemical reactions, reactions should be carried out without degradation.

2. Functional methacrylate ester monomer and polymer synthesis from oxirane compounds

2.1 Synthesis of aryloxy-2,3-epoxy propane (oxirane)

The oxirane compound is obtained from the epichlorohydrin with an arylalcohol. The synthesis reaction scheme is given in **Figure 1**.

A typical procedure for the reaction of arylalcohol with epichlorohydrin is as follows: arylalcohol (0.5 mol) and epichlorohydrin (1.5 mol) and sodium hydroxide (0.55 mol) are mixed with magnetic stirrer at 50°C for 10 h, and then

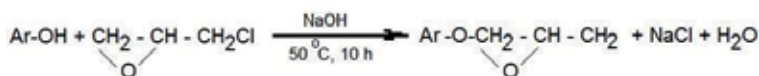


Figure 1.
Reaction scheme of aryloxy-2,3-epoxy propane.

the reaction mixture is stirred at room temperature for 15 h. The organic layer is washed several times with diethylether and dried over magnesium sulfate. After removing diethylether, the excess of epichlorohydrin is distilled at 50°C and 60 mmHg. The remaining reaction mixture is distilled at 110°C and 12 mmHg (oxirane product yield: 87%). The structure of the compound aryloxy-2,3-epoxy propane is identified by the FT-IR techniques. FT-IR (cm^{-1}): 3100–2800 (C—H); 1590 (C=C); 1250 (epoxy C—O); 950–770 (epoxy C—H).

2.2 Synthesis of aryloxy-2-hydroxypropyl methacrylate monomer

Oxirane compound is distilled off again at 110°C and 12 mmHg by vacuum distillation. In a reaction flask, 0.26 mol of oxirane, 0.54 mole of methacrylic acid, 0.30 mol of pyridine, and 100 ppm of hydroquinone are mixed in 200 ml of toluene solvent at 85°C for 24 h with a magnetic stirrer. After the reaction is complete, 30% sodium hydroxide solution is added until the mixture is taken up in ethereal separation funnel and basic. The basic aqueous phase obtained at the end of the extraction is extracted three times with diethylether in another separating funnel. The collected ethereal phases are taken to the separating funnel and extracted until neutral with water. The etheric phases are taken into a collection container and a sufficient amount of anhydrous magnesium sulfate is thrown into it and left to dry for 24 h. At the end of the filtration process, the mixture separated from magnesium sulfate is distilled off the toluene at 45°C and 50 mmHg. To the remaining mixture, 50 ppm of hydroquinone was added and vacuum distillation is carried out with monomer at 150°C and 1 mmHg (monomer yield: 65%). The synthesis reaction scheme is given in **Figure 2**.

The structure of the monomer is confirmed by the FT-IR and ^1H - and ^{13}C -NMR spectroscopic techniques. FT-IR (cm^{-1}): 3600–3200 (—OH); 3100–2800 (C—H); 1720 ($>\text{C}=\text{O}$); 1630 ($\text{CH}_2=\text{C}$); 1580 (aromatic, C=C); 1250 (C—O). ^1H -NMR (CDCl_3 , TMS): 8.0–6.8 (aromatics —H); 6.2–5.44 ($\text{CH}_2=\text{C}$); 4.25 (O—H); 1.8 (CH_3). ^{13}C -NMR (CDCl_3 , TMS): 157.2–113.8 (aromatics —C); 134.0–124.4 ($\text{CH}_2=\text{C}$); 165.6 ($>\text{C}=\text{O}$); 67.8 ($\text{CH}-\text{OH}$); 17.2 (CH_3).

2.3 Free radical polymerization of aryloxy-2-hydroxypropyl methacrylate monomer

Appropriate amounts of aryloxy-2-hydroxypropyl methacrylate monomer and chloroform and 2,2'-azobisisobutyronitrile (AIBN) as an initiator (2% of the monomer mass) are disposed in a polymerization tube and liquidated with nitrogen for 10 min. The sealed and waxed polymerization reaction tube is placed at $60 \pm 1^\circ\text{C}$ for 24 h in oil bath. The reaction product is poured dropwise into an abundant of diethylether. The obtained polymer is purified by re-precipitation with diethylether from a chloroform solution and the latest operation dried under vacuum oven (conversion 90%). The synthesis reaction scheme is given in **Figure 3**.

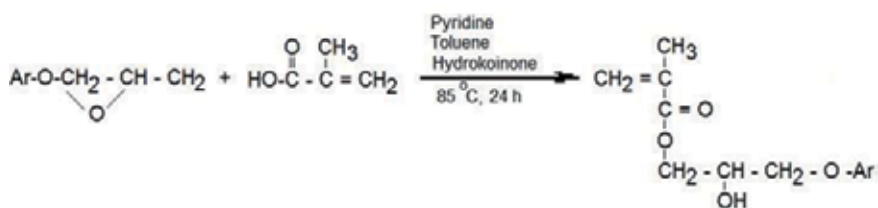


Figure 2.
Reaction scheme of aryloxy-2-hydroxypropyl methacrylate monomer.

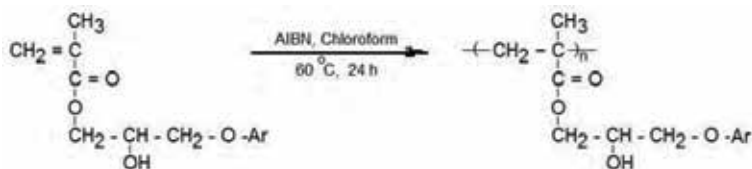


Figure 3.
Reaction scheme of poly aryloxy-2-hydroxypropyl methacrylate.

The formation of the homopolymer of aryloxy-2-hydroxypropyl methacrylate is confirmed by the FT-IR and $^1\text{H-NMR}$ spectroscopic techniques. The main description for the polymerization of the monomer is that the characteristic double bond (vinyl structure double bond) peak signal of the monomer in the FT-IR spectrum is fully depleted and does not peak in this region in the FT-IR spectrum of the polymer. This is because the addition polymerization proceeds through the opening of the pi bond in the vinyl group. This has been effectively observed in the synthesis and characterizations herein. Two signals altered in the FT-IR spectrum of the monomer: the stretching vibration band of the vinyl group $\text{C}=\text{C}$ at 1630 cm^{-1} and the absorption signal at 920 cm^{-1} assigned to the $\text{C}-\text{H}$ bending of geminal $=\text{CH}_2$.

The information is clearly seen in $^1\text{H-NMR}$ spectroscopy on polymer formation. The formation of polymer is clearly evident from the disappearing of the two singlets at 6.3 and 5.4 ppm of the vinyl protons and the wide peaks at 2.4–1.3 ppm due to the conversion to the aliphatic $-\text{CH}_2$ group.

3. Functional methacrylate ester monomer and polymer synthesis from arylacetylhalide compounds

3.1 Synthesis of arylacetylhalide

Arylacetyl chloride is prepared by reacting arylalcohol with chloroacetyl chloride using the K_2CO_3 . A typical procedure for the acylation reaction of arylalcohol with chloroacetyl chloride is as follows: arylalcohol (1 mol) and K_2CO_3 are dissolved in 20 ml of anhydrous benzene at 0°C , and then 1.1 mol of chloroacetyl-chloride is added dropwise to this solution. The reaction mixture is stirred at room temperature for 15 h. The organic layer is washed several times with diethylether and dried over MgSO_4 . After removing diethylether, α -chloro-arylacetyl chloride is crystallized from methanol (yield: 80%). The structure of the compound arylacetylhalide is identified by the FT-IR techniques. FT-IR (cm^{-1}): 3100–2800 ($\text{C}-\text{H}$); 1730 ($>\text{C}=\text{O}$); 1580 (aromatic, $\text{C}=\text{C}$). The synthesis reaction scheme is given in **Figure 4**.

3.2 Synthesis of aryloxycarbonyl methyl methacrylate monomer

Aryloxycarbonyl methyl methacrylate is synthesized as follows: a mixture of arylacetyl chloride (1 mol), sodium methacrylate (1.1 mol) in 100 ml acetonitrile and triethylbenzylammonium chloride (TEBAC) (0.1 mol) as a phase transfer

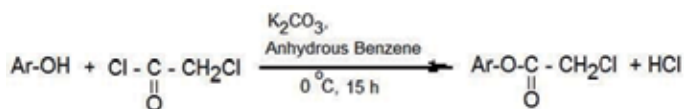


Figure 4.
Reaction scheme of arylacetylhalide.

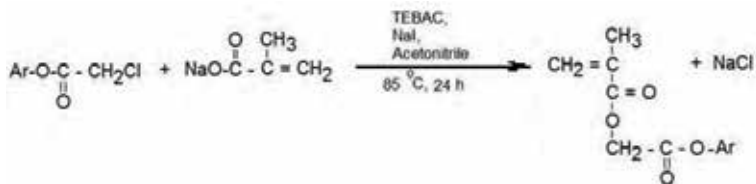


Figure 5.
 Reaction scheme of aryloxycarbonyl methyl methacrylate monomer.

catalyst better and sodium iodide (NaI) (0.1 mol) as catalyst are receipt in a three-neck round bottom flask equipped with a thermometer, magnetic stirrer, and heated to 85°C in a reflux condenser in the presence of 100 ppm hydroquinone. The reaction is continued for an additional 30 h. The reaction mixture is cooled to 20°C and moved to a separating funnel, washed sequentially with diethylether, 5% NaOH, and distilled water. The organic layer are spooled and dried over anhydrous magnesium sulfate (MgSO₄) for 24 h. Magnesium sulfate is filtered and the diethylether is removed from the organic layers with a rotary evaporator. The resulting monomer is purified by recrystallization from ethanol (yield: 85%). The synthesis reaction scheme is given in **Figure 5**.

The structure of the monomer is confirmed by the FT-IR and ¹H- and ¹³C-NMR spectroscopic techniques. FT-IR (cm⁻¹): 3100–2800 (C—H); 1730 (>C=O); 1630 (CH₂=C); 1580 (aromatic, C=C); 1250 (C—O). ¹H-NMR (CDCl₃, TMS): 7.9–6.6 (aromatics —H); 6.2–5.41 (CH₂=C); 1.8 (CH₃). ¹³C-NMR (CDCl₃, TMS): 157.1–113.4 (aromatics —C); 134.4–124.2 (CH₂=C); 165.2 (>C=O); 18.1 (CH₃).

3.3 Free radical polymerization of aryloxycarbonyl methyl methacrylate monomer

Homopolymer of aryloxycarbonyl methyl methacrylate is synthesized using 2,2'-azobisisobutyronitrile (AIBN) as an initiator (2% of the monomer mass) in 1,4-dioxane solution. The reaction mixture is de-aerated by passing nitrogen gas for 10 min, then the tube is tightly sealed and kept in a thermostatic oil bath at 60 ± 1°C for 24 h. The homopolymer is precipitated in excess methanol, purified by dissolution in 1,4-dioxane and reprecipitation in methanol. The homopolymer is dried in vacuum to constant weight (conversion 90%). The synthesis reaction path is given in **Figure 6**.

The formation of the homopolymer of aryloxycarbonyl methyl methacrylate is confirmed by the ¹H-NMR and FT-IR spectroscopic techniques. The information is clearly seen in ¹H-NMR spectroscopy on polymer formation. The formation of polymer is clearly evident from the disappearing of the two singlets at 6.3 and 5.4 ppm of the vinyl protons and the wide peaks at 2.4–1.3 ppm due to the conversion to the aliphatic-CH₂ group. The main description of the polymer is exactly the extinction of some characteristic peaks of the double bond in the FT-IR spectrum, and this has

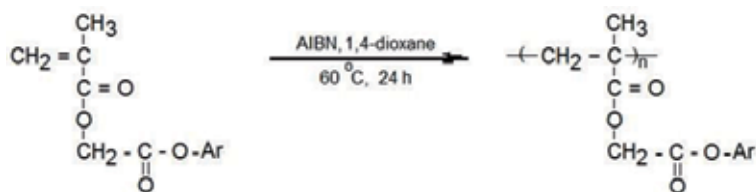


Figure 6.
 Reaction scheme of poly aryloxycarbonyl methyl methacrylate.

been effectively observed in the synthesis and characterizations herein. Two signals altered in the FT-IR spectrum of the monomer: the stretching vibration band of the vinyl group C=C at 1630 cm^{-1} and the absorption signal at 920 cm^{-1} assigned to the C—H bending of geminal=CH₂.

4. Functional methacrylate ester monomer and polymer synthesis from α -chloro-N-arylacетamide compounds

4.1 Synthesis of α -chloro-N-arylacетamide

α -chloro-N-arylacетamide is prepared by reacting arylamine with chloroacetylchloride using the K₂CO₃. A typical procedure is as follows: arylamine (1 mol) and K₂CO₃ were dissolved in 20 ml of anhydrous benzene at 0°C, and then 1.1 mol of chloroacetylchloride are added dropwise to this solution. The reaction mixture is stirred at room temperature for 15 h. The organic phase is washed several times with diethylether and dried over MgSO₄. After removing diethylether, α -chloro-N-arylacетamide is crystallized from methanol (yield: 80%). The synthesis reaction scheme is given in **Figure 7**.

The structure of the compound α -chloro-N-arylacетamide is identified by the FT-IR techniques. FT-IR (cm⁻¹): 3340 (NH); 3100–2800 (C—H); 1680 (>C=O); 1580 (aromatic, C=C).

4.2 Synthesis of arylamido methyl methacrylate monomer

Arylamido methyl methacrylate is synthesized as follows: 1.1 mol sodium methacrylate, 1 mol α -chloroacетamide, 0.1 mol NaI and 0.1 mol TEBAC and as catalyst are stirred in 100 ml acetonitrile at 80°C in a reflux condenser for 30 h in the presence of 100 ppm hydroquinone. After the solution is cooled to 20°C and neutralized with a 5% NaOH solution. The organic phase is washed a few times with water, and the water phase is washed with diethylether a several times. The diethyl ether phase and the acetonitrile phase are spooled and dried over anhydrous magnesium sulfate for 24 h. Diethyl ether and acetonitrile are removed with a rotary evaporator. The organic phases are collected and the residue is distilled at 130°C at 5 mmHg to give a colorless liquid (yield: 80%). The synthesis reaction scheme is given in **Figure 8**.

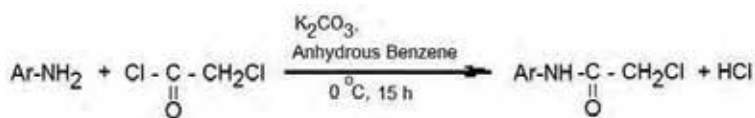


Figure 7.
Reaction scheme of α -chloro-N-arylacетamide.

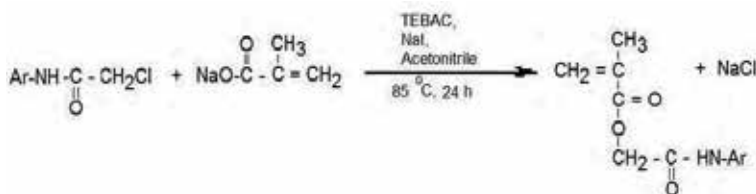


Figure 8.
Reaction scheme of arylamido methyl methacrylate monomer.

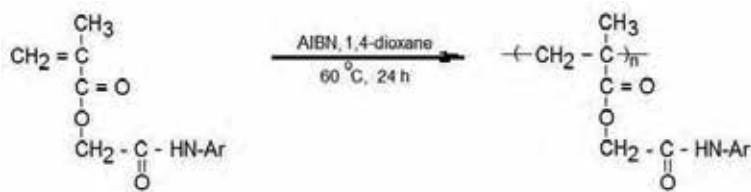


Figure 9.
Reaction scheme of poly arylamido methyl methacrylate.

The structure of the monomer is confirmed by the FT-IR and ^1H - and ^{13}C -NMR spectroscopic techniques. FT-IR (cm^{-1}): 3325 (NH); 3100–2800 (C—H); 1680 ($>\text{C}=\text{O}$); 1630 ($\text{CH}_2=\text{C}$); 1580 (aromatic, C=C); 1230 (C—O—C). ^1H -NMR (CDCl_3 , TMS): 9.1 (N—H); 8.0–6.7 (aromatics —H); 6.3–5.43 ($\text{CH}_2=\text{C}$); 1.8 (CH_3). ^{13}C -NMR (CDCl_3 , TMS): 157.1–113.4 (aromatics —C); 134.4–124.2 ($\text{CH}_2=\text{C}$); 168.1 ($>\text{C}=\text{O}$); 18.1 (CH_3).

4.3 Free radical polymerization of arylamido methyl methacrylate monomer

Arylamido methyl methacrylate monomer is freed from inhibitor by washing with a dilute KOH solution followed by distilled water and then drying over MgSO_4 . Appropriate amounts of arylamido methyl methacrylate monomer, 2,2'-azobisisobutyronitrile (AIBN) (2% of the monomer mass) and 1,4-dioxane are placed in a polymerization reaction tube and purged with nitrogen for 15 min. The closed mouth polymerization reaction tube is kept at $60 \pm 1^\circ\text{C}$ for 30 h in oil bath. The reaction product is poured dropwise into an abundant of n-hexane. The obtained polymer is purified by re-precipitation with n-hexane from a 1,4-dioxane solution and the latest operation dried under vacuum oven (conversion 90%). The synthesis reaction scheme is given in **Figure 9**.

The structure of poly arylamido methyl methacrylate is confirmed by the FT-IR and ^1H -NMR spectroscopic techniques. The main description for the polymerization of the monomer is that the characteristic double bond (vinyl structure double bond) peak signal of the monomer in the FT-IR spectrum is fully depleted and does not peak in this region in the FT-IR spectrum of the polymer. This is because the addition polymerization proceeds through the opening of the pi bond in the vinyl group. This has been effectively observed in the synthesis and characterizations herein. Two signals altered in the FT-IR spectrum of the monomer: the stretching vibration band of the vinyl group C=C at 1630 cm^{-1} and the absorption signal at 920 cm^{-1} assigned to the C—H bending of geminal= CH_2 .

The information is clearly seen in ^1H -NMR spectroscopy on polymer formation. The formation of polymer is clearly evident from the disappearing of the two singlets at 6.3 and 5.4 ppm of the vinyl protons and the wide peaks at 2.8–1.4 ppm due to the conversion to the aliphatic — CH_2 group.

5. Functional methacrylate ester monomer and polymer synthesis from aryl-1,3-dioxolane compounds

5.1 Synthesis of (aryl-1,3-dioxolane-4-yl) methanol

(Aryl-1,3-dioxolan-4-yl)methanol is prepared by reacting arylaldehyde with glycerin using the *p*-toluenesulfonic acid as catalyst. A typical procedure is as follows: Arylaldehyde (0.1 mol), glycerin (0.1 mol), *p*-toluenesulfonic acid (*p*-TOS)

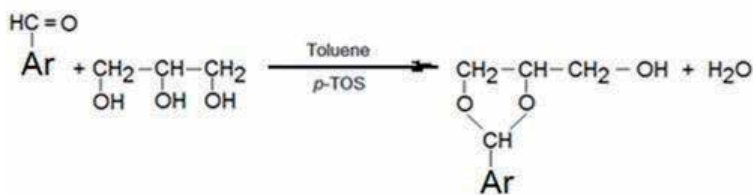


Figure 10.
Reaction scheme of (aryl-1,3-dioxolane-4-yl) methanol.

(0.5 g, as catalyst) and toluene (30 mL) are placed in a 100 mL three-necked reaction balloon fitted with a thermometer, condenser and a stirrer. The reaction mixture is refluxed at 115°C for 2 h with strong mixing. The reaction mixture is extracted a few times with diethyl ether and then 5% KOH solution, diethyl ether and toluene, respectively. The diethyl ether and toluene solvents are evaporated with rotary evaporator. The raw product is washed with water (40 mL × 3) and dried over anhydrous magnesium sulfate at overnight. The synthesis reaction scheme is given in **Figure 10**.

The structure of (aryl-1,3-dioxolane-4-yl) methanol is identified by the FT-IR and ¹H- and ¹³C-NMR spectroscopic techniques. FT-IR (cm⁻¹): 3500–3110 (O—H); 3100–2800 (C—H); 1570 (aromatic, C=C); 1180 (C—O—C). ¹H-NMR (CDCl₃, TMS): 7.48–7.0 (aromatics —H); 6.3–5.52 (CH₂=C); 4.0–3.7 (—O—CH); 4.17–4.11 (O—CH₂); 3.16 (—OH), 3.0 (CH₂). ¹³C-NMR (CDCl₃, TMS): 151.1–116.4 (aromatics —C); 134.4–124.2 (C₂=C); 63.1 (C₂); 68.8 (O—C₂); 77.3 (O—CH).

5.2 Synthesis of (aryl-1,3-dioxolane-4-yl) methyl acrylate monomer

(Aryl-1,3-dioxolan-4-yl)methanol (0.1 mol), triethyl amine (NR₃) (20 mL, as catalyst) and diethyl ether (40 mL) are filled in a 250 mL four-necked reaction balloon fitted with a thermometer, a condenser, a stirrer and an addition funnel including 15 mL acryloyl chloride. The acryloyl chloride is added drop wise to the solution with a dropping funnel. The temperature of the reaction mixture is hold by a cryostat at -5°C for 18 h. The reaction mixture is extracted a few times with 5% KOH solution and after dried over anhydrous magnesium sulfate for 24 h. The solvents are removed by the vacuum evaporator. The synthesis reaction scheme is given in **Figure 11**.

The structure of (aryl-1,3-dioxolane-4-yl) methyl acrylate is confirmed by the FT-IR and ¹H- and ¹³C-NMR spectroscopic techniques. FT-IR (cm⁻¹): 3100–2800 (C—H); 1727 (>C=O); 1630 (CH₂=C); 1570 (aromatic, C=C); 1190 (C—O—C). ¹H-NMR (CDCl₃, TMS): 7.6–7.0 (aromatics —H); 6.3–5.52 (CH₂=C); 5.8 (Ar—CH); 4.2–3.8 (—O—CH); 4.2–4.1 (O—CH₂); 3.0 (CH₂). ¹³C-NMR (CDCl₃, TMS): 166.2 (>C=O); 151.1–116.4 (aromatics —C); 130.4–122.2 (C₂=C); 103.2 (Ar—C₂); 63.1 (C₂); 68.8 (O—C₂); 87.2 (O—CH).

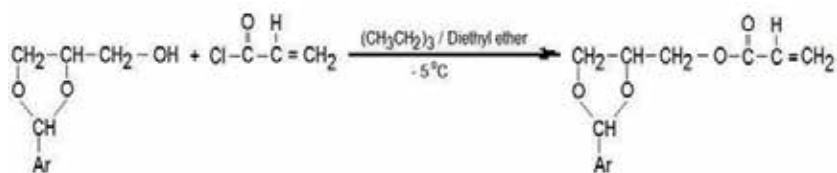


Figure 11.
Reaction scheme of (aryl-1,3-dioxolane-4-yl) methyl acrylate monomer.

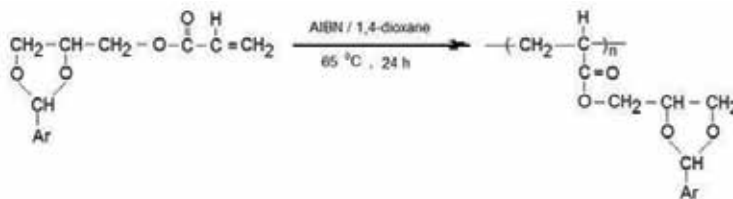


Figure 12.
Reaction scheme of poly(aryl-1,3-dioxolane-4-yl) methyl acrylate.

5.3 Free radical polymerization of arylamido methyl methacrylate monomer

Free radical polymerization reaction of (aryl-1,3-dioxolane-4-yl) methyl acrylate monomer is conducted in a polymerization reaction tube using 2,2'-azobisisobutyronitrile (AIBN) (1% of the monomer mass) as initiator in 10 mL of 1,4-dioxane, at 65°C with 90% conversion in 6 h. The formed polymer is precipitated in ethyl alcohol. The obtained polymer is dried under vacuum at 45°C for 24 h for constant weight. The synthesis reaction scheme is given in **Figure 12**.

The structure of poly(aryl-1,3-dioxolane-4-yl) methyl acrylate is confirmed by the FT-IR and ¹H-NMR spectroscopic techniques. The information is clearly seen in ¹H-NMR spectroscopy on polymer formation. The formation of polymer is clearly evident from the disappearing of the two singlets at 6.3 and 5.42 ppm of the vinyl protons and the wide peaks at 2.9–1.5 ppm due to the conversion to the aliphatic —CH₂ group. The main description of the polymer is exactly the extinction of some characteristic peaks of the double bond in the FT-IR spectrum, and this has been effectively observed in the synthesis and characterizations herein. Two signals altered in the FT-IR spectrum of the monomer: the stretching vibration band of the vinyl group C=C at 1630 cm⁻¹ and the absorption signal at 920 cm⁻¹ assigned to the C—H bending of geminal=CH₂.

6. Functional methacrylate ester monomer and polymer synthesis from benzofuran compounds

6.1 Synthesis of acetyl benzofuran

Synthesis of acetyl benzofuran is as follows: Potassium carbonate (K₂CO₃) (0.1 mol) and 2-hydroxybenzaldehyde (1 mol) are dissolved in 30 ml of absolute acetone. The reaction mixture is taken in a three-neck round bottom reaction balloon equipped with a magnetic stirrer, a thermometer, and cooled to 0°C. After then chloroacetone (1.1 mol) are added dropwise to this solution at 5°C, and stirred at 20°C for 16 h. The organic phase is washed a few times with distilled water and separation layer is filtered through filter paper and dried over anhydrous MgSO₄ overnight. Acetyl benzofuran compound is crystallized from ethyl alcohol. Yield: 85%. The synthesis reaction scheme is given in **Figure 13**.

The structure of acetyl benzofuran is identified by the FT-IR techniques. FT-IR (cm⁻¹): 3100–2800 (C—H); 1690 (>C=O); 1570 (aromatic, C=C).

6.2 Synthesis of bromo-acetyl benzofuran

Acetyl benzofuran (1 mol) is dissolved in 200 mL acetic acid, and after then bromo is added dropwise to this solution at 25°C for 2 h. After bromination reaction, the mixture is divided into ice-water. The separation layer is filtered through

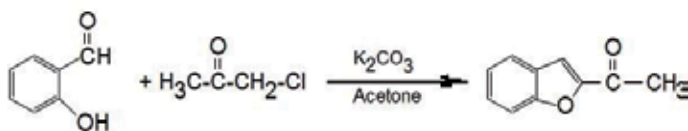


Figure 13.
Reaction scheme of acetyl benzofuran.

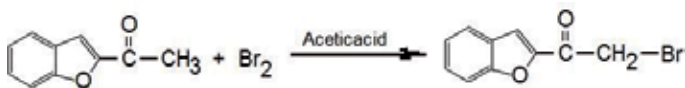


Figure 14.
Reaction scheme of bromo acetyl benzofuran.

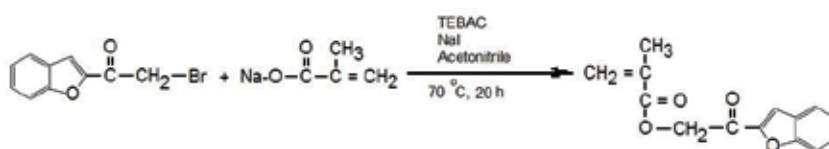


Figure 15.
Reaction scheme of acetyl benzofuryl methyl methacrylate monomer.

filter paper and dried over anhydrous magnesium sulfate (MgSO_4) overnight. Bromo-acetyl benzofuran compound is crystallized from ethyl alcohol. Yield: 85%. The synthesis reaction scheme is given in **Figure 14**.

The structure of bromo acetyl benzofuran is identified by the FT-IR techniques. FT-IR (cm^{-1}): 3100–2800 (C—H); 1690 ($>\text{C}=\text{O}$); 1570 (aromatic, C=C); 780 (CH—Br).

6.3 Synthesis of acetyl benzofuryl methyl methacrylate monomer

Sodium methacrylate (1.1 mol), bromo-acetyl benzofuran (1 mol), sodium iodide (0.1 mol) and triethylbenzylammoniumchloride (TEBAC) (0.1 mol) as catalyst are mixed in 100 mL acetonitrile at 70°C in a reflux condenser for 20 h in the beside of 100 ppm hydroquinone as an inhibitor. After then the solution is cooled to 20°C and neutralized with a 5% NaOH solution. The organic phase is washed with diethyl ether a few times. The diethyl ether and acetonitrile layers are spooled and dried over anhydrous magnesium sulfate (MgSO_4) overnight. Diethyl ether and acetonitrile are evaporated with a rotary evaporator. The organic layers are collected and the residue is crystallized from ethyl alcohol. Yield: 80%. The synthesis reaction scheme is given in **Figure 15**.

The structure of acetyl benzofuryl methyl methacrylate is confirmed by the FT-IR and ^1H - and ^{13}C -NMR spectroscopic techniques. FT-IR (cm^{-1}): 3100–2800 (C—H); 1735 ($>\text{C}=\text{O}$); 1685 (—C=O); 1630 ($\text{CH}_2=\text{C}$); 1580 (aromatic, C=C); 1190 (C—O—C). ^1H -NMR (CDCl_3 , TMS): 7.7–7.2 (aromatics —H); 6.3–5.48 ($\text{CH}_2=\text{C}$); 4.2–4.0 (O— CH_2); 1.5 (CH_3). ^{13}C -NMR (CDCl_3 , TMS): 178.2 (—C=O); 168.1 ($>\text{C}=\text{O}$); 148.1–116.2 (aromatics —C); 130.1–122.0 ($\text{CH}_2=\text{C}$); 68.8 (O— CH_2); 19.1 (CH_3).

6.4 Free radical polymerization of acetyl benzofuryl methyl methacrylate monomer

The preparation of homopolymer of Acetyl benzofuryl methyl methacrylate monomer is synthesized by free radical polymerization in 1,4-dioxane solvent

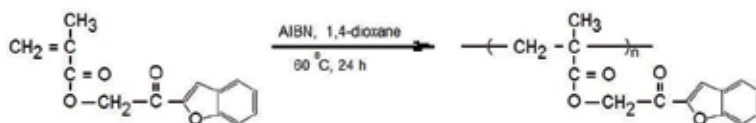


Figure 16.
Reaction scheme of poly acetyl benzofuryl methyl methacrylate.

using 2,2'-azobisisobutyronitrile (AIBN) as a free radical initiator. The homopolymer is purified by repeated reprecipitation from 1,4-dioxane and then filtered and dried until a constant weight is attained. The synthesis reaction path is given in **Figure 16**.

The structure of poly acetyl benzofuryl methyl methacrylate is confirmed by the FT-IR and $^1\text{H-NMR}$ spectroscopic techniques. The information is clearly seen in $^1\text{H-NMR}$ spectroscopy on polymer formation. The formation of polymer is clearly evident from the disappearing of the two singlets at 6.3 and 5.42 ppm of the vinyl protons and the wide peaks at 2.9–1.5 ppm due to the conversion to the aliphatic $\text{—CH}_2\text{—}$ group. The main description of the polymer is exactly the extinction of some characteristic peaks of the double bond in the FT-IR spectrum, and this real is effectively identified herein. Two signals altered in the FT-IR spectrum of the monomer: the stretching vibration band of the vinyl group $\text{C}=\text{C}$ at 1630 cm^{-1} and the absorption signal at 920 cm^{-1} assigned to the C—H bending of geminal =CH_2 .

7. Functional methacrylate ester monomer and polymer synthesis from photocrosslinkable functional group (pendant chalcone unit) compounds

7.1 Synthesis of hydroxyphenyl-methoxystyryl ketone (hydroxy chalcone)

Substituted benzaldehyde (1 mol) and substituted acetophenone (1 mol) are dissolved in 50 mL of ethyl alcohol and cooled at 18°C . An aqueous NaOH solution (1 mol in 40 mL of distilled water) is then added dropwise with constant mixing and as keeping the temperature constant at 18°C . After stirring the reaction mixture for 12 h at 20°C , it is neutralized with dilute HCl to isolate the compound. The obtained solid matter is filtered through filter paper, washed with ice cold water, dried and recrystallized from ethyl alcohol. Yield: 75%. The synthesis reaction scheme is given in **Figure 17**.

The structure of hydroxyl chalcone is identified by the FT-IR techniques. FT-IR (cm^{-1}): 3500–3200 (O—H); 3100–2800 (C—H); 1690 ($>\text{C}=\text{O}$); 1605 ($\text{—CH}=\text{CH—}$); 1570 (aromatic, $\text{C}=\text{C}$).

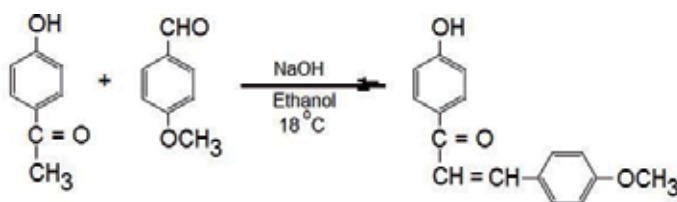


Figure 17.
Reaction scheme of hydroxyl chalcone.

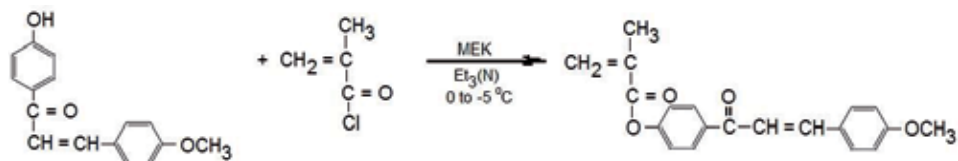


Figure 18.
Reaction scheme of methacryloyloxyphenyl-methoxystyryl ketone.

7.2 Synthesis of methacryloyloxyphenyl-methoxystyryl ketone

In a 250 mL three-necked flask, triethylamine (3 mol) and hydroxyphenyl-methoxystyryl ketone (1 mol) are dissolved in 100 mL of methyl ethyl ketone (MEK) and cooled between 0 and -5°C . Methacryloyl chloride (1.1 mol) in 50 mL of methyl ethyl ketone is then added drop by drop with mixing. After then, the reaction mixture is mixed for 3 h at 20°C and the precipitated quaternary ammonium salt is filtered off. Later, 100 ppm of hydroquinone is added to this solution and the MEK is removed by the vacuum evaporator. The raw product is dissolved in diethyl ether, washed one after another with a 5% aqueous potassium hydroxide solution and distilled water, dried over anhydrous magnesium sulfate (MgSO_4) and the diethyl ether is removed by the evaporator. The obtained material is recrystallized from methyl alcohol to get the shining yellow flakes of substituted methacryloyloxyphenyl-methoxystyryl ketone. Yield: 80%. The synthesis reaction scheme is given in **Figure 18**.

The structure of methacryloyloxyphenyl-methoxystyryl ketone is confirmed by the FT-IR and ^1H - and ^{13}C -NMR spectroscopic techniques. FT-IR (cm^{-1}): 3100–2800 (C-H); 1740 ($>\text{C=O}$); 1650 (C=O); 1630 ($\text{CH}_2=\text{C}$); 1605 (CH=CH); 1570 (aromatic, C=C); 1190 (C-O-C). ^1H -NMR (CDCl_3 , TMS): 8.1–6.9 (aromatics H); 6.3–5.78 ($\text{CH}_2=\text{C}$, and CH=CH); 3.84 (OCH_3); 1.8 (CH_3). ^{13}C -NMR (CDCl_3 , TMS): 178.0 (C=O); 166.8 ($>\text{C=O}$); 148.1–116.2 (aromatics C); 130.1–122.0 ($\text{CH}_2=\text{C}$, and CH=CH); 58.1 (OCH_3); 19.1 (CH_3).

7.3 Free radical polymerization of substituted methacryloyloxyphenyl-methoxystyryl ketone monomer

Substituted methacryloyloxyphenyl-methoxystyryl ketone is polymerized as a 3 molar solution in MEK using 2,2'-azobisisobutyronitrile (AIBN) as initiator at 70°C . The predetermined quantities of substituted methacryloyloxyphenyl-methoxystyryl ketone, the initiator (1 wt.% of monomer) and solvent are placed in a polymerization tube and the mixture is flushed with a slow stream of nitrogen for 20 min. Then, the tube is closed and placed in the thermostated oil bath at 70°C . After the specified time (12 h), the contents are added to excess methyl alcohol to precipitate the polymer. The crude polymer is purified by redissolving in 1,4-dioxane and reprecipitated by methyl alcohol, filtered, washed with methyl alcohol and dried under vacuum at 45°C for constant weight. Yield: 60%. The reaction scheme is shown below (**Figure 19**).

The structure of poly methacryloyloxyphenyl-methoxystyryl ketone is confirmed by the FT-IR and ^1H -NMR spectroscopic techniques. The information is clearly seen in ^1H -NMR spectroscopy on polymer formation. The formation of polymer is clearly evident from the disappearing of the two singlets at 6.3 and 5.78 ppm of the vinyl protons and the wide peaks at 2.7–1.3 ppm due to the conversion to the aliphatic CH_2 group. The main description of the polymer is exactly the extinction of some characteristic peaks of the double bond in the FT-IR

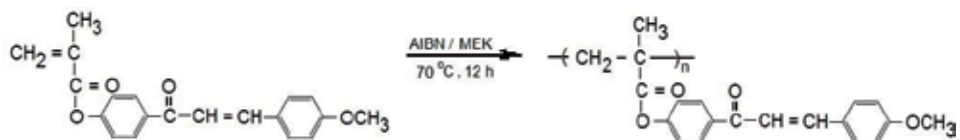


Figure 19.
Reaction scheme of poly methacryloyloxyphenyl-methoxystyryl ketone.

spectrum, and this real is effectively identified herein. Two signals altered in the FT-IR spectrum of the monomer: the stretching vibration band of the vinyl group C=C at 1630 cm⁻¹ and the absorption signal at 920 cm⁻¹ assigned to the C—H bending of geminal=CH₂.

8. Conclusion

In this paper, reaction pathway for the synthesis of new methacrylates having pendant amide, dioxolane, benzofuran and chalcone groups are described. Molecular structure information such as reaction scheme, Fourier transform infrared (FT-IR) and nuclear magnetic resonance spectroscopy of all the compounds is given. All of the methacrylates are used as photodegradable packaging materials and photoresists for microlithography. The increasing utility of photosensitive polymers in many applications such as microelectronics, printing and UV-curable lacquers, and inks is provided us with an incentive to obtain novel polymers.

Conflict of interest


The authors declare no conflict of interest.

Author details

Cengiz Soykan
Department of Materials Science and Nanotechnology, Faculty of Engineering,
University of Uşak, Uşak, Turkey

*Address all correspondence to: cengizsoykan@usak.edu.tr

IntechOpen

© 2020 The Author(s). Licensee IntechOpen. This chapter is distributed under the terms of the Creative Commons Attribution License (<http://creativecommons.org/licenses/by/3.0>), which permits unrestricted use, distribution, and reproduction in any medium, provided the original work is properly cited. 

References

- [1] Sherrington DC. Preparation, functionalization and characteristics of polymer supports. In: Hodge P, Sherrington DC, editors. *Polymer Supported Reactions in Organic Synthesis*. New York: Wiley; 1980. pp. 1-82
- [2] Kalachandra S, Turner DT, Burgess JP, Stejskal EO. Postirradiation reactions of monomer in poly(methyl methacrylate): Analysis by CP/MAS ¹³C NMR. *Macromolecules*. 1994;**27**(21):5948-5949. DOI: 10.1021/ma00099a003
- [3] Soykan C, Güven Ş, Coşkun R. Copolymers of 2-[(5-methylisoxazol-3-yl)amino]-2-oxo-ethyl methacrylate with ethyl methacrylate: Monomer reactivity ratios, thermal properties and antimicrobial activity. *Journal of Macromolecular Science, Part A: Pure and Applied Chemistry*. 2006;**43**:1619-1633. DOI: 10.1080/10601320600897031
- [4] Erol İ, Soykan C. Synthesis, characterization and polymerization of new methacrylate esters having pendant amide moieties. *Journal of Macromolecular Science, Part A: Pure and Applied Chemistry*. 2002;**A39**(5):405-417. DOI: 10.1081/MA-120003963
- [5] Soykan C, Erol İ, Türkmen H, Akçamur Y. New poly(methacrylate)s containing benzylpiperazine and methylpiperidine moieties. *Journal of Polymer Research*. 2004;**11**(3):181-187. DOI: 10.1023/B:POL.0000043400.92054.92
- [6] Erol İ, Soykan C. Synthesis and characterization of new aryl-oxycarbonyl methyl methacrylate monomers and their polymers. *Reactive and Functional Polymers*. 2003;**56**:147-157. DOI: 10.1016/S1381-5148(03)00052-X
- [7] İlter Z, Soykan C, Koca M. Synthesis, spectral and thermal properties of copolymers of (2-cyclopentylidene-1,3-dioxolane-4-yl)methyl methacrylate with styrene and acrylonitrile and determination of monomer reactivity ratios. *Journal of Polymer Science Part A: Polymer Chemistry*. 2003;**41**(19):2996-3005. DOI: 10.1002/pola.10892
- [8] İlter Z, Alhanlı F, Doğan F, Kaya İ. Synthesis and characterization of an acrylate polymer containing chlorine-1,3-dioxalane groups in side chains. *Chinese Journal of Polymer Science*. 2012;**30**(5):642-651. DOI: 10.1007/s10118-012-1155-x
- [9] Coşkun M, İlter Z. Copolymerization of (2-phenyl-1,3-dioxolane-4-yl)methyl methacrylate with alkyl methacrylates: Reactivity ratios and copolymer characterization. *Journal of Polymer Science, Part A: Polymer Chemistry*. 2002;**40**(8):1184-1191. DOI: 10.1002/pola.10174
- [10] İlter Z, Coşkun M, Erol İ. Copolymers of (2-cyclohexylidene-1,3-dioxolane-4-yl) methyl methacrylate with acrylonitrile and styrene: Synthesis, characterization, and monomer reactivity ratios. *Journal of Polymer Science, Part A: Polymer Chemistry*. 2001;**39**(13):2326-2331. DOI: 10.1002/pola.1209
- [11] İlter Z, Soykan C, Solmaz A. Copolymers of 7-methoxy-2-acetyl benzofuryl methylmethacrylate with styrene: Synthesis, characterization, reactivity ratios and determination of kinetic parameters with thermogravimetric analysis. *Journal of Macromolecular Science, Part A: Pure and Applied Chemistry*. 2015;**52**:175-185. DOI: 10.1080/10601325.2015.996937
- [12] Barim G, Altun Ö, Yayla MG. Methacrylate polymers having pendant

- chalcone moieties: Monomer reactivity ratios, thermal and optical properties. *Polymer (Korea)*. 2015;**39**(1):13-22. DOI: 10.7317/pk.2015.39.1.13
- [13] Subramanian K, Krishnasamy V, Nanjundan S, Rami Reddy AV. Photosensitive polymer: Synthesis, characterization and properties of a polymer having pendant photocrosslinkable group. *European Polymer Journal*. 2000;**36**(11):2343-2350. DOI: 10.1016/S0014-3057(00)00008-2
- [14] Brar AS, Malhotra M. Compositional assignments and sequence distribution of vinylidene chloride–methyl acrylate copolymers using one- and two-dimensional NMR spectroscopy. *Macromolecules*. 1996;**29**(23):7470-7476. DOI: 10.1021/ma960363c
- [15] Şahingöz R, Kanbur H, Voigt M, Soykan C. The determination of interface states and series resistance profile of Al/polymer/PEDOT-PSS/ITO heterojunction diode by I-V and C-V methods. *Synthetic Metals*. 2008;**158**:727-731. DOI: 10.1016/j.synthmet.2008.04.023
- [16] Şahingöz R, Soykan C, Yakuphanoglu F, Voigt M, Çetin H. The determination of the conduction mechanism and extraction of diode parameters of ITO/PEDOT-PSS/POLYMER/AL heterojunction diode. *Optical Materials*. 2006;**28**:962-965. DOI: 10.1016/j.optmat.2005.05.009
- [17] Tokaloğlu Ş, Yılmaz V, Kartal Ş, Delibaş A, Soykan C. Synthesis of a novel chelating resin and its use for selective separation and preconcentration of some trace metals in water samples. *Journal of Hazardous Materials*. 2009;**169**:593-598. DOI: 10.1016/j.jhazmat.2009.03.146
- [18] Soykan C, Şahan A, Yakuphanoglu F. Synthesis and semi-conducting properties of novel 2-(4-chloro-1-naphthoxy)-2-oxoethyl methacrylate with 2-(dimethylamino)ethyl methacrylate copolymers, quaternized amino groups. *Journal of Macromolecular Science, Part A: Pure and Applied Chemistry*. 2011;**48**(2):169-176. DOI: 10.1080/10601325.2011.537537
- [19] Ari H, Soykan C, Özpozan T. Preparation of organic/inorganic hybrid materials using aggregates of poly{2-methyl-N-[2-(phenylthio)phenyl]acrylamide-co-2-(trimethylsilyloxy)ethyl methacrylate} as precursor and vibrational investigation of the polymerization. *Journal of Macromolecular Science, Part A: Pure and Applied Chemistry*. 2013;**50**(10):1022-1041. DOI: 10.1080/10601325.2013.821847
- [20] Açıkbaş Y, Erdoğan M, Çapan R, Soykan C. Characterization and gas sensing properties of Langmuir-Blodgett thin films of poly(ClNOEMA-co-DEAEMA). *Sensor Letters*. 2016;**14**:474-483. DOI: 10.1166/sl.2016.3636
- [21] Açıkbaş Y, Çapan R, Erdoğan M, Bulut L, Soykan C. Optical characterization and swelling behaviour of Langmuir-Blodgett thin films of a novel poly[styrene(ST)-co-glycidyl methacrylate (GMA)]. *Sensors and Actuators B: Chemical*. 2017;**241**:1111-1120. DOI: 10.1016/j.snb.2016.10.025
- [22] Patel MB, Patel SA, Ray A, Patel KH. Synthesis, characterization, and antimicrobial activity of acrylic copolymers. *Journal of Applied Polymer Science*. 2003;**89**(4):895-900. DOI: 10.1002/app.11970
- [23] Patel MP, Shah B, Ray A, Patel KH. Acrylic homo- and co-polymers based on 2,4-dichlorophenyl methacrylate and 8-quinolinyl methacrylate. *Journal of Polymer Science-Taiwan*. 2004;**11**(1):65-73. DOI: 10.1023/B:JPOL.0000021779.30811.48

- [24] Patel MV, Dolia MB, Patel JN, Patel RM. Synthesis and characterization of novel acrylic copolymers: Determination of monomer reactivity ratios and biological activity. *Reactive and Functional Polymers*. 2005;**65**(3):195-204. DOI: 10.1016/j.reactfuncpolym.2005.08.002
- [25] Patel JN, Patel JR, Patel KH, Patel MP, Patel MR. Acrylic copolymers based on phenol: Synthesis, characterization, and antimicrobial activity. *Journal of Macromolecular Science, Part A Pure and Applied Chemistry*. 2007;**44**(4-6):395-402. DOI: 10.1080/10601320601188109
- [26] Patel MG, Patel HJ, Patel JR, Patel KH. Development and applications of novel acrylic copolymers. *International Journal of Polymeric Materials*. 2008;**57**(2):165-176. DOI: 10.1080/00914030701486179
- [27] Patel JR, Patel KH, Patel RM. Reactivity ratio of novel acrylic copolymer by NMR spectroscopy. *Colloid & Polymer Science*. 2009;**287**(1):85-90. DOI: 10.1007/s00396-008-1943-6
- [28] Patel HJ, Patel MG, Patel AK, Patel KH. Synthesis, characterization and antimicrobial activity of important heterocyclic acrylic copolymers. *Express Polymer Letters*. 2008;**2**(10):727-734. DOI: 10.3144/expresspolymlett.2008.86
- [29] Patel RT, Patel KH, Patel AR, Patel RM. Kinetic of 8-quinolinyl methacrylate polymerization by differential scanning calorimetry. *International Journal of Polymeric Materials and Polymeric Biomaterials*. 2000;**46**:71-79. DOI: 10.1080/00914030008054842
- [30] Vijayanand PS, Kato S, Kojima T. Synthesis and characterization of 3,5-dimethoxyphenyl methacrylate and methyl methacrylate copolymers: Determination of monomer reactivity ratios. *Journal of Macromolecular Science, Part A: Pure and Applied Chemistry*. 2007;**44**(3):277-283. DOI: 10.1080/10601320601077302
- [31] Zhang R, Yang J, Sun W, Shen Z. Synthesis and characterization of poly [4-(2-thiazolylazo) phenyl methacrylate]-co-poly(methyl methacrylate). *Journal of Applied Polymer Science*. 2007;**103**(4):2152-2157. DOI: 10.1002/app.25041
- [32] Thamizharasi S, Gnanasundaram P, Reddy BSR. Copolymerization of 4-acetyl phenylacrylate with methacrylate and butyl methacrylate: Synthesis, characterization and reactivity ratios. *European Polymer Journal*. 1997;**33**(9):1487-1494. DOI: 10.1016/S0014-3057(96)00270-4
- [33] Stanek LG, Heilmann SM, Gleason WB. Synthesis and monomer reactivity ratios of methyl methacrylate and 2-vinyl-4,4'-dimethylazlactone copolymers. *Journal of Polymer Science, Part A: Polymer Chemistry*. 2003;**41**:3027-3037. DOI: 10.1002/pola.10897
- [34] Loubat C, Batt-Coutrot D, Guyot B, Robin JJ, Boutevin B. Synthesis and monomer reactivity ratios of ethyl α -acetoxyacrylate and acrylic acid copolymers. *Polymer International*. 2005;**54**(11):1557-1563. DOI: 10.1002/pi.1884

Biodegradable Polymers: Opportunities and Challenges

Marieli Rosseto, Cesar V.T. Riguetto, Daniela D.C. Krein, Naiana P. Balbé, Lillian A. Massuda and Aline Dettmer

Abstract

The overuse of polymer materials from fossil sources has generated a large volume of waste that causes environmental impacts due to the degradation time. The technological advance has stimulated the search for alternatives that can contribute to sustainability. In this context, the use of biodegradable polymers, that use raw materials from renewable sources stand out because they have that ability to form films and come from abundant sources. Also, in the expectation of optimizing the environmental benefits in this process, it is possible to value the agroindustrial residues, using them as raw material in the synthesis of the polymer, the physical, chemical and mechanical properties of these polymers are important to evaluate the possible applications. The proposal of this chapter is to present current research on renewable sources, including agricultural and industrial residues, to obtain biodegradable polymers, highlighting their properties and possibilities of application.

Keywords: sustainability, waste, biodegradable, renewable, agroindustrial

1. Introduction

The increasing environmental impacts of pollution derived from fossil polymers are drawing attention to the need to produce sustainable materials. And the biodegradable polymers generated from renewable sources are an alternative to this problem [1]. They are made from renewable or synthetic sources that have the capacity to degrade by the action of microorganisms [2, 3].

In the search for biodegradable and renewable materials, the biopolymers that are gaining prominence are those that have greater availability: cellulose, chitosan, starch and proteins (collagen, soy, casein). As these sources are widely used in the food, pharmaceutical, agricultural, and other industries, material research has been developing in the quest to recover them from agroindustrial waste. These could be reinserted into the process as a source for synthesizing biodegradable polymers, as both industries and agriculture generate waste that is sometimes incorrectly disposed of in the environment.

Residues and by-products generated in larger quantities include fruit and vegetable residues (husks, seeds and stems), grain residues (rice, wheat, soy) and protein products (chitosan, gelatin, whey protein) [4]. Approximately 26% of food waste is generated from the beverage industry, followed by the dairy industry (21%), fruit and vegetables (14.8%), cereals processing (12.9%), preservation of meat products (8%), processing of oils of vegetable and animal origin (3.9%), among others (12.7%) [5].

The use of residues is seen as an opportunity for sustainability due to its ease of production and low cost, non-toxicity, biocompatibility, biodegradability, chemical and thermal stabilities [6]. Associated with the concern to replace materials of fossil origin, attention to the reuse of wastes/by-products of agricultural or agroindustrial origin is of extreme importance. In this way, in addition to contributing to the reduction of disposal of waste in landfills or the burning of landfills, the principle of reuse affects the economy in a positive way.

Despite these advantages, the water absorption is very high, due to the number of hydrophilic groups contained in the structure of the materials of renewable origin. To overcome this factor, techniques have been applied to improve the physical and mechanical properties of these materials, ensuring a better application performance. In addition, there is still a large gap between policy and implementation of these new technologies [7].

The following sections discuss the main sources of biodegradable polymers, aiming to know their specificities, so that to facilitate the link between possible sources to obtain them from agricultural or industrial waste, as well as the applicability of the material.

2. Sources for obtaining biodegradable polymers: opportunities

In the search for biodegradable and renewable materials, the biopolymers that are gaining prominence are those that present greater availability: cellulose, chitosan, starch and proteins.

These sources are widely used in the food, pharmaceutical and agricultural industries, causing the generation of large amounts of waste. This problem has aroused interest in research aimed at obtaining biopolymers from the recovery of the same, relating low cost, availability and sustainability.

2.1 Cellulose

Cellulose is the agroindustrial waste most reuse. Its main sources of production are mainly of vegetal origin (wood and cotton), however, it is also synthesized by algae, tunicates and some bacteria [8–10].

The cellulose molecule $((C_6H_{10}O_5)_n)$ has a linear ribbon-like conformation, and its compounds bound together by the so-called β_{1-4} , glycosidic bonds. The number of chain repeats n varying according to the source of the obtainment, wherein in wood, for example, is about 10,000 and 15,000 in cotton. These chains impart rigidity to the cellulose, providing good mechanical properties and thermal stability. However, cellulose dissolution is a difficult process and it is necessary to develop new techniques that allow the use of regenerated cellulose as a component of polymeric materials [11, 12].

The materials produced from regenerated cellulose acquire exceptional physical and chemical characteristics, as well as clear benefits for society, especially when minimizing environmental impacts. During the regeneration of the cellulose solution, physical and chemical treatments can be applied generating functional and biocompatible materials, organic hybrids or porous membranes, making the use of cellulose comprehensive [12].

In this sense, the cellulose modification has been the focus of several studies, aiming to evaluate it as a substitute raw material to obtain synthetic polymers, fibers, films and membranes, hydrogels and aerogels, bioplastics, beads and microspheres as shown in (Table 1).

Author	Objective of study
Fibers	
[13]	Obtaining of magnetically activated cellulose fibers by moist spinning cellulose/ Fe_3O_4 solution in 1-ethyl-3-methylimidazolium chloride.
[14]	Manufacture of regenerated cellulose multifilaments by means of pilot scale spinning equipment from the cellulose solution in NaOH/Urea.
Films and membranes	
[15]	Development of new cellulose films via low temperature solvents.
[16]	Manufacture of flexible, transparent and fortified regenerated films by crosslinking the cellulose with epichlorohydrin (ECH) in NaOH/Urea.
[17]	New method of preparation of hydrated membranes of cellulose in NaOH/Urea, employing a process of pregelatinization.
[18]	Direct production of films with cellulose nanocomposites from cellulose microfibers using nano-soldering based on ionic liquid.
[10]	Manufacture of optically clear paper from densely packed cellulose nanofibers.
Hydrogels and aerogels	
[19]	Manufacture of a series of cellulose hydrogels directly from the cellulose solution followed by crosslinking with epichlorohydrin (ECH) via heating and freezing.
[20]	Production of regenerated cellulose hydrogels made from lithium chloride/dimethylacetamide by slow coagulation with water.
[21]	Preparation of hydrogel from a cellulose solution in an ionic liquid of 1-butyl-3-methylimidazolium chloride and water at room temperature.
[22]	Carbonized aerogels after pyrolysis under nitrogen flow and doping with platinum nanoparticles.
Beads and microspheres	
[23]	Manufacture of cellulose beads from thin plates of Cellulose/NaOH solution in a water bath.
[24]	Preparation of macroporous spheres with viscose cellulose xanthogenate densified with high density tungsten carbide via thermal regeneration in water-in-oil suspension with starch as a porogenic.
Bioplastics	
[25]	Construction of new cellulose bioplastics (CBP) from cellulose hydrogels prepared by cellulose solution in NaOH/Urea via simple hot pressing.

Table 1.
Studies to obtain materials with cellulose in its composition.

Recent studies have turned their efforts to provide reuse and value adding to industrial waste. In order to convert lignocellulosic materials into nanocellulose, [26] used the residues of tobacco stalks after steam blasting followed by bleaching and refining to produce nanofibrillated cellulose (NFC), successfully reaching the objective of the study, and generating a promising alternative for the reuse of this residue organic.

Reference [27] extracted microcrystalline cellulose (MCC) and spherical nanocrystalline cellulose (SNCC) by acid hydrolysis from cotton fabric waste, concluding that the developed process is suitable for industrial scale application, since the generation of cotton waste is high, as well as the cellulose content contained in them (about 94%).

Reference [28] isolated microcrystalline cellulose powder (MCC) from waste paper from three sources (books, newspapers and cardboard), evaluating the effect of the

treatment using various concentrations of sodium hydroxide (NaOH) on the properties of the powders obtained, concluding that the lowest concentration, which was 5% (m/v) NaOH in the medium, was ideal for MCC isolation in these paper wastes.

Aiming to reduce the environmental impacts caused in aquatic life due to the contamination of water by complex substances such as petroleum and vegetable oils, [29] developed a hydrophobic aerogel with high sorption capacity, from cellulose nanofibres obtained from waste from the furniture industry, processed via acidic hydrolysis by steam explosion for oil sorption. The authors tested the sorption capacity of the aerogel produced in homogeneous media (pure oil and vegetable oil) and heterogeneous medium (oil in water), where it had high sorption capacity in both media, 19.55 and 19.21 $\text{g}_{\text{oil}} \text{g}_{\text{aerogel}}^{-1}$, for petroleum and oil respectively.

2.2 Chitosan

The chitosan is a molecule with a carbohydrate structure like cellulose, consisting of two types of repeating units, N-acetyl-D-glucosamine and D-glucosamine, linked by $\beta_{1,4}$ glycosidic bonds [30]. They are the most abundant organic compounds after cellulose [31].

It is widely distributed in the animal kingdom (shells of crustaceans and mollusks, the backbone of squid and the cuticle of insects) and vegetable (algae, protozoa and the cell wall of several fungal species) [32].

The degree of acetylation differentiates chitin from chitosan, when the polymer has a degree of acetylation greater than 50%, is called chitin, and when the degree of acetylation is less than 50%, it is called chitosan [33].

Reference [34] discuss the main methods of chitosan extraction, measure alkaline treatment, which is most commonly used at the industrial level, and sodium hydroxide (NaOH), which is commonly used for the deacetylation process. The enzymatic deacetylation that uses chitin deacetylases obtained from different biological sources, such as fungi and insects to effect treatment. And steam explosion, which performs a hydrothermal treatment where the chitin is treated with a blow gun, with saturation vapor at increased pressure and temperature for several minutes, followed by explosive decomposition.

There are several studies that provide application opportunities for a chitosan. For the food area: active films, antioxidants, antimicrobials, chitosan compounds, edible coatings, application in fruits and vegetables and application in seafood products [35]. [36] made a comparison between nano-composite films based on gelatin and starch modified by nanocellulose and chitosan for packaging applications. And [37] developed and evaluated an antioxidant film and pH indicator based on sources of chitosan and food waste. [38] incorporated the extract of mango leaves to the antioxidant film of chitosan for active food packaging.

In addition, it can be used in a number of areas, such as biomedicine, pharmaceuticals, food, agriculture, personal care products and the environmental sector [39]. [40] developed nanoparticles of chitosan coating for the treatment of brain diseases. [41] studied nanogels of chitosan as nanocarriers of polyoxometalates for breast cancer therapies. In the environmental area [41] have developed a lysozyme-chitosan biocomposite for the effective removal of dyes and heavy metals from aqueous solutions. [42] have made antibacterial and ecologically correct membranes of chitosan and polyvinyl alcohol for air filtration. In the area of agriculture [43] chitosan nanoparticle delivery systems for sustainable agriculture and [44] biocompatible chitosan nanoparticles loaded with agrochemicals for pest management.

However, there is a great waste of chitosan in marine waste from processing industries, there has been a significant increase in recent years, due to modern seafood processing practices that result in the accumulation of a large volume of

waste (skin, head, tails, shells, scales, spine). As the rate of biodegradation of this material is low because chitin is not soluble in water, this volume accumulates and consequently causing environmental impacts. [45, 46].

These marine residues are potential materials for extracting chitin and chitosan. This requires the recovery of chitosan present in these wastes. [47] extract and characterize the fish scale chitosan (*Labeo rohita*). While [48] make the extraction from abundant shrimp residues (exoskeleton - shells). Already [49] use as extraction source the blue crab. And [50] performed alkaline hydrolysis to recover the chitin and chitosan from the squid feather and used the residual water of this process to recover the proteins and evaluate the antioxidant action.

The challenge is to obtain materials with properties equivalent to fully synthetic products [45]. Since, in the preparation of films, for example, when only chitosan is used, there are disadvantages as poor mechanical and barrier properties due to the absorption of moisture [51]. The ideal would be to use materials that add these absent characteristics.

2.3 Starch

Starch can be found in many vegetables in the granule formula and its composition is basically from two polysaccharides: amylose (linear) and amylopectin (branched) [52]. It is one among foods that have significant energy source in the human diet. In addition to the use for consumption, the starch can be used for pharmaceutical and functional purposes and is widely used for its desirable physicochemical properties such as grain swelling, viscosity, gel formation capacity and water binding affinity [53].

The modification in the structure of starches is closely linked to the process of retrogradation, which generates a reorganization of the molecules present. Research on this phenomenon generally occurs in aqueous dispersions at different concentrations. Other factors that may be associated in the modification of starch are the disorganization and rupture of the granules, which occur in the presence of high temperatures [54].

When the starch is heated at a characteristic temperature called the gelatinization temperature (60–70°C) in aqueous solution, the swelling step of the grain occurs, where the amylose is solubilized. At temperatures lower than 100°C and without mechanical shear the granules have their integral structure and are characterized as viscoelastic [52].

In order to obtain improvements in starch properties, as well as to solve some problems, starch modification has occurred, that can occur genetically, physically, chemically or even enzymatically [55].

With genetically modified starches there are opportunities for starch production with improved functionality, for example with high levels of amylose and phosphates, with amylopectin short chains without the presence of amylose, and as properties one can mention stability to freezing and thawing [55].

As an example of physical modifications, high pressure homogenization has resulted in a physically modified starch having crystallinity reduction properties in the starch grain that could produce a hydrogel with stronger gel networks [56]. Modification by treatment of humidity and heat that generates interactions and new associations between the amylose and amylopectin structures, besides the ultrasound that can also be used as a physical method for the modification of starches [57].

Among the chemical modifications it is important to mention acid hydrolysis, acetylation, esterification, double modification and oxidation. The purpose of the chemical modification is to replace a new functional group that would add desired properties to the starch [58].

The modification of starch through enzymes mainly involves the use of hydrolyzing enzymes, an important aspect is that the enzyme must be free of components that can cause damage to starch molecules [39].

The starch after conversion into thermoplastic presents itself as an alternative for the replacement of polymers of fossil origin, mainly in relation to the properties and biodegradability of the final product. Further, on starch thermoplastic studies show that the higher proportion of amylose to amylopectin provides more flexibility and makes it even more thermoplastic [59].

Since starch can come from a variety of plant sources, it is therefore comprehensive and has high availability, recent studies highlight the use of this biopolymer through alternative sources such as starch recovery or reuse of waste in various applications, such as residual starch from the milling process, or maize residues to obtain bioethanol [60, 61] and applications as biodegradable films as shown in **Table 2**.

2.4 Proteins

Proteins are polymers of natural origin, consisting of peptide bonds, the result of hydrogen bonds, ionic bonds and cross-links between amines that can originate from plant or animal material [67]. Some examples of proteins that are used as substitution of polymers of petroleum origin are: soy protein, casein, collagen and some others not so used, as wheat gluten and ovalbumin, due to the low availability of the material [68].

2.4.1 Collagen

Collagen is a natural protein present in animals and is responsible for ensuring the structure that supports the skin and organs. Beyond the skins, it can be found in bones, cartilage and some other structures. Formed by amino acids, the collagen is structured by a helix triple consisting of proline, hydroxyproline and glycine molecules [69].

Author	Objective of study
[60]	To evaluate ethanol production by <i>Zymomonas mobilis</i> ZM4 and an industrial ethanol producing strain of <i>Saccharomyces cerevisiae</i> using as substrate residual starch of wet flour milling, supplemented with crushed wheat grains, with subsequent hydrolysis.
[61]	The residue flow of potato starch produced during chip manufacturing was used as an economical source to produce biomass and bioethanol by <i>Saccharomyces cerevisiae</i> .
[62]	Production of biodegradable films based on thermoplastic corn starch and starch extraction residues from <i>Pachyrhizus ahipa</i> .
[63]	Mechanical and chemical treatment of turmeric residue, aiming application in the production of films with improved properties.
[64]	Extraction and characterization of pineapple stems using common mechanical extraction with water.
[65]	The production of ethanol using as raw material an agroindustrial residue rich in complex starches, called thippi, which after combined treatment with steam and enzymatic hydrolysis, was subjected to mixed culture fermentation.
[66]	Recovery of mixed biopolymers composed of starch and curcuminoids from the extraction of supercritical fluid and pressurized liquid.

Table 2.
Studies from recovered starch.

The origin of this collagen can be derived from residues from slaughterhouses, as well as from fishing activities [70]. The volume of waste from these activities can generate high environmental impact, since there is very little reuse on them. Thus, their destination is usually for landfills, or mostly, in irregular deposits in nature, contributing to contamination of soil and water resources. The high volume and little reuse can be justified by the leftovers during the processing of the raw material and low commercial value of the by-products generated.

Collagen, in its natural form, has little application. Therefore, one chooses to extract the gelatin present in its composition for use. In order to obtain the gelatin, it is necessary for the collagen to undergo a hydrolysis process (acidic, alkaline or enzymatic), associated with high temperatures, to break the covalent bonds, releasing the gelatin molecules, through denaturation of the helix triple. After cooling the solution, the chains absorb the water, forming gelatin [69].

Gelatin is the result of water-soluble proteins, that after extraction, can be purified and concentrated, eliminating some salts or undesirable substances contained in its structure that may compromise its application. This is another factor that may imply its applicability, generating a water absorption in the material larger than the desired one. Depending on the origin of the residue, salts such as chromium and sodium can be found (residues of leather trimmings, for example). The presence of magnesium and chlorine can be observed due to alkaline or acidic hydrolysis, respectively, that was employed in the gelatin extraction process.

Collagen and gelatin are considered good materials for application in several areas, including medical, pharmaceutical and cosmetic areas [71]. For application in the health area, purification should be more complex, involving filtration steps, generally carried out by ultrafiltration membranes.

For the food area, as referred in films for food coating, gelatin extracted from fish waste (bone and cartilage) can be used without contraindications, however gelatin extracted from tanning waste leather is not allowed for use by legislation, due to chrome remnants that exist in the solution. Gelatin from leather residue can be reused to produce films for soil cover [72]. Studies on the use of this polymer for cover application have been increasing, due to the fact of the optimum biodegradability of the material.

For the leather waste there are also other alternatives, besides the use for extraction of gelatin. Many authors have studied its use as fertilizer, due to its high potential for containing nitrogen content in its composition [73]. For use as fertilizers, the residue can be treated by adding more essential mineral salts to the soil with phosphorus and potassium.

2.4.2 Soybean

Soybean is the main grain marketed in the world and is used in many processes to obtain different consumer goods. Because it is widely applied in the industry, it is also capable of generating a lot of waste. Soybean meal, considered as a by-product of the extraction of oil contained in grain for food production or biofuel, is mainly destined for animal feed [74].

Protein isolate from soybean has been the subject of many studies. Despite its high protein content, its reuse is restricted due to its high stiffness and low water resistance [75]. Materials that use soy protein have great potential for replacement of polymers of fossil origin. It can be used as an adhesive for food coatings, as packaging for use in horticulture, guaranteeing its function as both container and fertilizer [76].

When used as a base for packaging manufacture, the soy protein isolate has good advantages such as biodegradability and good gas barrier property. However, its low tensile strength makes its application difficult [77].

Techniques such as coatings and crosslinking are applied to the polymer matrix, resulting in a material with improved mechanical properties, as well as increasing the shelf life of the film.

The coating, when employed, provides low water permeability, while the crosslinking technique provides better mechanical properties when compared to the coating. In addition, it can be seen that the amount of hydrophilic groups is reduced.

Although it is shown as a more efficient technique, the crosslinking uses agents that can present certain toxicity, limiting its application in the food industry [75]. Thus, it is sought to use biological macromolecular materials, such as starch, chitosan, cellulose, for the formation of films [78].

2.4.3 Casein

Casein is the protein found in milk, of high nutritional value. It can be found in one of the residues that in recent years have generated many problems for dairy products: whey. Despite this being used in dairy production with its due treatment, was once considered as a by-product in the food industry.

Casein can be used in films for food coatings and pharmaceuticals, its main application despite the few studies on its excellent characteristics such as biodegradability, thermal stability and non-toxicity translate a high value-added material for use in drugs. Despite these advantages, the mechanical strength of the material is still quite limited [79, 80].

3. Challenges

Even with promising trends for applicability, biodegradable polymers obtained from renewable sources present some disadvantages, such as low mechanical properties, rapid degradation rate, high hydrophilic capacity, and in some cases, poor mechanical properties, especially in humid environments, rendering their application unviable [81, 82].

In this context divergent opinions arise about the acceptability of biodegradable polymers in industry. While some believe in their potential to replace petroleum polymers, others presume that their shortcomings, both in technical and economic aspects, hinder their rapid adoption, at least in the near future [83].

The challenge is to obtain materials with properties equivalent to synthetic products [45]. To achieve this objective, different techniques are studied to promote modifications of biodegradable polymers, as shown in **Table 3**.

Author	Material studied	Aim of the study/Results obtained
[84]	Cellulose	Evaluation of the mechanical barrier, and interfacial properties of Methylcellulose (MC) films reinforced Poly (caprolactone)-based biodegradable films. It was found that MC film contributed to the improvement of mechanical properties of the composites. It was found that the methylcellulose film acted as a satisfactory reinforcing agent, contributing to the improvement of the mechanical and oxygen barrier properties of the composites for packaging applications.
[85]		Simultaneously achieve impact strength and bending properties (flexural strength and tensile strength) by improving the impact strength of modified cardanol (PAA) -bound cellulose diacetate (CDA) by adding flexible resins. In conclusion, the impact resistance of PAA-bound CDA was dramatically increased by the addition of a small amount of olefinic resins (polyethylene and polypropylene).

Author	Material studied	Aim of the study/Results obtained
[86]	Chitosan	Evaluation of the effects of adding the silicone liquid rubber to formulations of chitosan and alginate membranes both with and without silver-containing antimicrobial agent, to improve the overall mechanical properties of the dressings. It found that membranes containing the silicone rubber had a more homogeneous appearance and adequate flexibility and adhesiveness, increasing in tensile strength, both with and without the antimicrobial agent. In addition, the membranes without the antimicrobial agent resulted in a decrease in absorption of all physiological solutions tested.
[87]	Chitosan and gelatin	Development chitosan/gelatin composite films embedded with various amounts of wool nanoparticles. In conclusion, it was found that incorporation of wool nanoparticles into chitosan/gelatin composite led to a reduction in swelling, moisture content, dissolution degree and degradation rate of the films. However, tensile strength and elongation at break decreased upon loading the films with wool nanoparticles.
[88]	Starch	Incorporation of saturated fatty acids in the development of films made of starch and the biodegradable synthetic polymer poly (butylene adipate-co-terephthalate) (PBAT), concluding that the incorporation of saturated fatty acids until 12 carbon atoms reduces the permeability to water vapor and improves the mechanical properties of films made of starch, glycerol, and PBAT produced by extrusion, contributing to the formation of a cohesive and homogeneous polymer matrix.
[89]		Investigation of polyol mixtures including glycerol as plasticizer and high molecular weight polyol such as xylitol, sorbitol and maltitol used to plasticize corn starch, it being understood that the extra addition of high molecular weight polyol together with glycerol favored an improvement of the thermal stability and mechanical strength of the starch composite.
[90]		Verification of the influence of starch oxidation with sodium periodate on the functionality of active films based on gelatin and starch, obtaining an improvement in the properties of strength and barrier to water vapor and oxygen, reducing the water absorption capacity.
[91]		Evaluation of the effect of irradiation on the physicochemical properties, rheological and in vitro digestibility of the Kithul starch (<i>Caryota urens</i>). Concluded that the irradiation decreased the pH, swelling index, amylose and moisture content of the starch, increasing the content of carboxylic acid, acidity and solubility.
[92]		Characterization of rice starch gels reinforced with enzymatically produced resistant starch, resulting in an increase in the gel strength of about 60%, while cohesion decreased and the elasticity remained stable.
[93, 94]	Gelatin	Crosslinking induced by the enzyme transglutaminase in gelatin films, evidencing improvements in the physical, chemical and mechanical properties of the films.
[95]	Casein and soybean	Development and characterization of novel melttable polymers and composites based on casein and soybean proteins. In addition to the investigation of the effect of inert (Al ₂ O ₃) and bioactive (tricalcium phosphate) ceramic reinforcements on the mechanical performance, water absorption and bioactivity behavior of injection molded thermoplastics, aiming at biomedical applications. And concluding that thermoplastics developed on the basis of casein and soy protein present an adequate range of mechanical properties and degradation as well as a bioactive character (especially when reinforced with bone-like ceramics) that may possibly allow its use as biomaterials in medicine.

Table 3.
Studies to improve the properties of biopolymers.

4. Conclusions

This chapter addressed a theoretical review of the opportunities and challenges of biopolymers, considering aspects such as generation and use of waste, sustainability and properties that make their applicability unfeasible.

In addition, it is necessary to continue the studies aimed at improving the poor properties of biopolymers, in order to contribute directly to scientific knowledge, ensuring sustainability, environmental preservation and consequently future generations.

Acknowledgements

This work was supported by the Foundation for Research Support of the State of Rio Grande do Sul (FAPERGS) and University of Passo Fundo (UPF) for space and research support.

Author details


Marieli Rosseto¹, Cesar V.T. Riguetto¹, Daniela D.C. Krein², Naiana P. Balbé², Lillian A. Massuda² and Aline Dettmer^{2*}

1 Postgraduate Program in Food Science and Technology (PPGCTA), Faculty of Agronomy and Veterinary Medicine (FAMV), University of Passo Fundo, Passo Fundo, Rio Grande do Sul, Brazil

2 Department of Chemical Engineering, Faculty of Engineering and Architecture (FEAR), University of Passo Fundo (UPF), Passo Fundo, Rio Grande do Sul, Brazil

*Address all correspondence to: alinedettmer@upf.br

IntechOpen

© 2019 The Author(s). Licensee IntechOpen. This chapter is distributed under the terms of the Creative Commons Attribution License (<http://creativecommons.org/licenses/by/3.0>), which permits unrestricted use, distribution, and reproduction in any medium, provided the original work is properly cited. 

References

- [1] Bhawani SA, Bhat AH, Ahmad FB, MNM I. Green polymer nano-composites and their environmental applications. In: Jawaid M, Khan MM, editors. *Polymer-based Nanocomposites for Energy and Environmental Applications*. 1st ed. Cambridge: Woodhead Publishing; 2018. pp. 617-633. DOI: 10.1016/b978-0-08-102262-7.00023-4
- [2] Ashter S. *Introduction to Bioplastics Engineering*. 1st ed. William Andrew: Merrimack; 2016. p. 300. DOI: 10.1016/b978-0-323-39396-6.00001-4
- [3] Masina N, Choonara YE, Kumar P, Du Toit LC, Govender M, Indermun S. A review of the chemical modification techniques of starch. *Carbohydrate Polymers*. 2017;**157**:1226-1236. DOI: 10.1016/j.carbpol.2016.09.094
- [4] Flôres SH, Rios AO, Iahnke AOS, Campo C, Vargas CG, Santos CDM, et al. Films for food from ingredient waste. In: Smithers GW, editor. *Reference Module in Food Science*. 1st ed. Melbourne: Elsevier; 2017. pp. 1-40. DOI: 10.1016/b978-0-08-100596-5.21366-8
- [5] Nayak A, Bhushan B. An overview of the recent trends on the waste valorization techniques for food wastes. *Journal of Environmental Management*. 2019;**233**:352-370. DOI: 10.1016/j.jenvman.2018.12.041
- [6] Habibi Y, Lucia LA, Rojas OJ. Cellulose nanocrystals: Chemistry, self-assembly, and applications. *Chemical Reviews*. 2010;**110**:3479-3500. DOI: 10.1021/cr900339w
- [7] Sindhu R, Gnansounou E, Rebello S, Binod P, Varjani S, Thakur IS, et al. Conversion of food and kitchen waste to value-added products. *Journal of Environmental Management*. 2019;**241**:619-630. DOI: 10.1016/j.jenvman.2019.02.053
- [8] Klemm D, Schumann D, Kramer F, Heßler N, Hornung M, Schmauder HP, et al. Nanocelluloses as innovative polymers in research and application. *Polysaccharides II*. 2006;**205**:49-96. DOI: 10.1007/12_097
- [9] Henriksson M, Berglund LA. Structure and properties of cellulose nanocomposite films containing melamine formaldehyde. *Journal of Applied Polymer Science*. 2007;**106**:2817-2824. DOI: 10.1002/app.26946
- [10] Nogi M, Iwamoto S, Nakagaito AN, Yano H. Optically transparent nanofiber paper. In: Wang X, Fu H, Peng A, Zhai T, Ma Y, Yuan F, Yao J, editors. *Advanced Materials*. Vol. 21. Weinheim: Wiley; 2009. pp. 1595-1598. DOI: 10.1002/adma.200803174
- [11] Simon J, Müller HP, Koch R, Müller V. Thermoplastic and biodegradable polymers of cellulose. *Polymer Degradation and Stability*. 1998;**59**:107-115. DOI: 10.1016/s0141-3910(97)00151-1
- [12] Wang S, Lu A, Zhang L. Recent advances in regenerated cellulose materials. *Progress in Polymer Science*. 2016;**53**:169-206. DOI: 10.1016/j.progpolymsci.2015.07.003
- [13] Sun N, Swatloski R, Maxim M, Rahman M, Harland A, Haque A, et al. Magnetite-embedded cellulose fibers prepared from ionic liquid. *Journal of Materials Chemistry*. 2008;**18**:283290. DOI: 10.1039/B713194A
- [14] Ruan D, Zhang L, Lue A, Zhou J, Chen H, Chen X, et al. A rapid process for producing cellulose multi-filament fibers from a NaOH/thiourea solvent system. *Macromolecular Rapid Communications*. 2006;**27**:1495-1500. DOI: 10.1002/marc.200600232
- [15] Yang Q, Qin X, Zhang L. Properties of cellulose films prepared from NaOH/

urea/zincate aqueous solution at low temperature. *Cellulose*. 2011;**18**:681-688. DOI: 10.1007/s10570-011-9514-2

[16] An L, Chen J, Bangal PR. Dissolving cellulose in a NaOH/thiourea aqueous solution: A topochemical investigation. *Macromolecular Bioscience*. 2007;**7**:1139-1148. DOI: 10.1002/mabi.200700072

[17] Liang S, Zhang L, Xu J. Morphology and permeability of cellulose/chitin blend membranes. *Journal of Membrane Science*. 2007;**287**:19-28. DOI: 10.1016/j.memsci.2006.10.002

[18] Yousefi H, Nishino T, Faezipour M, Ebrahimi G, Shakeri A. Direct fabrication of all-cellulose nanocomposite from cellulose microfibrils using ionic liquid-based nanowelding. *Biomacromolecules*. 2011;**12**:4080-4085. DOI: 10.1021/bm201147a

[19] Chang C, Zhang L, Zhou J, Zhang L, Kennedy JF. Structure and properties of hydrogels prepared from cellulose in NaOH/urea aqueous solutions. *Carbohydrate Polymers*. 2010;**82**:122-127. DOI: 10.1016/j.carbpol.2010.04.033

[20] Gindl W, Emsenhuber G, Maier G, Keckes J. Cellulose in never-dried gel oriented by an AC electric field. *Biomacromolecules*. 2009;**10**:1315-1318. DOI: 10.1021/bm801508e

[21] Kadokawa JI, Murakami MA, Kaneko Y. A facile preparation of gel materials from a solution of cellulose in ionic liquid. *Carbohydrate Research*. 2008;**343**:769-772. DOI: 10.1016/j.carres.2008.01.017

[22] Guilminot E, Gavillon R, Chatenet M, Berthon-Fabry S, Rigacci A, Budtova T. New nanostructured carbons based on porous cellulose: Elaboration, pyrolysis and use as platinum nanoparticles substrate for oxygen reduction electrocatalysis. *Journal of*

Power Sources. 2008;**185**:717-726. DOI: 10.1016/j.jpowsour.2008.08.030

[23] Sescousse R, Gavillon R, Budtova T. Wet and dry highly porous cellulose beads from cellulose-NaOH-water solutions: Influence of the preparation conditions on beads shape and encapsulation of inorganic particles. *Journal of Materials Science*. 2010;**46**:759-765. DOI: 10.1007/s10853-010-4809-5

[24] Xia H, Lin D, Yao S. Preparation and characterization of macroporous cellulose-tungsten carbide composite beads for expanded bed applications. *Journal of Chromatography. A*. 2007;**1175**:55-63. DOI: 10.1016/j.chroma.2007.10.004

[25] Wang Q, Cai J, Zhang L, Xu M, Cheng H, Han C, et al. A bioplastic with high strength constructed from a cellulose hydrogel by changing the aggregated structure. *Journal of Materials Chemistry A*. 2013;**1**:6678-6686. DOI: 10.1039/C3TA11130J

[26] Tuzzin G, Godinho M, Dettmer A, Zattera AJ. Nanofibrillated cellulose from tobacco industry wastes. *Carbohydrate Polymers*. 2016;**148**:69-77. DOI: 10.1016/j.carbpol.2016.04.045

[27] Xiong R, Zhang X, Tian D, Zhou Z, Lu C. Comparing microcrystalline with spherical nanocrystalline cellulose from waste cotton fabrics. *Cellulose*. 2012;**19**:1189-1198. DOI: 10.1007/s10570-012-9730-4

[28] Okwonna OO. The effect of pulping concentration treatment on the properties of microcrystalline cellulose powder obtained from waste paper. *Carbohydrate Polymers*. 2013;**98**:721-725. DOI: 10.1016/j.carbpol.2013.06.039

[29] Oliveira PB, Godinho M, Zattera AJ. Oils sorption on hydrophobic nanocellulose aerogel obtained from the wood furniture industry waste.

Cellulose. 2018;**25**:3105-3119. DOI: 10.1007/s10570-018-1781-8

[30] Roberts GAF. Chitin chemistry. 1st ed. Hong Kong: The Macmillan Press Ltd; 1992. p. 350. DOI: 10.1007/978-1-349-11545-7

[31] Panariello L, Coltelli MB, Buchignani M, Lazzeri A. Chitosan and nano-structured chitin for biobased anti-microbial treatments onto cellulose based materials. *European Polymer Journal*. 2019;**113**:328-339. DOI: 10.1016/j.eurpolymj.2019.02.004

[32] Khor E. The sources and production of chitin. In: Khor E. Chitin editors. *Fulfilling a Biomaterials Promise*. 1st ed. Victoria: Elsevier Science; 2001. pp. 63-72. DOI: 10.1016/B978-008044018-7/50005-1

[33] Gonil P, Sajomsang W. Applications of magnetic resonance spectroscopy to chitin from insect cuticles. *International Journal of Biological Macromolecules*. 2012;**51**:514-522. DOI: 10.1016/j.ijbiomac.2012.06.025

[34] Sivashankari PR, Prabakaran M. Deacetylation modification techniques of chitin and chitosan. In: Jennings JA, Bumgardner JD, editors. *Chitosan Based Biomaterials*. 1st ed. Cambridge: Woodhead Publishing; 2017. pp. 117-133. DOI: 10.1016/b978-0-08-100230-8.00005-4

[35] Muxika A, Zugasti I, Guerrero P, De La Caba K. Applications of chitosan in food packaging. In: Smithers GW, editor. *Reference Module in Food Science*. 1st ed. Melbourne: Elsevier; 2017. pp. 1-12. DOI: 10.1016/b978-0-08-100596-5.22400-1

[36] Noorbakhsh-Soltani SM, Zerafat MM, Sabbaghi S. A comparative study of gelatin and starch-based nano-composite films modified by nano-cellulose and chitosan for food packaging applications. *Carbohydrate*

Polymers. 2018;**189**:48-55. DOI: 10.1016/j.carbpol.2018.02.012

[37] Kurek M, Garofulić IE, Bakić MT, Ščetar M, Uzelac VD, Galić K. Development and evaluation of a novel antioxidant and pH indicator film based on chitosan and food waste sources of antioxidants. *Food Hydrocolloids*. 2018;**84**:238-246. DOI: 10.1016/j.foodhyd.2018.05.050

[38] Rambabu K, Bharath G, Banat F, Show PL, Cocolozzi HH. Mango leaf extract incorporated chitosan antioxidant film for active food packaging. *International Journal of Biological Macromolecules*. 2019;**126**:1234-1243. DOI: 10.1016/j.ijbiomac.2018.12.196

[39] Kaur S, Dhillon GS. Recent trends in biological extraction of chitin from marine shell wastes: A review. *Critical Reviews in Biotechnology*. 2013;**35**:44-61. DOI: 10.3109/07388551.2013.798256

[40] Yu S, Xu X, Feng J, Liu M, Hu K. Chitosan and chitosan coating nanoparticles for the treatment of brain disease. *International Journal of Pharmaceutics*. 2019;**560**:282-293. DOI: 10.1016/j.ijpharm.2019.02.012

[41] Pérez-Álvarez L, Ruiz-Rubio L, Artetxe B, Vivanco MD, Gutiérrez-Zorrilla JM, Vilas-Vilela JL. Chitosan nanogels as nanocarriers of polyoxometalates for breast cancer therapies. *Carbohydrate Polymers*. 2019;**213**:159-167. DOI: 10.1016/j.carbpol.2019.02.091

[42] Wang Z, Yan F, Pei H, Li J, Cui Z, He B. Antibacterial and environmentally friendly chitosan/polyvinyl alcohol blend membranes for air filtration. *Carbohydrate Polymers*. 2018;**198**:241-248. DOI: 10.1016/j.carbpol.2018.06.090

[43] Kashyap PL, Xiang X, Heiden P. Chitosan nanoparticle-based delivery

systems for sustainable agriculture. *International Journal of Biological Macromolecules*. 2015;**77**:36-51. DOI: 10.1016/j.ijbiomac.2015.02.039

[44] Sharma A, Sooda K, Kaur J, Khatri M. Agrochemical loaded biocompatible chitosan nanoparticles for insect pest management. *Biocatalysis and Agricultural Biotechnology*. 2019;**18**:101079-101085. DOI: 10.1016/j.bcab.2019.101079

[45] Knidri HE, Belaabed R, Addaou A, Laajeb A, Lahsini A. Extraction, chemical modification and characterization of chitin and chitosan. *International Journal of Biological Macromolecules*. 2018;**120**:1181-1189. DOI: 10.1016/j.ijbiomac.2018.08.139

[46] Yadav M, Goswami P, Paritosh K, Kumar M, Pareek N, Vivekanand V. Seafood waste: A source for preparation of commercially employable chitin/chitosan materials. *Bioresources and Bioprocessing*. 2019;**6**(1):8. DOI: 10.1186/s40643-019-0243-y

[47] Kumari S, Rath PK. Extraction and characterization of chitin and chitosan from (*Labeo rohita*) fish scales. *Procedia Materials Science*. 2014;**6**:482-489. DOI: 10.1016/j.mspro.2014.07.062

[48] Kadouche S, Farhat M, Lounici H, Fiallo M, Sharrock P, Mecherrri M, et al. Low cost chitosan biopolymer for environmental use made from abundant shrimp wastes. *Waste and Biomass Valorization*. 2016;**8**:401-406. DOI: 10.1007/s12649-016-9593-2

[49] Baron RD, Pérez LL, Salcedo JM, Córdoba LP, Sobral PJA. Production and characterization of films based on blends of chitosan from blue crab (*Callinectes sapidus*) waste and pectin from Orange (*Citrus sinensis* Osbeck) peel. *International Journal of Biological Macromolecules*. 2017;**98**:676-683. DOI: 10.1016/j.ijbiomac.2017.02.004

[50] Shavandi A, Hu Z, Teh S, Zhao J, Carne A, Bekhit A, et al. Antioxidant and functional properties of protein hydrolysates obtained from squid pen chitosan extraction effluent. *Food Chemistry*. 2017;**227**:194-201. DOI: 10.1016/j.foodchem.2017.01.099

[51] Sánchez-Ortega I, García-Almendárez BE, Santos-López EM, Amaro-Reyes A, Barboza-Corona JE, Regalado C. Antimicrobial edible films and coatings for meat and meat products preservation. *Scientific World Journal*. 2014;**2014**:1-18. DOI: 10.1155/2014/248935

[52] Miles MJ, Morris VJ, Orford PD, Ring SG. The roles of amylose and amylopectin in the gelation and retrogradation of starch. *Carbohydrate Research*. 1985;**135**:271-281. DOI: 10.1016/s0008-6215(00)90778-x

[53] Fuentes-Zaragoza E, Riquelme-Navarrete MJ, Sánchez-Zapata E, Pérez-Álvarez JAE. Resistant starch as functional ingredient: A review. *Food Research International*. 2010;**43**:931-942. DOI: 10.1016/j.foodres.2010.02.004

[54] Matignon A, Tecante A. Starch retrogradation: From starch components to cereal products. *Food Hydrocolloids*. 2017;**68**:43-52. DOI: 10.1016/j.foodhyd.2016.10.032

[55] Kaur B, Ariffin F, Bhat R, Karim AA. Progress in starch modification in the last decade. *Food Hydrocolloids*. 2012;**26**:398-404. DOI: 10.1016/j.foodhyd.2011.02.016

[56] Shahbazi M, Majzoobi M, Farahnaky A. Physical modification of starch by high-pressure homogenization for improving functional properties of κ -carrageenan/starch blend film. *Food Hydrocolloids*. 2018;**85**:204-214. DOI: 10.1016/j.foodhyd.2018.07.017

- [57] Dey A, Sit N. Modification of foxtail millet starch by combining physical, chemical and enzymatic methods. *International Journal of Biological Macromolecules*. 2017;**95**:314-320. DOI: 10.1016/j.ijbiomac.2016.11.067
- [58] Haq F, Yu H, Wang L, Teng L, Haroon M, Khan RU, et al. Advances in chemical modifications of starches and their applications. *Carbohydrate Research*. 2019;**476**:12-35. DOI: 10.1016/j.carres.2019.02.007
- [59] Teramoto N, Motoyama T, Yosomiya R, Shibata M. Synthesis, thermal properties, and biodegradability of propyl-etherified starch. *European Polymer Journal*. 2003;**39**:255-261. DOI: 10.1016/s0014-3057(02)00199-4
- [60] Davis L, Rogers P, Pearce J, Peiris P. Evaluation of *Zymomonas*-based ethanol production from a hydrolysed waste starch stream. *Biomass and Bioenergy*. 2006;**30**:809-814. DOI: 10.1016/j.biombioe.2005.05.003
- [61] Hashem M, Darwish SM. Production of bioethanol and associated by-products from potato starch residue stream by *Saccharomyces cerevisiae*. *Biomass and Bioenergy*. 2010;**34**:953-959. DOI: 10.1016/j.biombioe.2010.02.003
- [62] López OV, Versino F, Villar MA, Garcia MA. Agro-industrial residue from starch extraction of *Pachyrhizus ahipa* as filler of thermoplastic corn starch films. *Carbohydrate Polymers*. 2015;**134**:324-332. DOI: 10.1016/j.carbpol.2015.07.081
- [63] Maniglia BC, Tapia-Blácido DR. Structural modification of fiber and starch in turmeric residue by chemical and mechanical treatment for production of biodegradable films. *International Journal of Biological Macromolecules*. 2019;**126**:507-516. DOI: 10.1016/j.ijbiomac.2018.12.206
- [64] Nakthong N, Wongsagonsup R, Amornsakchai T. Characteristics and potential utilizations of starch from pineapple stem waste. *Industrial Crops and Products*. 2017;**105**:74-82. DOI: 10.1016/j.indcrop.2017.04.048
- [65] Patle S, Lal B. Investigation of the potential of agro-industrial material as low cost substrate for ethanol production by using *Candida tropicalis* and *Zymomonas mobilis*. *Biomass and Bioenergy*. 2008;**32**:596-602. DOI: 10.1016/j.biombioe.2007.12.008
- [66] Santanaa AL, Zabot GL, Osorio-Tobón F, Johnera JCF, Coelho AS, Schmiele M, et al. Starch recovery from turmeric wastes using supercritical technology. *Journal of Food Engineering*. 2017;**214**:266-276. DOI: 10.1016/j.jfoodeng.2017.07.010
- [67] Fombuena V, Sánchez-Nácher L, Samper MD, Juárez D, Baçart R. Study of the properties of thermoset materials derived from epoxidized soybean oil and protein fillers. *Journal of the American Oil Chemists' Society*. 2012;**90**:449-457. DOI: 10.1007/s11746-012-2171-2
- [68] Reiznautt QB, Garcia ITS, Samios D. Oligoesters and polyesters produced by the curing of sunflower oil epoxidized biodiesel with cis-cyclohexane dicarboxylic anhydride: Synthesis and characterization. *Materials Science and Engineering: C*. 2009;**29**:2302-2311. DOI: 10.1016/j.msec.2009.05.021
- [69] Sionkowska A. Current research on the blends of natural and synthetic polymers as new biomaterials: Review. *Progress in Polymer Science*. 2011;**36**:1254-1276. DOI: 10.1016/j.progpolymsci.2011.05.003
- [70] Silva RSG, Pinto LAA. Physical cross-linkers: Alternatives to improve the mechanical properties of fish

- gelatin. *Food Engineering Reviews*. 2012;**4**:165-170. DOI: 10.1007/s12393-012-9054-z
- [71] Sionkowska A, Wisniewski M, Kaczmarek H, Skopinska J, Chevallier P, Mantovani D, et al. The influence of UV irradiation on surface composition of collagen/PVP blended films. *Applied Surface Science*. 2006;**253**:1970-1977. DOI: 10.1016/j.apsusc.2006.03.048
- [72] Ocak B. Film-forming ability of collagen hydrolysate extracted from leather solid wastes with chitosan. *Environmental Science and Pollution Research*. 2017;**25**:4643-4655. DOI: 10.1007/s11356-017-0843-z
- [73] Dang X, Shan Z, Chen H. Biodegradable films based on gelatin extracted from chrome leather scrap. *International Journal of Biological Macromolecules*. 2018;**107**:1023-1029. DOI: 10.1016/j.ijbiomac.2017.09.068
- [74] Tian H, Guo G, Fu X, Yao Y, Yuan L, Xiang A. Fabrication, properties and applications of soy-protein-based materials: A review. *International Journal of Biological Macromolecules*. 2018;**120**:475-490. DOI: 10.1016/j.ijbiomac.2018.08.110
- [75] Xie DY, Song F, Zhang M, Wang XL, Wang YZ. Soy protein isolate films with improved property via a facile surface coating. *Industrial Crops and Products*. 2014;**54**:102-108. DOI: 10.1016/j.indcrop.2014.01.01
- [76] Schrader JA, Srinivasan G, Grewell D, McCabe KG, Graves WR. Fertilizer effects of soy-plastic containers during crop production and transplant establishment. *HortScience*. 2013;**48**:724-731. DOI: 10.21273/hortsci.48.6.724
- [77] Zheng P, Lin Q, Li F, Ou Y, Chen N. Development and characterization of a defatted soy flour-based bio-adhesive crosslinked by 1,2,3,4-butanetetracarboxylic acid. *International Journal of Adhesion and Adhesives*. 2017;**78**:148-154. DOI: 10.1016/j.ijadhadh.2017.06.016
- [78] Pan H, Jiang B, Chen J, Jin Z. Blend-modification of soy protein/lauric acid edible films using polysaccharides. *Food Chemistry*. 2014;**151**:1-6. DOI: 10.1016/j.foodchem.2013.11.075
- [79] Picchio ML, Paredes AJ, Palma SD, Passeggi MC Jr, Gugliotta LM, Minari RJ, et al. PH-responsive casein-based films and their application as functional coatings in solid dosage formulations. *Colloids and Surfaces, A: Physicochemical and Engineering Aspects*. 2018;**541**:1-9. DOI: 10.1016/j.colsurfa.2018.01.012
- [80] Picchio ML, Linck YG, Monti GA, Gugliotta LM, Minari RJ, Igarzabal CIA. Casein films crosslinked by tannic acid for food packaging applications. *Food Hydrocolloids*. 2018;**84**:424-434. DOI: 10.1016/j.foodhyd.2018.06.028
- [81] Demirgöz D, Elvira C, Mano JF, Cunha AM, Piskin E, Reis RL. Chemical modification of starch based biodegradable polymeric blends: Effects on water uptake, degradation behaviour and mechanical properties. *Polymer Degradation and Stability*. 2000;**70**:161-170. DOI: 10.1016/S0141-3910(00)00102-6
- [82] Shankar S, Rhim J. Effect of types of zinc oxide nanoparticles on structural, mechanical and antibacterial properties of poly(lactide)/poly(butylene adipate-co-terephthalate) composite films. *Food Packaging and Shelf Life*. 2019;**21**:100327-100333. DOI: 10.1016/j.fpsl.2019.100327
- [83] Meraldo A. Introduction to bio-based polymers. In: John R, Wagner Jr, editors. *Multilayer Flexible Packaging*. 2nd ed. Rochester: William Andrew; 2016. pp. 47-52. DOI: 10.1016/b978-0-323-37100-1.00004-1

- [84] Khan RA, Salmieri S, Dussault D, Sharmin N, Lacroix M. Mechanical, barrier, and interfacial properties of biodegradable composite films made of methylcellulose and poly (caprolactone). *Journal of Applied Polymer Science*. 2012;**123**:1690-1697. DOI: 10.1002/app.34655
- [85] Kiuchi Y, Soyama M, IJI M, Tanaka S, Toyama K. Improvement in impact strength of modified cardanol-bonded cellulose thermoplastic resin by using olefin resins. *Journal of Applied Polymer Science*. 2014;**131**:1-8. DOI: 10.1002/app.39829
- [86] Pires ALR, Moraes AM. Improvement of the mechanical properties of chitosan-alginate wound dressings containing silver through the addition of a biocompatible silicone rubber. *Journal of Applied Polymer Science*. 2015;**132**:1-9. DOI: 10.1002/app.41686
- [87] Eslahi N, Dadashian F, Nejad NH, Rabiee M. Evaluation of wool nanoparticles incorporation in chitosan/gelatin composite films. *Journal of Applied Polymer Science*. 2014;**131**:1-10. DOI: 10.1002/app.40294
- [88] Nobrega MM, Olivato JB, Grossmann MVE, Bona E, Yamashita F. Effects of the incorporation of saturated fatty acids on the mechanical and barrier properties of biodegradable films. *Journal of Applied Polymer Science*. 2012;**124**:3695-3703. DOI: 10.1021/bm201147a
- [89] Qiao X, Tang Z, Sung K. Plasticization of corn starch by polyol mixtures. *Carbohydrate Polymers*. 2011;**83659**:664. DOI: 10.1016/j.carbpol.2010.08.035
- [90] Moreno O, Cárdenas J, Atarés L, Chiralt A. Influence of starch oxidation on the functionality of starch-gelatin based active films. *Carbohydrate Polymers*. 2017;**178**:147-158. DOI: 10.1016/j.carbpol.2017.08.128
- [91] Sudheesh C, Sunooj KV, George J, Kumar S, Vikas, Sajeevkumar VA. Impact of γ - irradiation on the physico-chemical, rheological properties and in vitro digestibility of kithul (*Caryota urens*) starch; a new source of nonconventional stem starch. *Radiation Physics and Chemistry*. 2019;**162**:54-65. DOI: 10.1016/j.radphyschem.2019.04.031
- [92] Doan HXN, Song Y, Lee S, Lee BH, Yoo SH. Characterization of rice starch gels reinforced with enzymatically-produced resistant starch. *Food Hydrocolloids*. 2019;**91**:76-82. DOI: 10.1016/j.foodhyd.2019.01.014
- [93] Cheng S, Wang W, Li Y, Gao G, Zhang K, Zhou J, et al. Cross-linking and film-forming properties of transglutaminase-modified collagen fibers tailored by denaturation temperature. *Food Chemistry*. 2019;**271**:527-535. DOI: 10.1016/j.foodchem.2018.07.223
- [94] Al-Hassan A, Norziah MH. Effect of transglutaminase induced crosslinking on the properties of starch/gelatin films. *Food Packaging and Shelf Life*. 2017;**3**:15-19. DOI: 10.1016/j.fpsl.2017.04.006
- [95] Vaz CM, Fossen M, Van TRF, Graaf LA, Reis RL, Cunha AM. Casein and soybean protein-based thermoplastics and composites as alternative biodegradable polymers for biomedical applications. *Journal of Biomedical Materials Research Part A*. 2003;**65**:60-70. DOI: 10.1002/jbm.a.10416

Lignin as Sustainable Antimicrobial Fillers to Develop PET Multifilaments by Melting Process

Juliette Minet, Aurélie Cayla and Christine Campagne

Abstract

Nowadays, textiles functionalization is developing increasingly, fabrics are not only defined by the intrinsic properties of the fiber but some properties are also brought to provide them added value. Among the desired properties, antibacterial activity is targeted to improve the comfort and durability of textiles but many commercial products use chemical substances which are harmful for the environment (regulation 528/2012). The goal of this study was to use bio-based biocide which can be incorporated in the polyethylene terephthalate (PET) by melt spinning for the development of functional PET. This biocide had to resist to the PET processing temperature up to 264°C which was the maximum temperature of implementation. Two kinds of Kraft lignin and titanium dioxide as reference were added by melting way. The antimicrobial activity was characterized at low concentration (1 and 2 wt.%), to avoid a significant decrease in mechanical strength for the multifilaments and to maintain optimal rheological properties of the polymer for the melt spinning process. Filled PET pellets were obtained by twin screw extrusion step and the multifilaments by melt spinning step. Finally, knitting structures were developed for the evaluation of the antibacterial activity. The mechanical (tensile test) and thermal (DSC and TGA) properties of the filaments were characterized.

Keywords: antibacterial activity, melt spinning process, lignin, sustainable, filaments

1. Introduction

The textile industry is constantly in movement to develop functional and sustainable materials. Additional properties can be added to the intrinsic properties of the textile through its functionalization. One of the targeted properties is antibacterial activity to develop more durable textile because microbes damage fabrics or can develop bad odor. Antimicrobial textile is used in different fields such as medical, clothing or building. On the market, different kinds of textile structures developed with antimicrobial activity are commercialized, as example the X-static[®] product which is made by permanently bonding metallic silver to the surface of the fiber to inhibit the growth of bacteria [1]. Polyrey Sanitized[®] uses [2] silver ions for

hospital bedding or Cupron[®] which develops fabrics of natural or synthetic fibers with pure copper incorporate inside [3]. Textile can be functionalized at all stages of its transformation, during the extrusion for the mass-functionalization, by diffusion for the small molecules or with various surface treatments. The diffusion technic is similar to dyeing process, the diffused agent is carried within the fiber whereas others treatments as surface-functionalization, the agent is placed on the surface by padding or coating. Many textiles and filaments are marketed with antimicrobial activity by mass incorporation of fillers produced by extrusion. The active products are either organic or mineral agents and have to present a good thermal stability during the extrusion step for the incorporation of antibacterial component in the polymer. Amicor's[®] acrylic fibre used organic agent as triclosan for bringing the antibacterial properties [4]. Mineral agents as silver can be also incorporated in synthetic monofilament, for example, Trévira Bioactive[®] [5] and Meryl[®] Skinlife [6], respectively polyester and polyamide which present permanent antimicrobial properties. Nowadays, more and more commercial products are produced by extrusion with the addition of fillers into the thermoplastic polymer and silver nanoparticles are often selected [7–9]. However, environmental concerns of these particles are pointing despite the effective antibacterial properties and good resistance to high temperature because they are very toxic to aquatic life with long lasting effects. Its environmental impact leads to a European regulation (regulation 528/2012) of its use [10]. One way to reduce environmental impact is to substitute silver particles by sustainable, ecofriendly and efficient agents. The challenge, to continue the development of synthetic fiber by melt spinning, is the thermal resistant of agents to processing temperatures of polymer. For reducing the diffusion of the antibacterial agent in the environment, the mass functionalization by extrusion and melt spinning process seems to be the best way to obtain durable textile. Some bio-based agents as chitosan [11] or eugenol [12], present interesting antibacterial activity. Chitosan, obtained after a deacetylation of chitin which is structural element in the crustaceans exoskeleton, may interact with the bacteria membrane and damage it. Indeed, chitosan can alter permeability of membrane cell leading to release of the protein material and other intracellular components and can be accompanied by some lysis of the cell [11]. Eugenol, major constituent of cloves, is effective against a wide range of bacteria, Gram-negative as *E. coli*, *P. vulgaris* or Gram-positive as *S. aureus* [12]. However, a lot of these agents cannot be used for extrusion because of their degradation temperature too low during this step. One other kind of sustainable product which can be incorporate in a polymer to give antibacterial properties is lignin [13–17]. Lignin is a complex and irregular biopolymer and the International lignin institute [18] describes it as an organic substance that binds the cells, fibres and vessels together. It composes wood and the lignified elements of plants and gives the rigidity to the cell wall of the vascular plants [15, 18, 19]. This is the second most abundant organic polymers after cellulose on earth [18] however, it is considered as waste material and low value by-product in the paper industry [19]. Lignin is derived from the polymerization of *p*-coumaryl, coniferyl and sinapyl alcohols, it is cross-linked phenolic polymers [19, 20] but chemical structure cannot be precisely defined because all lignins have some variations in their composition [18]. Indeed, lignin contains many different functional groups, like hydroxyl, methoxyl, carbonyl and carboxylic groups which can be found in different proportions in its structure according to its origin and extraction processes applied [20]. This functional groups lead to polymers several different properties such as specific antioxidant properties [14, 16, 21], UV stabilization effect [22, 23] or antibacterial activity [18, 19, 22–25]. Cazacu et al. define antibacterial activity of several lignin (Alcell[®] lignin, Kraft lignin and hydrolysis lignin) according to the nature bacteria, its origin, its chemical structure and also its

concentration in cultivation medium and the type of microorganisms [19]. Therefore, lignin has shown antibacterial properties, and also in polyvinyl alcohol (PVA), in polyethylene (PE) and in poly(lactic acid) (PLA) [18, 19, 22–25]. Indeed, the activity of the PVA with lignin nanoparticles (LNP) for active packaging was demonstrated for two kinds of bacteria (*Xanthomonas arboricola* pv. pruni and *Pectobacterium carotovorum* subsp. Odoriferum) by Yang et al. [24]. They have demonstrated a well dispersion of the LNP could generate a nucleation effect in PVA and they have validated the synergetic antioxidation effect of LNP with the chitosan [24]. LNP and cellulose nanocrystals (CNC) at 1 and 3 wt.% in PLA present also a synergetic effect but in terms of transparency and UV light blocking aptitude not for antibacterial effect, LNP had better result without the addition of CNC as showed Yang et al. [22]. The antibacterial efficiency of 2 wt.% Björkman lignin was also described in PE film by Gregorova et al., against *E. coli* and *S. aureus* and its activity was compared with common used synthetic antibacterial effective additives [25]. Lignin showed good antibacterial activity compare to known biocides which is harmful for the environment [25]. Without mention antibacterial activity of lignin, Faruk et al. [35] showed the influence of lignin incorporation (Kraft lignin, organosolv lignin and soda lignin) in thermoplastics mostly in polypropylene and polyethylene but also in polyamide, polystyrene, polyvinyl chloride and even more at 0–80 wt.% of lignin were tested. They concluded that the addition of lignin can improved greatly the thermal stability but it depends on the miscibility between lignin and thermoplastics and the types of lignin had an influence on the blending [24]. Unfortunately, in most cases the mechanical strength decreased because of their low compatibility but can be improved with the change of lignin and new blending methods [24]. Furthermore, lignin enhanced the flame retardancy and allows to use it as a carbon source in intumescent systems [13, 24]. This review mentioned the study of Canetti and Bertini which dealt with thermal properties of the composites (PET + lignin) [26]. The analysis showed the degradation temperature and thermal stability in nitrogen decreased with the addition of filler, therefore the lignin content had not to be too high [26].

In this study, polyethylene terephthalate (PET) which is the synthetic polymer the most common in textile [27], was chosen for its high mechanical strength, toughness and fatigue resistance [27, 28]. Different antimicrobial products were incorporated in PET and the purpose was to identify agent with optimal antibacterial properties and with sufficient thermal stability for resisting to the extrusion and spinning process. Rheological property of the polymer had to be adapted to present fluidity compatible with the melt spinning process. The antimicrobial activity had to be observed with small concentration of product, without causing a considerable decrease in the textile's mechanical strength, antimicrobial product selected as a reference was titanium dioxide (TiO₂) because of its high photoactivity, it had been the subject of many studies as antibacterial, self-cleaning or antifogging surfaces [17, 29] and for the bio-based compounds were two kinds of Kraft lignins: Domtar lignin (DL) and Kraft lignin (KL).

2. Materials and methods

2.1 Materials

PET RT 5120 used in this study was supplied by INVISTA Resins & Fibers GmbH. The glass transition temperature of pellets is 82°C and its crystallization temperature 174°C with crystallinity content around 34%. Two kinds of Kraft lignins were incorporated in PET: Kraft lignin (KL) and Domtar lignin (DL).

KL was purchased from Sigma Aldrich and DL from UPM Biochemicals, Finland (European distributor of Domtar BioChoice™ lignin). KL was a pure grade lignin with purity level >98%, with a pH between 5.5 and 7.5 and DL represented industrial grade lignin with a lower purity level (~95%). Titanium dioxide (TiO₂), known for his antibacterial property [17, 29], had been used as a reference. Aeroxide® TiO₂P₂₅ was purchased from EVONIK Industries.

2.2 Textile structures development

Production of antibacterial textile structures requires firstly functional pellets (PET + lignin or TiO₂) produced by extrusion. Then PET nanocomposites were used in melt spin equipment for the development of multifilaments. Finally, a textile structure was obtained by knitting for the characterization of antibacterial activity.

2.2.1 Extrusion

The preparation of PET/fillers compounds by extrusion, requires a drying stage in a vacuum oven at 80°C during 12 h for removing any absorbed water and for avoiding the hydrolyze phenomena of PET. Lignins or TiO₂ incorporation into the PET, with different weight percentages (1 and 2 wt.%), was realized thanks to a co-rotating intermeshing twin-screw extruder from Thermo Haake (L/D = 25). For each blend, the rotational speed was 100 rpm and the five heating zones temperatures of the extruder were fixed ranging from 252 to 260°C. A granulator cut the extruded rod into cylindrical pellets which were dried again for the spinning step.

2.2.2 Melt spinning

Multifilament yarns were obtained by a melt spinning process using the Spinboy I manufactured by Busschaert Engineering spinning device. The extruded blend (PET + fillers) pellets passed through a single-screw extruder heated from 255 to 265°C which brought them in molten state. The spinning temperatures of extruder zones were defined in **Table 1**. They were injected through two dies, containing each 40 holes with a diameter of 1.2 mm, thanks to a volumetric pump. Two bundles of monofilaments were obtained, cooled down by air and then covered with a spin finish oil to ensure multifilament cohesion along the process. The multifilament continuous yarn was hot drawn between two rolls with varying speeds (S1 and S2 defined in **Table 1**) before winding. The theoretical drawing of multifilament was given by the draw ratio (DR), Eq. (1):

$$DR = \frac{S_2}{S_1} \quad (1)$$

Two draw ratios were applied, 2 and 4 by keeping the first roll at the same speed (200 m/min). DR = 4 was obtained when rollers reach the maximum speed at which the multifilaments were spinnable, for optimal drawing. The blend PET/KL

		Extruder zones				Dies	S1 (m/min)	S2 (m/min)	DR
T°C	257	255	264	264	260	262	200	200	2
							400	800	4

Table 1.
Spinning temperatures and roller speeds according to draw ratio (DR).

was not spinnable with DR = 4 because the heap of LK powder blocks the dies which prevents the formation of filaments.

2.2.3 Knit fabric

Developed multifilaments (PET + lignin; PET + TiO₂) were used for the development of A4 format textile structures by manual knitting machine. The knit fabric had to have a large pore structure for the antibacterial test (agar), so that bacteria can breathe underneath the knit. Indeed, bacteria used in this study, multiply in the presence of oxygen, they are called aerobic. All samples were knitted in rib 1 × 1 with 69 needles and E8 gauge. For antibacterial test, the knitting structures were desired for removing the presence of oil and surfactant at the yarns surface. Three steps were required for the desizing; the first one is several cycles in a soxhlet containing petroleum ether during 4 h. Fabrics were dried during at last 12 h, and then underwent a second soxhlet in ethanol during the same time as before. Three cleanings in distilled water under ultrasound (37 Hz) for 20 min released residual products from the sizing. After drying the knits during 12 h, they could be characterized.

2.3 Characterizations methods

2.3.1 Thermal properties

Thermogravimetric analyses (TGA) under air were performed using a TA 2050 Instruments. A sample of 10 ± 0.5 mg of filler or pellet was placed in an open platinum pan. Loss weight measurements were carried out from 20 to 700°C at a heating rate of 10°C/min in a 50 ml/min flow of nitrogen. Degradation temperature was studied after 5 wt.% loss weight. Differential scanning calorimetry (DSC) characterizations of multifilaments were performed on a 2920 Modulated DSC (TA Instruments) with typically 10 ± 0.2 mg of dry material. The manipulation carried out under nitrogen atmosphere (with a flow of 50 ml/min) consisted in two identical cycles, the first one being devoted to the elimination of the thermal history of the nanocomposite previously extruded. The first and the second cycle had the same temperature variation: from -20 to 200°C at 10°C/min, an isotherm at 200°C during 3 min and a cooling stage at 10°C/min to return to -20°C. Analyses were made on the second cycle. The crystallinity degree (χ) of PET in blend was calculated according to Eq. (2):

$$\chi(\%) = \frac{\Delta H_m}{(1 - m_{\text{filler}}) * \Delta H_m^0} \quad (2)$$

where m_{filler} is the theoretical content (wt.%) of fillers introduced in PET; ΔH_m^0 is the reference enthalpy defined as heat of a 100% crystalline sample (117.6 J/g); ΔH_m is the melting enthalpy.

2.3.2 Mechanical properties

Mechanical properties were tested to control that the multifilaments with fillers keep sufficient mechanical properties for undergoing to a textile transformation. The mechanical tests were realized on monofilaments extracted from the multifilament yarn. The count of 10 samples was measured in decitex (dTex) by Vibroskop LENZING INSTRUMENTS and each monofilament was tested to define

its tensile strength. These tests were carried out following the standard NF EN ISO 5079 on a tensile testing machine from Zwick (1456). The force sensor used was 10 N. All the tests were made at standard atmosphere ($20 \pm 2^\circ\text{C}$; $65 \pm 5\%$). The length of the sample was 20 mm and the deformation rate 20 mm/min. All the results represented an average value of 10 tests.

2.3.3 Morphology

The longitudinal view of multifilaments was observed with an optical microscope. The Nikon eclipse LV100POL with advanced research image analysis was used to analyze the dispersion of the fillers into PET. The morphology of PET with 1 and 2 wt.% KL and DL blends was studied using a Field Emission Gun-Scanning Electron Microscope (FEG-SEM) to analyze the distribution of lignin in the polymer. The technology used was Jeol JSM7600F with Oxford EDX (energy dispersive X-ray spectrometry) analysis.

2.3.4 Interfacial energy

The interfacial energy between the PET and the fillers were determined from the surface energy of each components by the sessile drop technique. Lignins films were created and were tested with a drop of water and diiodomethane which were polar and apolar liquid with a known surface tension (**Table 2**). Surface energy could be expressed as a sum of several components as in Eq. (3): polar (p), dispersive (d), ionic (i), covalent (c), metallic (m), etc. [30].

$$\gamma_S = \gamma_S^p + \gamma_S^d + \gamma_S^i + \gamma_S^c + \gamma_S^m + \dots \quad (3)$$

Only two components, polar and dispersive, are taken into account; the other terms are defined as negligible.

γ_L^d is the dispersive component and γ_L^p is the polar component of liquids.

θ was considered as the angle of the liquid on the solid. The Fowkes method allows to determinate the polar and dispersive components of the surface energy from the contact angles obtained on this solid with various liquids [31, 32].

The equation of Owen and Wendt [33] (4) with two unknowns allows to define the surface energy of the solid:

$$\gamma_L(1 + \cos\theta) = 2\sqrt{\gamma_S^d \gamma_L^d} + 2\sqrt{\gamma_S^p \gamma_L^p} \quad (4)$$

γ_S is the surface tension of lignins (mN/m); γ_L is the surface tension of the liquid (mN/m); γ^p is the polar component (mN/m); γ^d is the dispersive component (mN/m).

Surface energy of lignins and PET allow to measure interfacial energy with Eq. (5) between x/PET and x is the lignin KL or DL [34]:

(mN/m)	γ_L	γ_L^d	γ_L^p
Water	72.6	21.6	51.0
Diiodomethane	50.8	48.5	2.3

Table 2.
Water and diiodomethane components of the surface tension (γ_L).

$$\gamma_{x/PET} = \gamma_x + \gamma_{PET} - \frac{4 \gamma_x^d \gamma_{PET}^d}{\gamma_x^d + \gamma_{PET}^d} - \frac{4 \gamma_x^p \gamma_{PET}^p}{\gamma_x^p + \gamma_{PET}^p} \quad (5)$$

x is the lignin KL or DL.

2.3.5 Antibacterial activity

Antimicrobial tests have been run on each lignin powder and desizing knitted structures. First of all, knits were cut and autoclave steam sterilization was carried out at 120°C during 20 min to ensure other bacteria were not going to grow during the test. In test tubes, nutrient broth and bacteria were mixed and then cultured for 24 h at 37°C, which was the optimal temperature for bacteria growth. The culture solution was diluted and 250 µL of this solution with a concentration of ~105 CFU/ml was poured onto sterilized petri dishes with the solid culture medium (agar) that was adapted to the bacteria. Then 50 mg of each lignin powder was spread or knit fabrics (4 × 3 cm) were positioned in different petri dishes. Qualitative test was made with the Agar diffusion test. During this test, two different types of bacteria, described lower, were studied. This difference could be detected by staining technique: Gram-negative has an outer membrane. Indeed, antibacterial effect depends on the gram and the genus of the bacteria. The first was a Gram-positive bacterium, genus *Staphylococcus epidermidis* ATCC® 12228™, it is a bacterium that is found on the skin and is therefore constantly in contact with clothing textiles. The second bacterium tested was Gram-negative, genus *Escherichia coli* ATCC® 25922™. It is found mainly in the intestines of mammals and will serve as a reference for all Gram-negative bacteria.

Once the knits or the powders were positioned in contact with bacteria in petri dishes, they were placed in an oven for 24 h at 37°C for incubation. The antibacterial halo around the powder could be defined but for the textile, there is no diffusion of agent out of the fiber. Therefore, knits have been removed for defining antibacterial activity by contact underneath the knit.

3. Results and discussion

The comparison of the two lignins properties was realized with several tests out of characterization. First, fillers were tested to evaluate their antibacterial efficiency and their thermal resistance to high temperatures. Secondly, dispersion variations between fillers in PET were analyzed thanks to the mechanical properties of monofilament and finally the thermal and antibacterial properties of the textile material were characterized. Mechanical tests were also used to check if the yarn could be used and be enough resistant for an outdoor textile application.

3.1 Fillers properties

TGA tests on fillers were performed to define each degradation temperatures of lignins and the antibacterial test characterized their activities against two bacteria.

3.1.1 Thermal stability properties

The results in **Table 3** showed that the fillers presented thermal stability with the processing temperature of the PET (264°C) during melt spinning. In **Table 3**, degradation temperature (T_d) of KL and DL were close to the PET processing

Fillers	KL	DL	TiO ₂
Td (°C)	253	232	>700
Loss weight at 264°C (wt.%)	6.1	7.6	1.6

Table 3.
Degradation temperature of KL, DL and TiO₂.

temperature at 264°C whereas TiO₂ was very resistant up to over 700°C. The degradation at 264°C for both lignins was <8 wt.%. Therefore, KL and DL could be used by melt spinning as filler in the PET.

3.1.2 Antibacterial properties

Lignins powder were first tested with the agar diffusion test and qualitative test as explained in Section 2.3, antibacterial activity to confirm the antibacterial properties of lignins and the results are shown in **Figure 1**.

The black line delimits the halo which means that no bacteria are present around the lignin thanks to its antibacterial activity. Two kinds of bacteria were tested: *S. epidermidis* and *E. coli*, as explained. Against Gram-positive bacteria, halos were created around powders, so KL and DL were efficient. However, there was less diffusion of lignins with Gram-negative bacteria but a small halo could be noticed. Their effectiveness after an exposition at high temperature during 5 min were verified. The powders still demonstrated antibacterial activity with the same inhibition zone against bacteria after this thermal treatment.

3.2 Influence of dispersion on mechanical properties

The influence of fillers dispersion was characterized by the mechanical properties of the monofilaments. Optical microscope and SEM observations have completed the characterization of the dispersion. The interfacial energy of polymer and fillers gave information concerning the affinity of fillers and explained this dispersion.

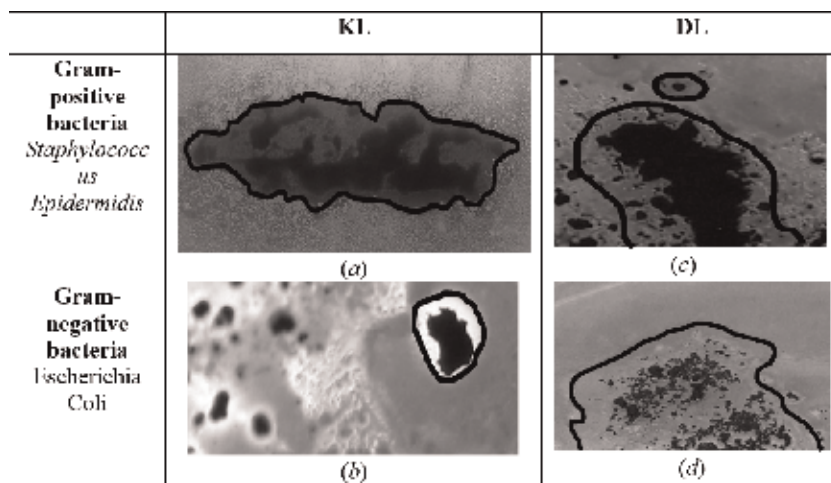


Figure 1.
Anti-bacterial results on (a) KL against *S. epidermidis*, (b) KL against *E. coli*, (c) DL against *S. epidermidis*, and (d) DL against *E. coli*.

3.2.1 Mechanical properties

Count (dTex) was measured on monofilament extracted from multifilament yarns and the same monofilament was used for tensile test.

Figure 2 represents counts of multifilaments realized, for 1 and 2 wt.% of TiO₂, KL and DL and for virgin PET. The monofilament with KL was less regular and the standard deviation of monofilament count with KL was higher than others. The count with DR = 4 was always slightly smaller than DR = 2, indeed multifilaments at DR = 4 were more stretched. Virgin PET was used as reference, and the introduction of TiO₂ or DL did not significantly modify the average count of the monofilaments extracted from the multifilament. On the other hand the incorporation of KL increased the count which could be explained by the agglomeration of fillers in PET.

Figure 3(a) represents the tenacity and **(b)** the elongation at break according to the fillers content. The dotted line is for DR = 4 and the continuous line for DR = 2. In **Figure 3(a)**, the incorporation of KL and DL fillers decreased the tenacity of the PET by almost 40% no matter the type of lignin. Both lignins weakened the monofilament but thanks to the good mechanical properties of PET, the multifilament could be still transformed into textile structure. The fillers content had low effect on the elongation at break except for KL, the tenacity continue to reduce with 2 wt.%. Moreover, when DR = 4 the material was more resistant than at DR = 2, because the macromolecules had been more oriented in the direction of the stress during drawing in the glassy state. In **Figure 3(b)**, all values of elongation

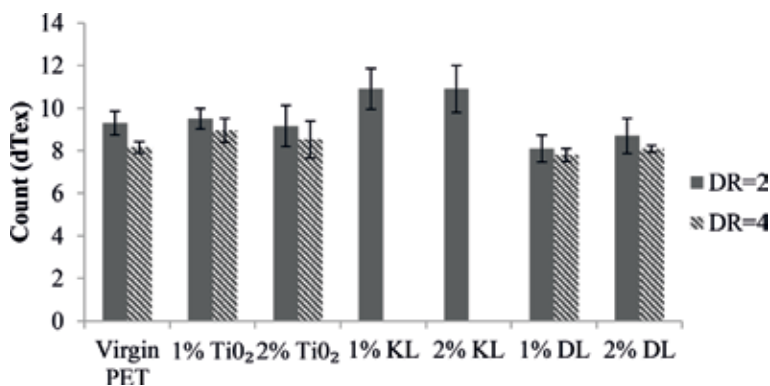


Figure 2. Counts of monofilaments: virgin PET, 1 and 2 wt.% of TiO₂, KL and DL according the draw ratio (DR).

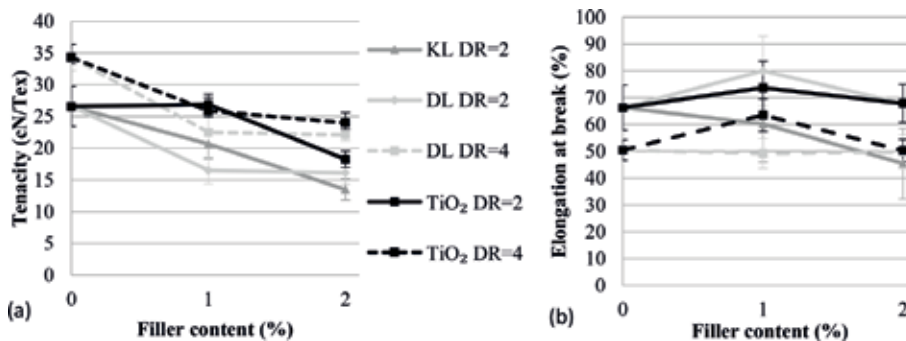


Figure 3. (a) Tenacity at break and (b) elongation at break according to fillers content.

at break were between 50 and 80%, the latter being weakly impacted by the adding of fillers. Elongation at break increased slightly with 1 wt.% TiO₂ and DL (DR = 2) but not significantly according to standard deviation. Indeed, the standard deviation is higher for 1 wt.% DL in comparison with the other measures. The incorporation of 1 and 2 wt.% KL decreased the elongation at break and this value decreased with the draw ratio leading to the orientation of the macromolecules. The more content of KL was, the weaker and less elastic the filament was. For DL there was no general trend, there was a decrease in mechanical properties with 1 wt.% and the properties were stable at 2 wt.%.

3.2.2 SEM and optical microscope

Figures 4 and **5** are respectively the SEM pictures and images from optical microscope. In the SEM pictures KL caused asperities on the surface of filaments and showed that it is not regular, unlike the wire with DL which is longitudinally regular. Microscopy analyzes show that KL forms agglomeration while DL is homogeneously dispersed. In **Figure 5(a)** and **(b)**, the optical microscope showed many agglomerates of KL in PET, especially with 2 wt.%. The higher the filler content, the more defects there were. Most of agglomerates were larger than 100 μm and some of them appeared to the naked eye as in **Figure 6**. DL presented a better dispersion in PET as seen in **Figure 5(c)** and **(d)**. The count of the yarn with KL was higher because of the poor dispersion and the heap of powder that increased the thickness. Agglomerates were arranged randomly along the filament which was explained the big standard deviation of the count in Section 3.2.1.

3.2.3 Interfacial energy

Interfacial energy was calculated with formulas in Section 2.3.3, Interfacial energy for explaining the difference of homogeneity between lignins in the PET. **Tables 4** and **5** show respectively the surface energy of DL, KL and PET and the interfacial energy between KL/PET and DL/PET.

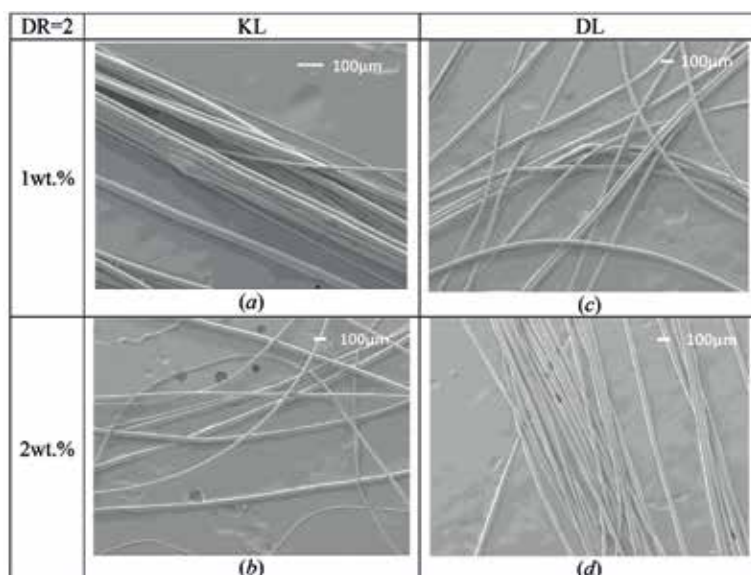


Figure 4. SEM of multifilaments (a) PET + 1 wt.% KL, (b) PET + 2 wt.% KL, (c) PET + 1 wt.% DL, and (d) PET + 2 wt.% DL.

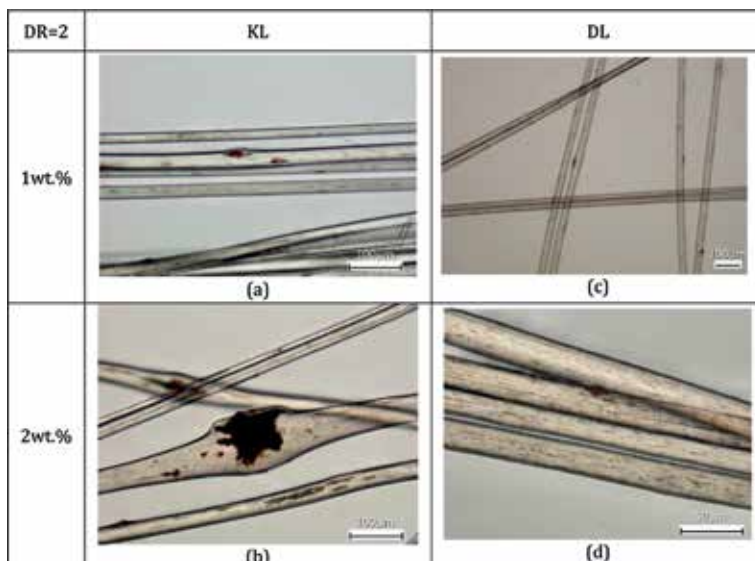


Figure 5. Optical images of multifilaments (a) PET + 1 wt.% KL, (b) PET + 2 wt.% KL, (c) PET + 1 wt.% DL, and (d) PET + 2 wt.% DL.

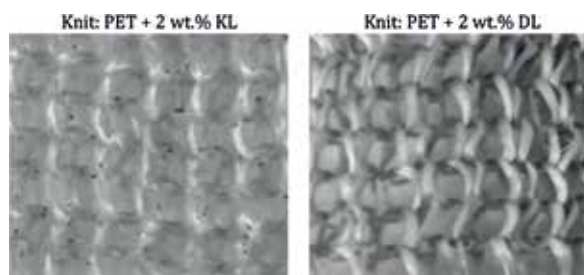


Figure 6. View of knit fabrics PET + 2 wt.% KL and PET + 2 wt.%.

(mN/m)	γ_s	γ_s^p	γ_s^d
KL	55.4	25.3	30.1
DL	53.8	15.9	37.9
PET	44.6	4.9	39.7

Table 4. Surface tension polar and dispersive of KL, DL and PET.

$\gamma_{KL/PET}$ (mN/m)	$\gamma_{DL/PET}$ (mN/m)
15.1	5.9

Table 5. Interfacial energy of KL and PET ($\gamma_{KL/PET}$) and DL and PET ($\gamma_{DL/PET}$).

Table 5 had showed that the interfacial energy for DL in PET was smaller than for KL, which means that the affinity between DL and PET is better than KL. A higher interfacial energy ($\gamma_{KL/PET}$) shows a low affinity which caused

agglomerates as seen in the optical microscope images. Omar Faruk et al. [24] have explained that when lignin was pure the blending was better, but in this case, it was the opposite because as seen in Section 2.1, KL has slightly higher purity than DL. The difference could be explained by the side-chain of each lignin, which account for the difference of the interfacial energy with PET.

3.2.4 Thermal properties

Knowing the thermal properties of the filament allowed to determine the crystallinity content of the polymer, to understand its behavior at different temperatures. DSC measured the crystallinity content, melting and glass temperature. The crystallinity content has been calculated as explain in Section 2.3, differential scanning calorimetry and are presented in **Figure 7**.

Figures 7 and 8 introduce the results obtained for the filaments with DR = 2 because results were similar for both DR. Tc is the crystallinity temperature measured on the second cycle of curves obtained by DSC analysis. **Figures 7 and 8** show the values according to the percentage of fillers in the PET. For all fillers, the incorporation enhanced the crystallinity content but for KL and TiO₂, the percentage of filler had no impact. For both lignins, crystallinity temperature increase and the crystallization start beforehand. The crystallinity content and temperature of DL increased with the percentage; therefore, DL can be defined as nucleating agent and its effect increase slightly with the fillers content.

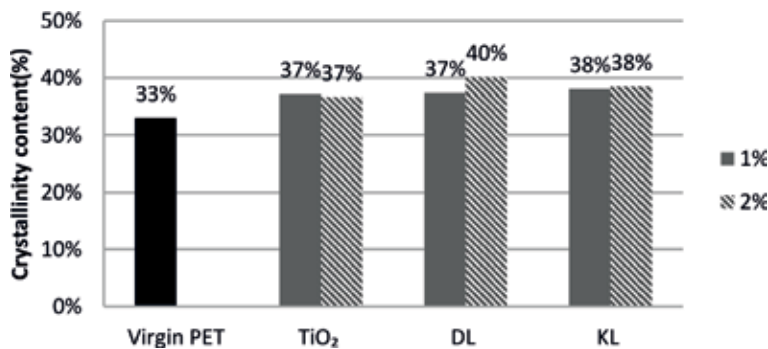


Figure 7. Crystallinity content of multifilaments DR = 2 virgin PET, and filled PET with TiO₂, LD or LK at 1 or 2 wt.%.

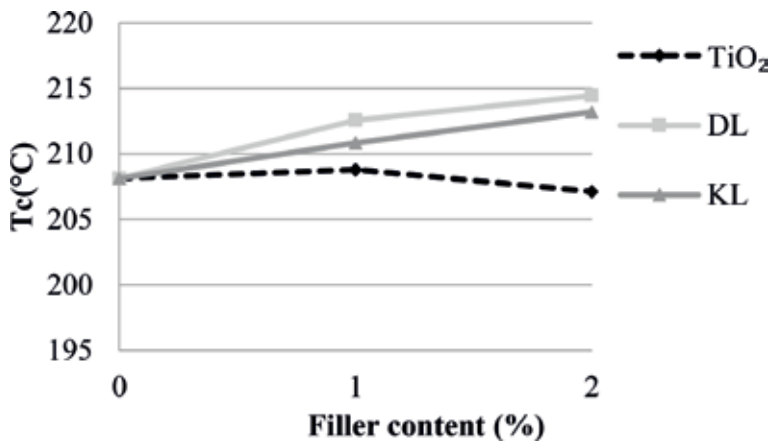


Figure 8. Crystallinity temperatures according to filler content for TiO₂, LD and LK, DR = 2.

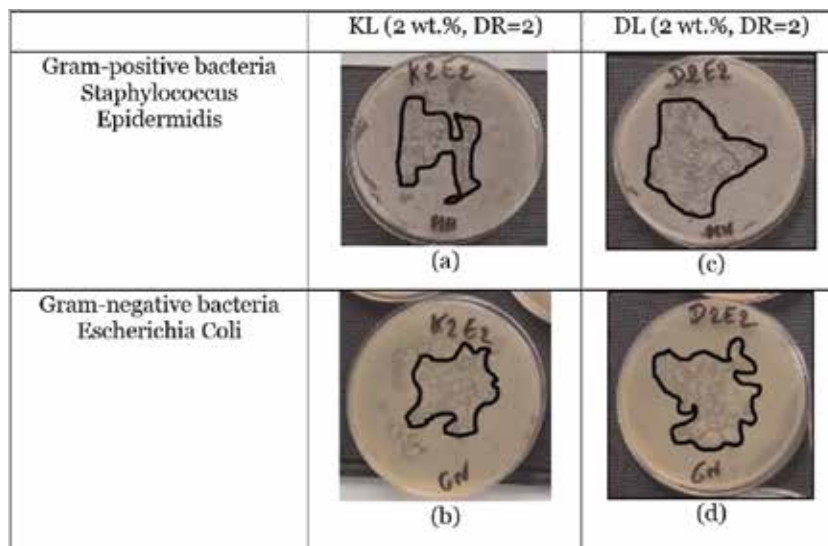


Figure 9. Anti-bacterial results on desizing knitted fabric based on PET filled with (a) KL against *S. epidermidis*, (b) KL against *E. coli*, (c) DL against *S. epidermidis*, and (d) DL against *E. coli*.

Integration of lignin at 1, 2 wt.% or TiO₂ did not modify the thermal stability of the PET and the degradation temperatures were always around 400 ± 2°C (which was the accuracy of TGA device). These fillers did not have any influence on thermal transition, nor on the glass transition and melting temperature. Whatever the draw ratio, fillers and their content, the glass temperature was always the same, close to 78 ± 2°C and the melting temperature is 256 ± 2°C. The fillers did not impact the thermal properties except DL which behaves as a nucleating agent.

3.3 Antibacterial properties

Antibacterial tests were run on knit fabrics with 2 wt.% of lignins, results were shown in **Figure 9**. Black lines show the antibacterial halos after removing textile. Bacterial growth was analyzed below the desizing knit fabric for avoiding the presence of impurities.

For PET knitting structures, the results were good, in contact with *E. coli* bacteria. DL appeared to have slightly better efficiency. Nevertheless, the results with *S. epidermidis* bacteria were quite similar. Both of them were efficient against Gram-positive bacteria. As seen in SEM and optical microscope images, the poor dispersion of KL causes agglomerates which are randomly along the filament. The contact between KL and the bacteria is different according to the area of the yarn in contact during the test, the antibacterial effect will be better where agglomerates are present and ineffectual when no KL. Whereas, the homogeneous dispersion of the DL with PET allow to guarantee an uniform antibacterial effect everywhere in the textile.

4. Conclusion

Antibacterial properties create added value for textiles to be durable and prevent bad odors. However, many antibacterial products are noxious for the environment. The aim of the study was to replace harmful biocide by eco-friendly and durable

agent. Melt spinning process was chosen because it restricts the diffusion of the antibacterial product in the environment. The filler selected was lignin, a biopolymer and two kinds of Kraft lignins were compared. The dispersion of fillers in the PET, the thermal and the mechanical properties and antibacterial activity were taken into account. First of all, the incorporation of both lignins in PET was a success for the development of multifilaments by melt spinning. As seen before, they have a significant impact on mechanical properties of the monofilaments with the incorporation of lignin into PET and we have observed a decrease of the tenacity. But these new mechanical properties do not have an effect on the use of yarns in the textile process. The poor dispersion of KL does not have a significant influence on the tenacity of the monofilament in comparison with DL. KL presents a low affinity with PET, remains on the surface and creates thickness defects. The dispersion of KL is not homogeneous within the filament and does not guarantee an antibacterial activity along the multifilament. However, DL has low interfacial energy with PET, which allows intimate mixing with the polymer. The thermal properties demonstrate DL as a nucleating agent because its crystallinity content and temperature increase, so DL intensifies the crystallinity of the PET. Finally, KL and DL have a positive activity against Gram-positive bacteria. Nevertheless, DL appears to have slightly better efficiency against Gram-negative bacteria despite its smaller specific surface area. Consequently, Domtar lignin seems to be a good candidate to replace silver nanoparticles. From this point on, testing the durability of anti-bacterial properties will be interesting to see the behavior of DL at weather conditions (temperature, humidity, UV) and by washing to equate to rain.

Acknowledgements

The authors would like to thank CENTEXBEL, project partner, for taking SEM and optical microscope images as well as for antibacterial tests. The authors would like to thank as well Christian Catel, technician in the field of microbiology and chemistry, for all the antibacterial tests made in ENSAIT, Guillaume Lemort, technician in research project for spinning multifilaments, Romain Danjou and Robin Hamed Mekbel, students in ENSAIT, for the mechanical tests carried out. The Duratex project is financed within the Interreg V program France-Wallonia-Flanders, a crossborder collaboration program with financial support from the European Fund for Regional Development and co-financed by the province of West Flanders and the Walloon Region.

Author details

Juliette Minet, Aurélie Cayla* and Christine Campagne
ENSAIT, GEMTEX, Roubaix, France

*Address all correspondence to: aurelie.cayla@ensait.fr

IntechOpen

© 2019 The Author(s). Licensee IntechOpen. This chapter is distributed under the terms of the Creative Commons Attribution License (<http://creativecommons.org/licenses/by/3.0>), which permits unrestricted use, distribution, and reproduction in any medium, provided the original work is properly cited. 

References

- [1] Noble Biomaterials Inc. 2016. Available from: <http://noblebiomaterials.com/xstatic-textiles/>
- [2] Polyrey. 2018. Available from: <http://en.polyrey.com/sanitized-en>
- [3] Cupron Inc. 2018. Available from: <http://www.cupron.com/>
- [4] Amicor® Pure. The world's leading 'intelligent' fibre for healthy living and sleeping. 2004. Available from: <http://www.amicorpure.co.uk/>
- [5] Available from: http://www.fidivi.com/images/stories/prodotti/pdf_generici/english/Bioactive_eng.pdf
- [6] Available from: <http://www.nylstar.com/shops/yarns/250-meryl-skinlife>
- [7] Mtimet I. Elaboration of antibacterial surfaces containing silver nanoparticles [thesis]. FR: INSA de Rouen; 2011
- [8] Chadeau E. Caractérisation des propriétés antibactériennes de textiles fonctionnalisés avec de l'argent ou du PolyHexaMéthylène Biguanide (PHMB) [thesis]. Université Claude Bernard—Lyon I; 2011
- [9] Panacek A, Kvitek L, et al. Silver colloid nanoparticles: Synthesis, characterization, and their antibacterial activity. *Journal of Physical Chemistry B*. 2006;**110**(33):16248-16253
- [10] ECHA. Available from: <https://echa.europa.eu/fr/regulations/biocidal-products-regulation/product-types>
- [11] Kong M, Guang Chen X, Xing K, Hyun PJ, et al. Antimicrobial properties of chitosan and mode of action: A state of the art review, *International Journal of Food Microbiology*. 2010;**144**:51-63
- [12] Marchese A, Barbieri R, et al. Antimicrobial activity of eugenol and essential oils containing eugenol: A mechanistic viewpoint. *Critical Reviews in Microbiology*. 2017;**43**(6): 668-689
- [13] Brebu M, Vasile C. Thermal degradation of lignin—A review, *Cellulose Chemistry and Technology*. 2010;**44**(9):353-363
- [14] Domenek S, Louaifi A, et al. Potential of lignins as antioxidant additive in active biodegradable packaging materials. *Journal of Polymers and the Environment*. 2013; **21**(3):692-701
- [15] Smolarski N. High-Value Opportunities for Lignin: Unlocking its Potential. Paris: Frost & Sullivan; 2012. pp. 1-15
- [16] Pouteau C, Dole P, Cathala B, Averous L, Boquillon N. Antioxidant properties of lignin in polypropylene. *Polymer Degradation and Stability*. 2003;**81**(1):9-18
- [17] Carre G. Compréhension des mécanismes lors de la photocatalyse appliquée à la dégradation des microorganismes. In: *Application au Traitement de l'air et Aux Textiles Auto-décontaminants*. PhD Thesis, University of Strasbourg (France); 2013
- [18] Available from: <http://www.ili-lignin.com/aboutlignin.php>
- [19] Cazacu G, Capraru M, Popa VI. Advances in natural polymers. In: *Advances Concerning Lignin Utilization in New Materials*. Vol. 18. 2013. pp. 255-312
- [20] N-E. El Mansouri, Salvadó J. Analytical methods for determining functional groups in various technical lignins. *Industrial Crops and Products*. 2007;**26**(2):116-124

- [21] Vinardell MP, Ugartondo V, Mitjans M. Potential applications of antioxidant lignins from different sources. *Industrial Crops and Products*. 2008;**27**:220-223
- [22] Yang W, Fortunati E, Dominici F, Giovanale G, Mazzaglia A, Balestra GM, et al. Synergic effect of cellulose and lignin nanostructures in PLA based systems for food antibacterial packaging. *European Polymer Journal*. 2016;**79**:1-12
- [23] Thakur VK, Thakur MK, Raghavan P, Kessler MR. Progress in green polymer composites from lignin for multifunctional applications: A review. *ACS Sustainable Chemistry and Engineering*. 2014;**2**:1072-1092
- [24] Yang W, Owczarek JS, et al. Antioxidant and antibacterial lignin nanoparticles in polyvinyl alcohol/chitosan films for active packaging. *Industrial Crops and Products*. 2016;**94**: 800-811
- [25] Gregorova A, Redik S, et al. Lignin-Containing Polyethylene Films with Antibacterial Activity. Brno, Czech Republic, EU; 2011;**9**:21-23
- [26] Canetti M, Bertini F. Influence of the lignin on thermal degradation and melting behaviour of poly(ethylene terephthalate) (PET) based composite. *e-Polymers*. 2009;**9**(1). Retrieved 1 June 2019, from DOI: 10.1515/epoly. 2009.9.1.596
- [27] CIRFS. Available from: <https://www.cirfs.org/man-made-fibers/Product-and-production-process>
- [28] Venkatachalam S, Nayak SG, Labde JV, Gharal PR, Rao K, Kelkar AK. In: Saleh HE-D, editor. *Degradation and Recyclability of Poly (Ethylene Terephthalate), Polyester*. InTech; 2012. DOI: 10.5772/48612. Available from: [https://www.intechopen.com/books/polyester/degradation-and-](https://www.intechopen.com/books/polyester/degradation-and-recyclability-of-poly-ethylene-terephthalate-)
- recyclability-of-poly-ethylene-terephthalate-
- [29] Gumy D, Morais C, Bowen P, et al. Catalytic activity of commercial of TiO₂ powders for the abatement of the bacteria (*E. coli*) under solar simulated light: Influence of the isoelectric point. *Applied Catalysis B: Environmental*. 2006;**63**:76-84
- [30] De Gennes P-G, Brochard-Wyart F, Quere D. *Capillarité: Interfaces mobiles*. In: *Gouttes, Bulles, Perles et Ondes*. Editions Belin; 2002. pp. 11-37. ISBN: 978-2-7011-4055-1
- [31] Fowkes M. Attractive forces at interfaces. *Industrial and Engineering Chemistry*. 1964;**56**(12):40-52
- [32] Leroux F. *Etude des traitements par plasma à pression atmosphérique— Applications à l'industrie textile* [thesis]. France: Valenciennes and Hainaut-Cambresis University; 2007
- [33] Owen DK, Wendt RC. Estimation of the surface free energy of polymers. *Journal of Applied Polymer Science*. 1969;**13**(8):1741-1747
- [34] Cayla A. *Elaboration de détecteurs souples de température—Mise en œuvre et caractérisation de multifilaments à base de polymères immiscibles chargés en nanotubes de carbone* [thesis]. France: Université des sciences et technologiques de Lille; 2010
- [35] Omar Faruk, Mohini Sain, William Andrew. Lignin reinforcement in thermoplastic composites. *Lignin in Polymer Composites*. 2015:95-114. ISBN: 9780323355667

Edited by Arpit Sand and Elsayed Zaki

This book, *Organic Polymers*, covers aspects that are of immediate concern to a new entrant to the field of polymers. Taken as a whole, these eight chapters aim to help the readers easily assimilate other specialized and exhaustive treatises on the subject. Topics dealing with the chemistry and technology of polymers are presented in a careful and logical manner so as to provide an easy and enjoyable read. Several examples and analogies are included so to make the main concepts easy to follow and tables and figures are included so that the book can serve, to a limited extent, as a hand book dealing with polysaccharides with different parameters. This book is meant for students studying polysaccharides and those working on graft copolymers and other allied polymer industries but without a formal educational background in organic polymers.

Published in London, UK

© 2020 IntechOpen

© Warayut Sansri / iStock

IntechOpen

